DEPARTMENT OF AERONAUTICS AND ASTRONAUTICS

UNIVERSITY OF WASHINGTON

Photothermoviscoelasticity

STATUS REPORT

NASA CONTRACT NSG 401

E. H. Dill

R. J. H. Bollard

July 1965

NATIONAL AERONAUTICS AND SPACE ADMINISTRATION OFFICE OF GRANTS

AND RESEARCH CONTRACTS

STATUS REPORT

NASA Research Grant NsG 401

for

Photothermoviscoelasticity Research

with the

University of Washington

Principal Investigators:

Dr. R. J. H. Bollard
Dr. E. H. Dill

Principal Personnel:

Dr. M. E. Fourney
Mr. C. W. Fowlkes
Mr. P. Ramanaiah

Department of Aeronautics and Astronautics.

Table of Contents

Introduction:

This report reviews the status of the photothermoviscoelasticity research project being conducted in the Department of Aeronautics and Astronautics at the University of Washington under Research Grant NsG-401. Parts of this report have been compiled in a form suitable for a NASA Technical Note and will be submitted for approval in the immediate future.

The research program is directed to establishing a procedure for the stress analysis of geometrically complex structures containing viscoelastic materials in total or in part and subjected to transient temperature and/or non-proportional boundary loadings. A primary objective has been the development of routine experimental procedures for obtaining such stress states. As detailed in this report such a routine procedure and the necessary equipment have been developed for linear viscoelastic materials. The experimental procedure employs and extends the techniques of photoelasticity. The necessary interpretative procedures employ the basic mathematical hypotheses and formulation presented herein.

Under the existing grants, the fundamental mathematical formulation of the relationships between the dielectric characteristics and the mechanical state of linear viscoelastic birefringent materials was formulated and experimentally verified. Since the observable fringe patterns obtained in a polariscope are related directly to the dielectric characteristics it is possible to relate these patterns to the mechanical state. To reach this point in the continuing research program the following developments were necessary:

(a) suitable transparent birefringent viscoelastic plastics for which it is possible to tailor the mechanical properties;

(b) apparatus for the optical and mechanical characterization
of the viscoelastic plastics:

(c) a rotating element photoviscoelastic bench:

(d) apparatus and techniques for obtaining thermal properties
and the measurement of temperature effects on the optical
and mechanical characteristics:

(e) experimental techniques for conducting photothermoviscoelastic
observations in the polariscope and the interpretation of
these photographically recorded observations:

As with any well conceived experiment the development is built on
an exhaustive analytic investigation of the optical and mechanical behavior
of viscoelastic materials. The first part of this report presents a survey
of the results of these studies. Details appear in the open literature
as referenced. Fundamental hypotheses made in this analytic formulation
required experimental verification and these are reported in the second part.
In the concluding section of this part the application to a typical thermo-
viscoelastic problem is illustrated. The example chosen is that of a
pressure and thermally loaded solid propellant motor grain cross-section
which is a problem presenting severe difficulties in theoretical analysis.
The method is applicable to any thermally and mechanically loaded structure
containing linear viscoelastic material and which can be modeled as a two-
dimensional specimen. The same method is directly applicable to three-
dimensional models by using imbedded polariscopes but the experimental tech-
niques are much more difficult.

The appendices describe in detail aspects of the interpretative techniques, the nature and characterization of the birefringent visco-elastic plastics used and the apparatus developed. Particular attention is drawn to the rotating element photoviscoelastic bench which was first successfully used in 1962 but continues to be modified and improved to suit the increasingly complex experiments as we reach for the general all-purpose equipment and techniques.

I. Theory

1. Basic Ideas.

This section provides an analytical basis for understanding the optical properties of birefringent viscoelastic materials and for the application of these materials in experimental stress analysis. In order to determine the state of stress in a viscoelastic body, the basic idea is to manufacture a model from a transparent birefringent material and then determine the stress state of the model by observation of the model in a polariscope. In the viscoelastic case, it is necessary to have a complete record of the history of isochromatic fringe order and isoclinic angle in order to determine the stress at the present time.

The classical theory of linear viscoelasticity is reviewed in section 2.

The theory of propagation of light in a dielectric at rest is described in section 3. It is shown that the isoclinic angle at any time is determined by the orientation of the principal axes of the dielectric tensor and the fringe order at any time is proportional to the difference in principal indices of refraction (see reference 1).

In section 4, the relationship between optical characteristics and mechanical state is explored. This is the core of the problem. A theory sufficiently general to interpret behavior at small strain is presented.

2. Viscoelasticity.

2.1. Basic Equations:

In this section some results are cited which are used to interpret our experiments. The experiments have been purposely limited to small displacements and quasi-static loads; that is, conditions are such that the classical linear theory can be used and inertia terms neglected. The usual cartesian tensor indicial notation and summation convention are used.

In rectangular cartesian coordinates, the equilibrium equations are

$$\partial_m \sigma_{km} + f_k = 0 \tag{2.1-1}$$

The body force f_k will be negligible in our experiments. The σ_{km} are the components of the stress tensor which is symmetric. The symbol ∂_m will mean partial derivative with respect to the coordinate x^m, throughout the following discussion.

The components of the strain tensor ϵ_{km} are related to the displacement vector u_k by

$$\epsilon_{km} = \tfrac{1}{2} (\partial_k u_m + \partial_m u_k) \tag{2.1-2}$$

In order to write the stress-strain relations it is convenient to introduce the deviatoric stress s_{km} and deviatoric strain e_{km} defined by

$$s_{km} = \sigma_{km} - 1/3 \, \sigma_{rr} \, \delta_{km}$$

$$\tag{2.1-3}$$

$$e_{km} = \epsilon_{km} - 1/3 \, \epsilon_{rr} \, \delta_{km}$$

where δ_{km} denotes the Kronecker delta. Then, for an isotropic material

$$s_{km} = \int_0^t 2G\,(t-\tau)\,\dot{e}_{km}\,(\tau)\,d\tau \qquad (2.1\text{-}4)$$

$$1/3\,\sigma_{rr} = \int_0^t K\,(t-\tau)\,\dot{\epsilon}_{rr}\,(\tau)\,d\tau \qquad (2.1\text{-}5)$$

Where the dot refers to the derivative with respect to the variable indicated and σ_{rr} and ϵ_{rr} are the mean hydrostatic stress and strain respectively.

The inverses of equations (2.1-4) and (2.1-5) are

$$2e_{km} = \int_0^t J\,(t-\tau)\,\dot{s}_{km}\,(\tau)\,d\tau \qquad (2.1\text{-}6)$$

$$\epsilon_{rr} = \int_0^t 1/3\,B\,(t-\tau)\,\dot{\sigma}_{rr}\,(\tau)\,d\tau \qquad (2.1\text{-}7)$$

The functions $G(t)$, and $K(t)$, or $J(t)$ and $B(t)$ characterize the material and have the names;

$J(t)$ – shear creep compliance

$B(t)$ – bulk creep compliance

$G(t)$ – shear relaxation modulus

$K(t)$ – bulk relaxation modulus

The functions are related by Volterra integral equations:

$$\int_0^t G\,(t-\tau)\,J\,(\tau)\,d\tau = t \qquad (2.1\text{-}8a)$$

$$\int_0^t K\,(t-\tau)\,B\,(\tau)\,d\tau = t \qquad (2.1\text{-}8b)$$

Given $J(t)$; $G(t)$ can be calculated by solving (2.1-8a) similar to the method shown in Appendix A.1.

We now recall some results for special deformations. First, consider a uniaxial stress field which is approximated by the tension test. If $\sigma_{11} \pm 0$ while the other components of stress are zero, the deviatoric stresses are

$$s_{11} = 2/3 \ \sigma_{11}, \quad s_{22} = -1/3 \ \sigma_{11}, \quad s_{33} = -1/3 \ \sigma_{11} \qquad (2.1-9)$$

and the others are zero. From equation (2.1-3), (2.1-6), and (2.1-7),

$$\epsilon_{11} = \int_{0}^{t} D(t-\tau) \ \dot{\sigma}_{11} \ d\tau \qquad (2.1-10)$$

$$\epsilon_{22} = \epsilon_{33} = -\int_{0}^{t} \nu(t-\tau) \ D(t-\tau) \ \dot{\sigma}_{11}(\tau) \ d\tau \qquad (2.1-11)$$

Where,

$$D(t) \equiv 1/3 \ J(t) + 1/9 \ B(t) \qquad (2.1-12)$$

$$\nu(t) \equiv \frac{3 \ J(t) - 2 \ B(t)}{6 \ J(t) + 2 \ B(t)} \qquad (2.1-13)$$

The pair of functions $D(t)$ and $\nu(t)$ also characterize the material and have the names

$D(t)$ - tensile creep compliance

$\nu(t)$ - "Poisson's Ratio" for creep[*]

---

[*] The definition chosen here leads to $\epsilon_y = -\nu \ \epsilon_x$ for the uniaxial creep test. This definition is not a unique generalization of the idea of Poisson's ratio for elastic materials.

Solving equations (2.1-12) and (2.1-13) we have

$$J = 2 (1 + \nu) D$$

$$B = 3 (1 - 2\nu) D \qquad\qquad (2.1-14)$$

Thus the bulk creep compliance and the shear creep compliance and, by (2.1-8), the relaxation moduli can all be calculated from the functions $\nu(t)$ and $D(t)$ occurring in the equations describing the tensile test.

The inverse of (2.1-10) is

$$\sigma_{11} = \int_0^t E(t-\tau)\,\dot{\epsilon}_{11}(\tau)\,d\tau \qquad\qquad (2.1-15)$$

The new functions is related to the tensile creep compliance by the **Volterra integral equation**

$$\int_0^t D(t-\tau)\,E(\tau)\,d\tau = t \qquad\qquad (2.1-16)$$

and has the name:

$E(t)$ — tensile relaxation modulus

The complete solution to a problem in linear viscoelasticity is determined by equations (2.1-1) — (2.1-3) and a pair of the stress-strain relations such as (2.1-4) and (2.1-5)

The solution must satisfy certain boundary conditions. Usually the displacement vector is given over part of the boundary while the stress vector F_k is given over the remainder. The stress vector is related to the stress tensors by

$$F_k = \sigma_{km}\,n_m \qquad\qquad (2.1-17)$$

where n_m are the components of the unit normal to the surface.

2.2. Elasticity:

The theory of linear elastic materials may be viewed as a special case in the theory of viscoelasticity when

$$J(t) = J_o \, h(t) \qquad (2.2-1)$$

and

$$B(t) = B_o \, h(t) \qquad (2.2-2)$$

where $h(t)$ is a unit step function

$$h(t) = \begin{cases} 0, & t < 0 \\ 1, & t \geq 0 \end{cases} \qquad (2.2-3)$$

Then

$$G = G_o \, h(t)$$
$$K = K_o \, h(t) \qquad (2.2-4)$$

and

$$D(t) = D_o \, h(t)$$
$$E(t) = E_o \, h(t) \qquad (2.2-5)$$

The elastic constants G_o, E_o, ν_o, and K_o are related:

$$G_o = \frac{E_o}{2\,(1+\nu_o)} \qquad (2.2-6)$$

$$K_o = \frac{E_o}{3\,(1-2\nu_o)} \qquad (2.2-7)$$

The field equations become

$$\partial_m \, \sigma_{km} + f_k = 0 \qquad (2.2-8)$$

$$\varepsilon_{km} = \tfrac{1}{2}\,(\partial_k \, u_m + \partial_m \, u_k) \qquad (2.2-9)$$

$$s_{km} = \sigma_{km} - 1/3\, \sigma_{rr}\, \delta_{km} \tag{2.2-10}$$

$$e_{km} = \varepsilon_{km} - 1/3\, \varepsilon_{rr}\, \delta_{km} \tag{2.2-11}$$

$$s_{km} = 2G_o\, e_{km} \tag{2.2-12}$$

$$1/3\, \sigma_{rr} = K_o\, \varepsilon_{rr} \tag{2.2-13}$$

Thus, time plays the role of a parameter and does not appear explicitly in the field equations.

2.3. Proportional Loading:

An important class of problems are those for which the stress vector on the surface has the form

$$F_k = \overline{F}_k\, (x^1, x^2, x^3)\, f(t) \tag{2.3-1}$$

This is termed proportional loading. Let us determine under what conditions the stress field has the form

$$\sigma_{km} = \overline{\sigma}_{km}\, (x)\, f(t) \tag{2.3-2}$$

where $\overline{\sigma}_{km}$ can be determined from the theory of elasticity.

The boundary conditions (2.1-17) give

$$\overline{\sigma}_{km}\, n_m = \overline{F}_k \tag{2.3-3}$$

In the absence of body force, the equilibrium equations (2.1-1) give

$$\partial_m \overline{\sigma}_{km} = 0 \tag{2.3-4}$$

The deviatoric stresses are

$$s_{km} = \overline{s}_{km}\, f(t) \tag{2.3-5}$$

where

$$\bar{s}_{km} = \bar{\sigma}_{km} - 1/3 \ \bar{\sigma}_{rr} \ \delta_{km} \tag{2.3-6}$$

The stress-strain relations (2.1-6) and (2.1-7) gives

$$2 \ e_{km} = 2 \ \bar{e}_{km} \ g(t) \tag{2.3-7}$$

$$\varepsilon_{rr} = \bar{\varepsilon}_{rr} \ k(t)$$

where

$$2 \ \bar{e}_{km} = 1/G_o \ \bar{s}_{km} \tag{2.3-8}$$

$$\bar{\varepsilon}_{rr} = 1/3K_o \ \bar{\sigma}_{rr} \tag{2.3-9}$$

$$g(t) = G_o \int_0^t J \ (t-\tau) \ \dot{f} \ (\tau) \ d\tau \tag{2.3-10}$$

$$k(t) = K_o \int_0^t B \ (t-\tau) \ \dot{f} \ (\tau) \ d\tau \tag{2.3-11}$$

The constants G_o and K_o are arbitrary constants.

Substituting equations (2.3-7) into the strain displacement equations (2.1-2), we see that the displacements can have the form

$$\bar{\varepsilon}_{km} = \tfrac{1}{2} \ (\partial_k \ \bar{u}_m + \partial_m \ \bar{u}_k) \tag{2.3-12}$$

$$u_k = \bar{u}_k \ (\underset{\sim}{x}) \ g(t) \tag{2.3-13}$$

only if $g(t) = k(t)$ or $\varepsilon_{rr} = 0$; that is, only when $B(t)$ is proportional to $J(t)$ by a constant factor.

From equations (2.1-14)

$$B(t) = 3/2 \ \frac{1-2 \ \nu(t)}{1 + \nu(t)} \ J(t) \tag{2.3-14}$$

Thus B(t) is proportional to J(t) only when ν is constant. Further, $\varepsilon_{rr} = 0$ only when ν is a constant equal to $\frac{1}{2}$.

If ν is constant, then the stress and displacement are determined by (2.3-2) and (2.3-13) where the barred quantities satisfy the equations (2.3-3), (2.3-4), (2.3-8), (2.3-9), (2.3-19), i.e. the equations of elasticity, provided the boundary conditions of the viscoelastic problem agrees with (2.3-1), and (2.3-13).

In fact, ν is never constant for any material. But it frequently happens that the variation in ν with time is slight or the effect of changes in ν on the solution to the elasticity problem is slight. In these cases the stress field under proportional loading can be approximated by the elasticity solution.

2.4. Plane Stress:

If the displacements u^1, u^2 are independent of x^3 and $\sigma_{33} = 0$, the equations of section 2.1 can be simplified to the following

$$\partial_3 \sigma_{\alpha 3} = 0 \tag{2.4-1}$$

$$\varepsilon_{\alpha\beta} = \tfrac{1}{2} (\partial_\alpha u_\beta + \partial_\beta u_\alpha) \tag{2.4-2}$$

$$s_{\alpha\beta} = \sigma_{\alpha\beta} - 1/3 \; \sigma_{rr} \delta_{\alpha\beta} \tag{2.4-3}$$

$$e_{\alpha\beta} = \varepsilon_{\alpha\beta} - 1/3 \; \varepsilon_{rr} \delta_{\alpha\beta} \tag{2.4-4}$$

$$2e_{\alpha\beta} = \int_{t_0}^{t} J(t-\tau) \dot{s}_{\alpha\beta}(\tau) \, d\tau \tag{2.4-5}$$

$$\varepsilon_{rr} = \int_{0} 1/3 \; B(t-\tau) \, \dot{\sigma}_{\alpha\alpha}(\tau) \, d\tau \tag{2.4-6}$$

The Greek indices have the range 1, 2 and all quantities are functions of x^α and t.

The equations (2.4-1) - (2.4-6) define a plane stress problem. There is an important class of plane stress problems for which the solution is independent of the material properties which we now consider. In this case, the stress can be calculated from the corresponding elasticity solution.

Equations (2.4-1) are satisfied by the Airy stress function F

$$\sigma_{\alpha\beta} = \varepsilon_{\alpha\gamma} \varepsilon_{\beta\delta} \partial_\gamma \partial_\delta F \qquad (2.4\text{-}7)$$

Where $\varepsilon_{\alpha\beta}$ is the permutation symbol.

Eliminating the displacements from (2.4-2) gives

$$\varepsilon_{\alpha\delta} \varepsilon_{\beta\tau} \partial_\tau \partial_\delta \varepsilon_{\alpha\beta} = 0 \qquad (2.4\text{-}8)$$

These are the compatibility relations.

Substituting (2.4-7) into (2.4-3) - (2.4-6) and the result into (2.4-8) leads to

$$\nabla^4 F = \partial_\alpha \partial_\alpha \partial_\beta \partial_\beta F = 0 \qquad (2.4\text{-}9)$$

If the boundary conditions are solely on stress, the equations (2.4-9) and the stress boundary conditions completely determine the stress independent of the material properties and the stress is the same as for an elastic material.

2.5. <u>Short Time Solution</u>:

We consider now a suddenly applied load and determine the solution immediately after loading (that is, immediately after all wave propagation effects are completed).

The stress and strain fields are related by (2.1-4) and (2.1-5). For a step change at time zero,

$$s_{km} = 2G(o) \ e_{km} \tag{2.5-1}$$

$$1/3 \ \sigma_{rr} = K(o) \ \varepsilon_{rr} \tag{2.5-2}$$

Further, from (2.1)

$$G(o) \ J(o) = 1 \tag{2.5-3a}$$

$$K(o) \ B(o) = 1 \tag{2.5-3b}$$

The **constitutive relations are** identical to the elasticity equations with elastic moduli equal to the values of the relaxation modulus at time zero. Therefore the stress distribution at the instant of loading will be the same as given by the elasticity solution for shear modulus. $G = G(o)$ and bulk modulus $K = K(o)$ or Poisson ratio $\nu = \nu(o)$

2.6. <u>Long Time Solution</u>:

The viscoelastic materials usually encountered have a fading memory. That is, the stress due to a step change in strain decreases in time. The result is that when loads are maintained at a constant value, an equilibrium state is reached such that no further change in stress or strain occurs.

By (2.1-4) and (2.1-5)

$$s_{km}(\infty) = \int_0^\infty G(\infty) \, \dot{e}_{km}(\tau) \, d\tau$$
$$= G(\infty) \, e_{km}(\infty)$$

(2.6-1)

$$1/3 \, \sigma_{rr}(\infty) = K(\infty) \, \varepsilon_{rr}(\infty)$$

(2.6-2)

The constitutive equations coincide with linear elasticity with moduli equal to the values of the relaxation functions at time infinity. Consequently, if the surface loads remain constant, the stress state will eventually approach that of the elasticity solution for shear modulus $G = G(\infty)$ and Poisson ratio $\nu = \nu(\infty)$.

2.7. Wave Propagation:

We consider here a propagating discontinuity in acceleration. Such discontinuities are always accompanied by discontinuities in gradient of strain. They propagate at speeds characteristic of the material. The speed of propagation of such disturbances is often found to coincide with the speed of propagation of infinitesimal harmonic fields where such problems can be solved. Thus we may suppose the speed of propagation of discontinuities will be the same as the speed of propagation of a disturbance introduced by small impact on the end of a rod.

Consider a surface across which some function f is discontinuous. Let [f] denote the difference of the values of f on each side of the surface at any instant.

Now consider the uniaxial stress field. The balance of linear momentum gives

$$\left[\frac{\partial \sigma_{11}}{\partial x^1} \right] \quad \cdot \quad \circ \left[\frac{\partial^2 u_1}{\partial t^2} \right] \tag{2.7-1}$$

Let

$$s = \left[\frac{\partial^2 u_1}{\partial x^1 \partial x^1} \right] \tag{2.7-2}$$

Then from the kinematics of singular surface, the jump in acceleration is

$$\left[\frac{\partial^2 u_1}{\partial t^2} \right] = U^2 s \tag{2.7-3}$$

where U **is the speed of propagation** of the surface. Thus

$$\left[\frac{\partial \sigma_{11}}{\partial x^1} \right] = \rho U^2 s \tag{2.7-4}$$

From the constitutive relation for uniaxial stress; equations (2.1-15),

$$\sigma_{11} = E(o)\,\epsilon_{11}(t) + \int_0^t \dot{E}(t-\tau)\,\epsilon_{11}(\tau)\,d\tau \tag{2.7-5}$$

Differentiating

$$\frac{\partial \sigma_{11}}{\partial x} = E(o)\,\frac{\partial^2 u_1}{\partial x^1 \partial x^1} + \int_0^t \dot{E}(t-\tau)\,\frac{\partial \sigma_{11}}{\partial x^1}(\tau)\,d\tau \tag{2.7-6}$$

This relation applies on each side of the wave. Thus,

$$\left[\frac{\partial \sigma_{11}}{\partial x^1} \right] = E(o)s \tag{2.7-7}$$

The second term in (2.7-6) is the same on both sides of the wave since the change in the integrand at a discrete point does not change the value of the integral.

From (2.7-7) and (2.7-4)

$$U^2 = \frac{E(o)}{\rho} \tag{2.7-8}$$

That is, the speed of propagation is determined by the value of the tensile relaxation modulus at time zero.

2.8. Temperature Effects:

Each of the material property functions is temperature dependent. That is, if the tensile test is conducted at different temperatures, the tensile creep compliance is a different function of time. In many instances this temperature dependence can be described by an empirical relation involving the so-called "time-temperature equivalence". The material is then termed thermo-rheologically simple.

Let $G(t)$ be the relaxation modulus at constant temperature T and $\overline{G}(t)$ be the relaxation modulus at some reference temperature T_o, see Fig. (2.1) Suppose that the effect of temperature on the short time modulus and long time modulus is such that:

$$G(o) = \overline{G}(o) \tag{2.8-1}$$

$$G(\infty) = \overline{G}(\infty) \tag{2.8-2}$$

In this case, there always exists a pair of times for which G and $\overline{G}$ have the same value

$$G(t) = \overline{G}(\xi) \qquad (2.8-3)$$

The time ξ is called the reduced time. It depends on the temperature T of the test and the time t at which the ordinate G is measured. Empirical evidence suggest that for many materials

$$\xi = a(T)t. \qquad (2.8-4)$$

The function a(T) of temperature is known as a temperature shift factor (in the sense of shifting the curves if Fig. (2.1) were plotted on log time).

Similar results are thought to describe the isothermal values of the other material property functions.

Isothermal experiments cannot determine the nature of the stress-strain relationship for tests in which the temperature varies with time and no experimental evidence is available. A possible generalization which is compatible with the isothermal observations was proposed by Morland and Lee[2]. Their idea is that rate of change of the modulus is determined by the instantaneous temperature.

If G (t) is the relaxation modulus measured at varying temperature T(t), then (2.8-3) holds. Thus

$$\frac{dG}{dt} = \frac{d\overline{G}}{d\tau} \frac{d\xi}{dt} \qquad (2.8-5)$$

The fundamental hypothesis is

$$\frac{d\xi}{dt} = a(T) \qquad (2.8-6)$$

This agrees with (2.8-4) in the isothermal case. If temperature is a function of time for a given particle,

$$\xi(t) = \int_0^t a\, (T(t))\, dt \tag{2.8-7}$$

This generalizes (2.8-4) to the case of varying temperature.

Now suppose the same temperature variation occurs but the strain is applied at time τ. Let $E_\tau(t)$ be the resulting relaxation modulus. Again assuming that the initial and final values are independent of temperatures, there exists a function $\xi_\tau(t)$ such that

$$F_\tau(t) = \overline{G}\,(\xi_\tau) \tag{2.8-8}$$

and

$$\frac{dF_T}{dt} = \frac{d\overline{G}}{d\xi_\tau} \cdot \frac{d\xi_T}{dt}.$$

The fundamental hypothesis is

$$\frac{d\xi_T}{dt} = a(T) \tag{2.8-9}$$

Since

$$F_\tau\,(\tau) = \overline{G}\,(o) \tag{2.8-10}$$

we must have

$$\xi_\tau\,(\tau) = o \tag{2.8-11}$$

Thus,

$$\xi_\tau = \int_0^t a\,(T\,(t))\, dt$$

$$\xi_T = \int_0^t a(T(t))\, dt - \int_0^\tau a(T(t))\, dt$$

$$= \xi(t) - \xi(\tau) \qquad\qquad (2.8\text{-}12)$$

The stress due to continuously changing strain is then

$$s_{ij} = \int_0^t 2\, \overline{G}\left(\xi(t) - \xi(\tau)\right)\, \dot{e}_{ij}(\tau)\, d\tau \qquad\qquad (2.8\text{-}13)$$

3. <u>Birefringence</u>.

3.1. <u>Ideal Dielectric</u>:

In this section, we review a theory of birefringence based upon the description of light as an electromagnetic wave propagating in an anisotropic dielectric. Our experiments are purposely limited to quasi-static deformations. Thus, during the time of passage of an electromagnetic wave, the displacements of the material are negligible. The equations of a dielectric at rest can therefore be used. Furthermore, since we intend to observe only relative intensity of light transmitted, the absorption and dispersion will be neglected. The equations of an anisotropic dielectric then have the following form:

$$\text{curl } \underset{\sim}{H} - \frac{\partial D}{dt} = 0 \qquad\qquad (3.1\text{-}1)$$

$$\text{curl } \underset{\sim}{E} + \frac{\partial B}{\partial t} = 0 \qquad\qquad (3.1\text{-}2)$$

$$D_i = \varepsilon_o K_{ij} E_j \qquad\qquad (3.1\text{-}3)$$

$$\underset{\sim}{H} = \frac{1}{u_o} \underset{\sim}{B} \qquad\qquad (3.1\text{-}4)$$

Here, $\underset{\sim}{E}$ is the electric field; $\underset{\sim}{B}$ is the density of magnetic flux; $\underset{\sim}{H}$ is the potential of free current; $\underset{\sim}{D}$ is the potential of free charge. ε_o and u_o are fundamental properties of the material in which the propagation occurs. K_{ij} will be termed the dielectric tensor. The fields $\underset{\sim}{D}$ and $\underset{\sim}{B}$ are also subject to the relations

$$\text{div } \underset{\sim}{B} = 0 \qquad\qquad (3.1\text{-}5)$$

$$\text{div } \underset{\sim}{D} = 0$$

However, these relations are not independent of (3.1-1) and (3.1-2)

3.2. Plane Wave:

We will consider only the case when the direction of propagation coincides with one of the principal axes of the dielectric tensor.

Let us choose the coordinate axes parallel to the principal axes of the dielectric tensor K_{ij} and take $x^3 = z$ to be the direction of propagation of the wave. A plane wave can then be represented by the real or imaginary part of the terms:

$$E = a\, e^{i\varphi} \qquad (3.2\text{-}1)$$

$$B = b\, e^{i\varphi} \qquad (3.2\text{-}2)$$

$$D = d\, e^{i\varphi} \qquad (3.2\text{-}3)$$

$$H = h\, e^{i\varphi} \qquad (3.2\text{-}4)$$

$$\varphi = kz - \omega t \qquad (3.2\text{-}5)$$

where k is the wave number; ω is the angular frequency; a, b, d, and h are constant complex vectors.

The field equations (3.1-1) - (3.1-4) imply (see reference 7) that only two such plane waves are possible. In each case the direction of d and a coincide with one of the remaining principal axes, and b and h coincide with the other. The index of refraction defined by

$$N = \frac{kc}{\omega} \qquad (3.2\text{-}6)$$

has the value

$$N = \sqrt{K} \qquad (3.2\text{-}7)$$

where K is the principal value of the dielectric tensor associated with the axis along $\underline{a}$. The field equations (3.1-5) are satisfied trivially.

3.3. Dielectric Slab:

We consider a slab of dielectric of thickness h bounded by planes which are surfaces of constant values of z, and the z-axis is a principal axis of K. Choose the remaining coordinate axes along the principal axes of K.

If a plane transverse wave is incident on one surface then part of the wave is transmitted and part is reflected. A similar transmission and reflection occurs at the second surface. Thus, there are five electromagnetic waves as shown in Fig. 3.1 .

If the incident wave is such that the electric field coincides with one of the principal axis K, then the electric field of each wave has that same direction. The incident field

$$\underline{E}_1 = \underline{a}_1 \, e^{i\varphi} \tag{3.3-1}$$

and the transmitted field

$$\underline{E}_5 = \underline{a}_5 \, e^{i\varphi} \tag{3.3-2}$$

are parallel and (see reference 7)

$$\underline{a}_5 = C \, \underline{a}_1 \tag{3.3-3}$$

where

$$C = \frac{4 N e^{-i \, k_o h}}{(1+N)^2 \, e^{-ikh} - (1-N)^2 \, e^{-ikh}} \tag{3.3-4}$$

where k is the wave number given by (3.2-11) and (3.2-12) corresponding to the principal axis along $\underline{E}$.

3.4. Plane Polariscope:

A monochromatic transverse wave is obtained by passing mono-chormatic light through a polarizer. This wave is incident on the dielectric slab. The coordinating axes are principal axes of K_{ij} and the wave propagates along the z axis. The incident waves can be represented as the sum of two waves, each parallel to one of the remaining principal axes. The formula (3.3-3) applies to each wave. The transmitted wave is then passed through a second polaroid.

The transmitted wave is given by

$$E = A (C_1 \cos \alpha \cos \beta + C_2 \sin \alpha \sin \beta) e^{i(k_o z - \omega t)} \qquad (3.4-1)$$

where A is the amplitude of the incident wave; α is the angle between the x_1-axis and the axis of the polarizer; β is the angle between the x_2-axis and the axis of the analyzer; $k_o = \omega/c$; and the constants C_1 and C_2 are given by the formulas (3.3-4) with $k = k_1$ or $k = k_2$ respectively (see reference 7).

Equation (3.4-1) can be put in the form

$$F = AK_1 \cos \alpha \cos \beta \, e^{i \, (k_o z - \omega t - k_o h t_1)}$$
$$+ AK_2 \sin \alpha \sin \beta \, e^{i \, (k_o z - \omega t - k_o h t_2)} \qquad (3.4-2)$$

where

$$K_n = \frac{2 N_n}{\sqrt{4N_n^2 \cos^2 k_n h + (1+N_n^2)^2 \sin^2 k_n h}} \qquad (3.4-3)$$

$$\tan \theta_n = \frac{1 + N_n^2}{2N_n} \quad \tan k_n h \qquad (3.4-4)$$

Either the real or imaginary part of E is the amplitude of light transmitted. The imaginary part is

$$I = Q \sin (k_o z - \omega t - k_o h + \chi) \qquad (3.4-5)$$

where

$$Q \cos \chi = A K_1 \cos \alpha \cos \beta \cos \theta_1$$
$$+ A K_2 \sin \alpha \sin \beta \cos \theta_2 \qquad (3.4-6)$$

and

$$Q \sin \chi = A K_1 \cos \alpha \cos \beta \sin \theta_1$$
$$+ A K_2 \sin \alpha \sin \beta \sin \theta_2 \qquad (3.4-7)$$

For the case $\beta = \alpha + \pi/2$, i.e. the polarizer and analyzer are crossed. Then

$$4 Q^2 = A^2 \sin^2 2\alpha (K_1^2 + K_2^2 - 2K_1 K_2 \cos 2m\pi) \qquad (3.4-8)$$

$$n = \frac{\theta_2 - \theta_1}{2\pi} \qquad (3.4-9)$$

For the case $\beta = \alpha$, i.e. the polarizer and analyzer are parallel,

$$Q^2 = A^2 (K_1^2 \cos^4\alpha + K_2^2 \sin^4 \alpha + 2 K_1 K_2 \cos^2 \alpha \sin^2\alpha \cos 2m\pi) \qquad (3.4-10)$$

For the materials used in photoanalysis, N_1 is equal to N_2 in the natural state where they have a value of about 1... In the deformed state, N_1 and N_2 change by terms of about 10^{-5}. In such cases, the minimum values of equation (3.4-8) occur at nearly integer values of n and

$$n \doteq \frac{h\omega}{2\pi c} (N_2 - N_1) \qquad (3.4\text{-}11)$$

The minimum values of equation (3.4-10) occur approximately where n is an odd-multiple of $\frac{1}{2}$. The locus of all such points form lines on the model which are called isochromatic lines.

From equation (3.4-8), there will be zero light intensity at those points for which the principal axis of the dielectric tensor **coincide with the axis of the polarizer-analyzer**. The locus of all such points form lines on the model which are called isoclinic lines.

The variable n is called the fringe order and the difference in principal indices of refraction is termed the birefringence

$$\Delta = N_1 - N_2 \qquad (3.4\text{-}12)$$

4. <u>Rheo-optical Effect</u>.

4.1. <u>General Law</u>:

The optical character of the material is determined by the dielectric tensor K_{ij} and therefore by any other tensor from which the dielectric tensor can be calculated.

The tensor which has the same principal axes as $\underset{\sim}{K}$ and which has the principal values equal to the principal waves speeds is given by

$$V_{ij} = c \; \overline{K_{ij}}^{-\frac{1}{2}} \tag{4.1-1}$$

where c is the velocity of light in free space. This tensor completely determines $\underset{\sim}{K}$ and is used by Read.[4]

The tensor K_{ij}^{-1} plays a direct role in the solution of the electromagnetic field equations. It was used by Mindlin.[3]

The tensor which has the same principal axes as K_{ij} and which has principal values equal to the principal indices of refraction is given by

$$N_{ij} = K_{ij}^{\frac{1}{2}} \tag{4.1-2}$$

Let us call N_{ij} the refraction tensor. The principal axes of N_{ij} are determined by the isoclinic and the difference in principal values of N_{ij} is determined by the isochromatic fringe order as shown in Section 3.

Since the tensor N_{ij} is most directly related to the experimental observations, it will be used to formulate the mechanical-optical law.

If a high polymer is maintained at constant strain, the fringe order is observed to decrease. The material is said to experience.

optical relaxation at constant strain. The behavior is similar to the stress relaxation observed at constant strain. Thus, we hypothesize that the refraction tensor depends upon the history of deformation with a fading memory.

We will consider in this report only small displacements. The fading memory functional may be approximated in the case of small displacement gradients. In the case of anisotropic material, the relation becomes

$$N_{ij}(t) = N_o \delta_{ij} + \delta_{ij} \int_0^t A(t-\tau) \dot{e}_{kk}(\tau) d\tau \qquad (4.1-3)$$

$$+ 2 \int_0^t B(t-\tau) \dot{e}_{ij}(\tau) d\tau$$

Let

$$R_{ij} = N_{ij} - 1/3 N_{kk} \delta_{ij} \qquad (4.1-4)$$

denote the deviatoric part of N_{ij}. Then

$$R_{ij} = \int_0^t 2 B(t-\tau) \dot{e}_{ij}(\tau) d\tau \qquad (4.1-5)$$

where e_{ij} is again the deviatoric part of the strain tensor. The function $B(t)$ gives the birefringence at constant strain. It may, therefore, be termed the optical relaxation modulus.

The inverse relation of (4.1-5) is

$$2 e_{km} = \int_0^t C(t-\tau) \dot{R}_{km}(\tau) d\tau \qquad (4.1-6)$$

The functions $C(t)$ and $B(t)$ are related by a volterra integral equation of the type (2.1-8).

Combining the stress-strain relation (2.1-6) with (4.1-5) gives

$$R_{ij} = \int_0^t \psi(t-\tau) \dot{s}_{km}(\tau) d\tau \qquad (4.1-7)$$

The functions $B(t)$ and $\psi(t)$ are related by

$$\psi = \int_0^t B(t-\tau)\ \dot{J}(\tau)\ d\tau \qquad (4.1-8)$$

The function $\psi(t)$ gives the fringe order at constant stress. It, therefore, characterizes the optical creep at constant load.

The inverse of (4.1-7) is

$$s_{km} = \int_0^t \Phi(t-\tau)\ \dot{R}_{km}(\tau)\ d\tau \qquad (4.1-9)$$

The functions $\xi(t)$ and $\psi(t)$ are related by a Volterra integral equation of the type (2.1-8).

4.2. Stress and Strain Birefringence:

Consider the possibility

$$B(t) = B_o\ h(t) \qquad (4.2-1)$$

where $h(t)$ is the unit step function. Then, equation (4.1-5) becomes

$$R_{ij} = 2\ B_o\ e_{ij}$$
$$\xi(t) = \frac{1}{B_o}\ G(t) \qquad (4.2-2)$$
$$\psi(t) = B_o\ J(t)$$

In this case, the birefringence is proportional to the difference in principal strains and the isoclinic angle coincides with the principal axis of strain. A material characterized by equations (4.2-2) may be termed strain birefringent.

Consider the possibility

$$\psi(t) = \psi_o \, h(t) \tag{4.2-3}$$

Then, equation (4.1-7) becomes

$$R_{ij} = \psi_o \, s_{ij}$$

$$C(t) = \frac{1}{\psi_o} \, J(t) \tag{4.2-4}$$

$$B(t) = \psi_o \, G(t)$$

In this case, the birefringence is proportional to the difference in principal stresses and the isoclinic angle coincides with the principal axes of stress. A material characterized by equations (4.2-4) may be termed stress-birefringent.

Consider an elastic material which is stress-birefringent. Substituting equation (2.2-12) into equations (4.2-4) leads to an equation of the form (4.2-2). Thus, a stress-birefringent elastic material is also strain-birefringent. Similarly, a strain-birefringent elastic material is stress-birefringent.

Consider the possibility

$$\psi(t) = \alpha \, h(t) + \tfrac{1}{2}\beta \, J(t) \tag{4.2-5}$$

Then, equation (4.1-7) and (2.1-6) lead to

$$R_{ij} = \alpha \, s_{ij} + \beta \, e_{ij} \tag{4.2-6}$$

This relation is often in fair agreement with the experimental data.

The list of such special cases of the representation of Section 4.1 is endless. Such equations as (4.2-2), (4.2-4), and (4.2-6) are certainly not universal but may describe some special materials accurately enough for some applications. Such representations as (4.2-6) may be useful in qualitative reasoning, i.e. to exercises of "physical intuition".

4.3. Slow or Rapid Motions:

The constitutive relations (4.1-5) are of the same form as (2.1-4) and the function $B(t)$ is generally found to be of the same character as $G(t)$. Thus, the same approximation theorems hold for both relations.

For a step change in strain, the instantaneous value of the **refraction tensor is given by**

$$R_{ij} = 2\ B(o)\ e_{ij} \qquad\qquad (4.3\text{-}1)$$

Thus every material with fading memory is strain-birefringent for sufficiently rapid strain. As shown in Section 2.6, such a material is also elastic in this time region, it is therefore also stress-birefringent for rapid deformation.

If the strains are maintained constant, the refraction tensor approach the value given by

$$R_{ij} = 2\ B(\infty)\ e_{ij} \qquad\qquad (4.3\text{-}2)$$

Thus every material with fading memory is strain-birefringent for

sufficiently slow deformation. As shown in Section 2.6, such a material
is also elastic, it is therefore also stress-birefringent for slow
deformations.

4.4. Temperature Dependence:

Each of the material property functions is temperature dependent.
If the tensile test is conducted at different temperatures, the optical
creep compliance ψ is a different function of time. From the similarity
of the mechanical and optical behavior, we may expect that certain
materials will have an optical behavior which is thermo-rheologically
simple.

Let the reduced time be defined by

$$\xi(\tau) = \int_0^\tau b(T(\tau)) \, d\tau \qquad (4.4-1)$$

The function $b(T)$ of temperature may be termed the optical shift factor.
We then define an optically thermo-rheologically simple material by
the constitutive relation

$$R_{ij} = \int_0^t 2 \, \overline{B} \, (\xi(t) - \xi(\tau)) \, \dot{e}_{ij} \, (\tau) \, d\tau \qquad (4.4-2)$$

where $B(t)$ is the optical relaxation modulus for an isothermal test
at reference temperature $\overline{T}$. This generalizes equation (4.1-5).

It may happen that the mechanical and optical shift factors are
the same. However, this must be determined experimentally.

II. Experiments

5. Summary:

The material from which the model is manufactured must have
the same mechanical characteristics as the prototype. Therefore,
one must be able to prepare a polymer of pre-determined relaxation
modulus. Our procedure is to mix liquid epoxy resins with plastizer
and hardener, and then cast a sheet of material. The model is then
cut from the sheet. By varying the proportions of the ingredients,
the relaxation times can be changed over a wide range. This procedure
is described in Appendix A.2.

The optical properties of the model material are determined from
the tensile creep test. This gives the fringe order at constant
stress $\sharp$. The stress at constant fringe order η is then calculated
by solving an integral equation (Appendix A.1.).

We consider here only plane stress problems. A model is then
loaded and heated and the temperature, fringe order, and isoclinic
angle are recorded at each point as a function of time. By using
equation (4.1-9) and the previously determined function η, the difference
in principal stresses and the orientation of principal stresses can
be determined.

6. Basic Formulae for Plane Stress:

Our experiments all deal with plane stress problems (Section 2.4). The only non-zero stress components are σ_x, σ_y, τ_{xy}.

The principal stresses in the plane are the stress components related to the axes making an angle θ with the x-y axes:

$$\tan \theta = \frac{2 \tau_{xy}}{\sigma_x - \sigma_y} = \frac{2 s_{xy}}{s_x - s_y} \tag{6.0-1}$$

The principal stresses are given by

$$\sigma_1 = \sigma_x \cos^2 \theta + \sigma_y \sin^2 \theta + 2 \tau_{xy} \sin \theta \cos \theta$$

$$\sigma_2 = \sigma_x \sin^2 \theta + \sigma_y \cos^2 \theta - 2 \tau_{xy} \sin \theta \cos \theta \tag{6.0-2}$$

or

$$\sigma_1 - \sigma_2 = (\sigma_x - \sigma_y) \cos 2\theta + 2 \tau_{xy} \sin 2\theta$$

$$= (s_x - s_y) \cos 2\theta + 2 s_{xy} \sin 2\theta \tag{6.0-3}$$

Thus, the deviatoric stress components

$$s_x = \sigma_x - 1/3 (\sigma_x + \sigma_y)$$

$$s_y = \sigma_y - 1/3 (\sigma_x + \sigma_y) \tag{6.0-4}$$

$$s_{xy} = \tau_{xy}$$

completely determine the angle θ and the difference $(\sigma_1 - \sigma_2)$ of the principal stresses in the plane.

Solving (6.0-1) and (6.0-2),

$$\sigma_x = \sigma_1 \cos^2 \theta + \sigma_2 \sin^2 \theta$$

$$\sigma_y = \sigma_1 \sin^2 \theta + \sigma_2 \cos^2 \theta \qquad (6.0\text{-}5)$$

$$\tau_{xy} = (\sigma_1 - \sigma_2) \sin \theta \cos \theta$$

Thus

$$s_x - s_y = \sigma_x - \sigma_y = (\sigma_1 - \sigma_2) \cos 2\theta$$

$$(6.0\text{-}6)$$

$$s_{xy} = \tau_{xy} = \tfrac{1}{2}(\sigma_1 - \sigma_2) \sin 2\theta$$

Similar results hold for the refraction tensor when the z-axis is

a principal axis:

$$R_x - R_y = N_x - N_y = (N_1 - N_2) \cos 2\varphi = \Delta \cos 2\varphi$$

$$(6.0\text{-}7)$$

$$R_{xy} = N_{xy} = \tfrac{1}{2} (N_1 - N_2) \sin 2\varphi = \tfrac{1}{2} \Delta \sin 2\varphi$$

The relation (4.1-7) leads to

$$\Delta \cos 2\varphi = \int_o^t \psi (t-\tau) \frac{d}{d\tau} [(\sigma_1 (\tau) - \sigma_2 (\tau)) \cos 2\theta (\tau)] \, d\tau$$

$$(6.0\text{-}8)$$

$$\Delta \sin 2\varphi = \int_o^t \psi (t-\tau) \frac{d}{d\tau} [(\sigma_1 (\tau) - \sigma_2 (\tau)) \sin 2\theta (\tau)] \, d\tau$$

The relation (4.1-9) leads to

$$(\sigma_1 - \sigma_2) \cos 2\theta = \int_o^t \phi (t-\tau) \frac{d}{d\tau} [\Delta (\tau) \cos 2\varphi (\tau)] \, d\tau$$

$$(6.0\text{-}9)$$

$$(\sigma_1 - \sigma_2) \sin 2\theta = \int_o^t \phi (t-\tau) \frac{d}{d\tau} [\Delta (\tau) \sin 2\varphi (\tau)] \, d\tau$$

7. <u>Material Calibration</u>:

The mechanical and optical properties of the material were determined by the tensile creep test. A constant uniaxial stress was applied and the strain and birefringence were recorded as described in Appendix A.2. The test was repeated for several stress levels at each of several temperatures. The thermal properties of the material were determined as described in Appendix A.4. The mechanical and thermal properties are not used in the experimental stress analysis; they merely serve to identify the material tested. Only the optical creep function is needed to interpret the observed fringe pattern.

For the tensile creep test, the principal axis of stress, strain, **and refraction coincide. Equation** (6.0-8) **leads to**

$$\Psi(t) = \frac{\Delta(t)}{\sigma} \tag{7.0-1}$$

where, by (3.4-11),

$$\Delta(t) = \frac{2\pi c}{h} n(t) \tag{7.0-2}$$

From (2.1-10)

$$D(t) = \frac{\varepsilon_x(t)}{\sigma} \tag{7.0-3}$$

From (2.1-11),

$$\nu(t) = - \frac{\varepsilon_y(t)}{\varepsilon_x(t)} \tag{7.0-4}$$

Then $J(t)$ and $B(t)$ can be calculated from (2.1-14):

$$J = 2(1+\nu) D$$
$$B = 3(1-2\nu) D \tag{7.0-5}$$

The constant stress σ is applied and the intensity of light transmitted is measured by a photocell. The successive peaks on the intensity curve correspond to integer values of the fringe order n. By observing the time of occurrence the optical creep function $\psi(t)$ can be determined from (7.0-1) and (7.0-2). A graph of ψ determined at room temperature for mix A is shown in Fig. 7.1. The results of tests at various temperatures are shown in Fig. 7.2. for mix B. These two mixes were of the same proportions of raw material but show a slight difference in their mechanical and optical properties.

The longitudinal and lateral strains were also measured at room temperature for mix A. The tensile creep compliance $D(t)$ computed by (7.0-3) as shown in Fig. 7.3, and the transverse contraction ratio $\nu(t)$ is shown in **Fig. 7.4.** Because of the small change in thickness the lateral strains are difficult to measure, and the large band of experimental data in Fig. 7.4 is due to this experimental error rather than any real variation of material properties. The shear creep compliance $J(t)$ and bulk creep compliance $B(t)$ calculated from (7.0-5) are shown in Fig. 7.5 and 7.6. In the tests at higher temperatures of mix B, only the longitudinal strain was measured. The tensile creep compliance is shown in Fig. 7.7.

If the dependence of the final data on temperature is neglected in Fig. 7.2, then the temperature dependence of the optical creep function over this small change of temperature can be reasonably well described by a temperature shift factor as defined by (4.4-1) and (4.4-2). The optical and mechanical shift factors are shown in Fig. 7.8.

The optical creep function is also reasonably well described by the empirical relation (4.2-5), and (4.2-6) with $\alpha = 0.15 \times 10^{-5}$ in/lb^2 and $\beta = 0.3 \times 10^{-2}$. The resulting representation is shown in Fig. 7.9.

The speed of propagation of a wave in a rod was measured as described in Appendix A.5. The value of the relaxation modulus at time zero is then calculated from (2.7-8). Since

$$D(o) = \frac{1}{E(o)} \qquad (7.0\text{-}6)$$

the initial value of D (t) is then known.

In order to analyze the photoviscoelastic data it is necessary to calculate the inverse of the optical creep function ψ (t) related to ϕ (t) by

$$\int_{o}^{t} \phi(t) \, \psi(t-\tau) \, d\tau = t \qquad (7.0\text{-}7)$$

This equation is solved by a numerical technique in conjunction with the digital computer as described in Appendix A.1. The results are shown in Fig. 7.10 for one case.

8. Test I.

A sheet was bonded to metal blocks along opposite edges as shown in Fig. 8.1. The blocks are essentially rigid compared to the polymer. By loading the blocks a state of nearly plane stress is obtained in the sheet. If the load on the block is constant, the problem is one of proportional loading as described in Section 2.3. If the time variation of Fig. 7.4, can be neglected, then the stresses will be constant. Experience with elasticity problems leads us to think that variation of ν should not have a strong effect. Therefore, we choose this configuration for some preliminary tests.

In the first test, the model was "sheared" by constant loads P_1. As shown in Section 2.3, if the variation in ν is neglected, the stress will be constant and be the same as if the material were elastic. The stress state in an elastic material was determined by standard photoelastic means. It was found that the shear stress varied along the centerline as shown in Fig. 8.2. By symmetry, the point in the center of the specimen experiences a pure shear stress, i.e. $\sigma_x = \sigma_y = 0$. Thus, we expect constant loads P_1 to give a constant state of stress

$$\sigma_x = 0$$
$$\sigma_y = 0 \qquad\qquad (8.0\text{-}1)$$
$$\tau_{xy} = \tau$$

at the center. The particle at the center experiences a creep test.

By the formula of Section 6.

$$n(t) = \frac{h\omega}{2\pi c} \; \Delta(t) = \frac{h\omega}{2\pi c} \; 2\tau \; \psi(t) \tag{8.0-2}$$

The experimental results are shown in Fig. 8.3. They agree with the expected value. The small deviation may be due to non-linear behavior caused by the rather large stress applied.

We then decided to demonstrate the fact that the isoclinic angle does not coincide with the principal axes of stress. By first applying a load P_2 and then, at a later time t_o, applying the load P_1, the principal axes of stress can be made to rotate. The isoclinic angle can be simultaneously measured.

The weight of the frame alone caused some shear stress to which we may regard as having reached an equilibrium state. By (4.3-2), (2.6-1) and the formula of Section 4.1,

$$N_{xy} = \psi(\infty) \; \tau_o$$
$$\tag{8.0-3}$$
$$N_x - N_y = 0$$

The loads P_2 result in a state of stress at the center with $\tau_{xy} = 0$. We assumed that the stress σ_y was negligible and σ_x was approximately equal to the average stress:

$$\sigma_x = \sigma, \qquad t > 0$$
$$\sigma_y = 0 \tag{8.0-4}$$
$$\tau_{xy} = 0$$

where the x_1 direction has been designated as x and the x_2 direction as y.

The values of the refraction tensor are

$$N_{xy} = 0$$

$$N_x - N_y = \psi(t)\,\sigma \qquad (8.0\text{-}5)$$

The **shear load** P_1 applied at time t_o results in stresses:

$$\tau_{xy} = \tau \qquad\qquad t > t_o$$

$$\sigma_x = 0 \qquad\qquad (8.0\text{-}6)$$

$$\sigma_y = 0$$

The values of the refraction tensor are

$$N_{xy} = \psi\,(t-t_o)\,\tau$$

$$N_x - N_y = 0 \qquad (8.0\text{-}7)$$

Since the problem is linear, the response to the three stress states can be superimposed. The combined values of the refraction tensor for $t > t_o$ are determined by adding (8.0-3), (8.0-5), and (8.0-7):

$$N_{xy} = \psi(\infty)\,\tau_o + \psi\,(t-t_o)\,\tau$$

$$(8.0\text{-}8)$$

$$N_x - N_y = \psi\,(t)\,\sigma$$

The isoclinic angle is given by

$$\tan 2\rho = \frac{2N_{xy}}{N_x - N_y} \qquad (8.0\text{-}9)$$

Thus,

$$\tan 2\, \varphi \;=\; \frac{\psi(\infty)}{\psi(t)} \;\; \frac{2\tau_o}{\sigma} \;+\; \frac{\psi(t-t_o)}{\psi(t)} \;\; \frac{2\tau}{\sigma} \tag{8.0-10}$$

$$=\; \frac{\psi(\infty)}{\psi(t)} \;\; \tan 2\vartheta_o \;+\; \frac{\psi(t-t_o)}{\psi(t)} \;\; \tan 2\vartheta$$

The angle φ predicted by (8.0-10) is compared with the observed isoclinic angle in Fig. 8.4. The agreement is within experimental deviation.

9. Test II.

A specimen shown in Fig. 9.1 was cut from a sheet as described in Appendix A.2. The model has a circular outer boundary and an irregular inner boundary. A uniform normal pressure was applied along the outer boundary and the model was heated by a heater along the inner boundary. The polaroid was cut to the shape of the model and placed in contact with it. Transparent plastic guards were then placed around the material to minimize heat loss at the surface. The procedures are described in Appendix A.7.

It was shown in Section 2.4 that the stress field in a plane stress problem with stress boundary conditions and uniform temperature is the same as if the material were elastic. In particular, the stress is independent of the material properties. Thus, if the unheated model is subjected to constant external pressure, the stress at any point should be constant. Each particle experiences creep at constant stress. The isoclinic angle at each point is then constant and coincides with the principal axes of stress. Take the coordinate axes along the principal axes. Then equations (6.0-8) and (7.0-2) lead to

$$n(t) = \frac{h}{2\pi c} \Delta(t) = \frac{h}{2\pi c} \psi(t) [\sigma_1 - \sigma_2] \qquad (9.0\text{-}1)$$

Since $\psi(t)$ is known from the tensile test, Section 7, the expected fringe order can be calculated, to within a constant factor. The actual fringe pattern was recorded with a movie camera. A typical frame is shown in Fig. 9.2. The expected fringe order is compared with the observed fringe order at several points in Fig. 9.3 and the agreement is satisfactory.

If the temperature of the model is not uniform then the stress field will not be constant even when the boundary pressure is constant. However, by means of (6.0-9), the difference in principal stresses and directions of principal stress can be calculated by integration over the observed history of fringe order and isoclinic angle.

In the present test, the model was heated until a steady non-uniform temperature distribution was reached. This temperature was maintained throughout the loading. Thus each particle experiences isothermal deformations. Equation (6.0-9) applies to each point but the function ψ will be different for each point because the temperature is different.

We expected that the stress at the inner boundary due to a step change in boundary pressure would be large at first, then diminish, but finally increasing to initial value. As shown in Section 2.5, the initial stress should be the same as for an elastic material and therefore, neglecting the effect of temperature on the value of $G(o)$ and $K(o)$, the stress should be the same as in the uniform temperature test of Fig. 9.3. The hotter points on the inner boundary then begin to relax. The modulus $G(t)$ becomes much smaller at the hotter points. Consequently, they "carry a smaller portion of the load", and the stress will decrease at the hotter points. As described in Section 2.6 the stress at long times is the same as for an elastic material; therefore, neglecting the effect of temperature on $G(\infty)$ and $K(\infty)$, the stress should approach that observed in the uniform temperature test.

The fringe order actually observed at a point is shown in Fig. 9.4.

At a point on the boundary the principal axis of stress are normal to the boundary at all times. Choose the coordinate axis along the principal axis of stress. Then, in (6.0-9), $\theta = \phi = 0$ and $\sigma_2 = 0$;

$$\sigma_1 = \int_0^t \Phi\,(t-\tau)\,\dot{\Delta}\,(\tau)\,d\tau \qquad (9.0\text{-}2)$$

The stress calculated using the observed fringe order and the function $\Phi(t)$ calculated from the optical creep function $\psi(t)$ for the particle temperature, is shown in Fig. 9.5. It has the expected character. The exact analytical solution is unknown and so no comparison is possible.

III. Conclusion

For the quasi-static problems of loaded structures containing linear viscoelastic materials an experimental technique has been developed. The experimental technique employs optically birefringent viscoelastic plastics from which models are prepared and observed in a photoelastic bench under the same loading states as in the prototype structure. The mechanical properties of the plastics can be tailored to those of the prototype. The observed fringe patterns in the photoelastic bench can be interpreted by employing the theory detailed in this report and the experimental characterization both optical and mechanical of the birefringent plastic. The technique permits quantitative stress analysis of engineering structural problems which are analytically extremely difficult or intractable. Such problems exist in solid propellant rocket motor grains where the motor is exposed to thermal and handling loads, in highly heated structures as exist in re-entry vehicles and will exist in supersonic transport aircraft, etc. The developed equipment and techniques are established and are in the process of being refined so they can be used routinely in an engineering analysis or design study.

IV. Plans for Continuing Effort.

In an effort to build upon the knowledge and experience gained in the first phase of this research program, and to make the results more meaningful to the engineer and designer who will in the future be faced with this type of problem, the following areas of continuing study have been defined.

(a) existing techniques, both experimental and interpretative, will be refined for the quasi-static and linear material behavior problems.

(b) an extension of the thoery to include non-linear and non-thermo-rheologically simple material will be made.

(c) an effort will be made to coordinate experimental techniques and numerical analyses to develop economical techniques to analyze engineering structural problems which currently are intractable.

(d) dynamic studies will be undertaken. It will thus be necessary to dynamically characterize the material which will of necessity involve wave propagation studies. This will involve development of dynamic equipment for the high resolution optical bench which will be used in dynamic photoelastic and photoviscoelastic studies.

References:

1. E. G. Coker and L. N. G. Filon: Photoelasticity, 2nd. edition, Cambridge
   University Press, 1957.

2. R. D. Mindlin: "A Mathematical Theory of Photoviscoelasticity."
   J. Appl. Phys., 20: 206-216. 1949. (See also Appl. Mech. Rev.
   4: 164. 1951).

3. W. T. Read, Jr.: "Stress Analysis for Compressible Viscoelastic Materials."
   J. Appl. Phys., 21: 671-674. 1950.

4. F. H. Dill: "Photothermoviscoelasticity." The Trend in Engineering.
   (Published by University of Washington). 14: 14-16. 1962.

5. E. H. Dill: "On Phenomenological Rheo-Optic Constitutive Relations."
   J. Polymer Sci., Part C, No. 5, Pp. 67-74. 1964.

6. E. H. Dill: "A Theory of Photothermoviscoelasticity." Proc. Fourth
   Intern. Cong. Rheology, John Wiley and Sons, N.Y. 1964.

7. E. H. Dill and C. W. Fowlkes: "Photoviscoelastic Experiments I."
   The Trend in Engineering. (Published by University of Washington),
   16: 5-9. 1964.

8. E. H. Dill: "Photoviscoelasticity." Proc. International Conference
   on the Mechanics and Chemistry of Solid Propellants. 1965.
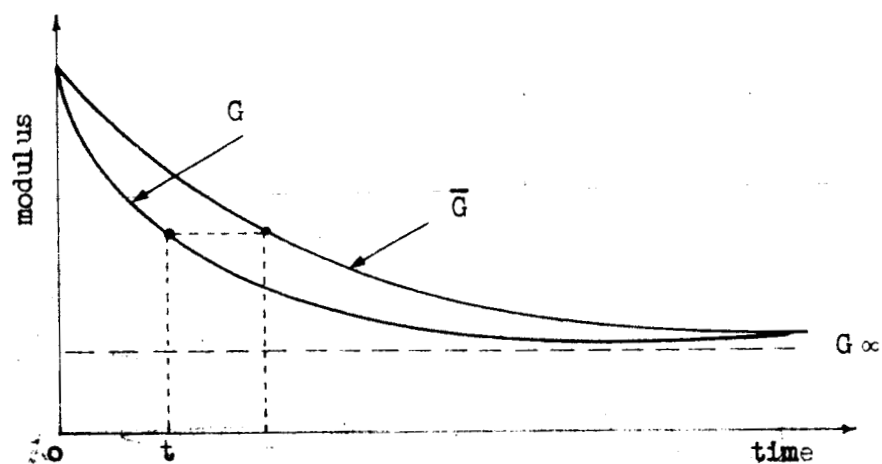
Fig. 2.1.   Isothermal Relaxation Moduli
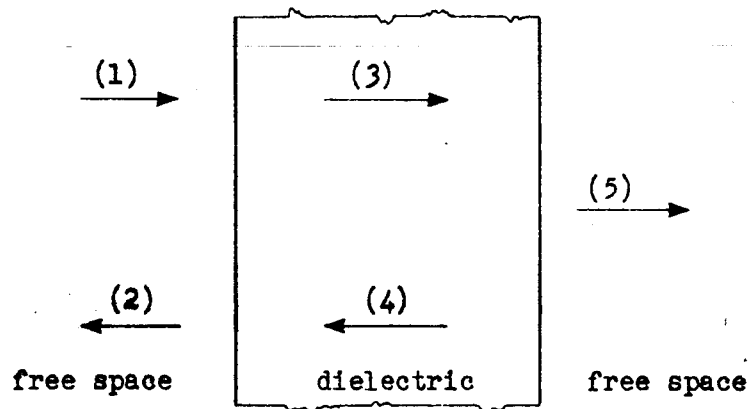
Fig. 3.1. Dielectric Slab
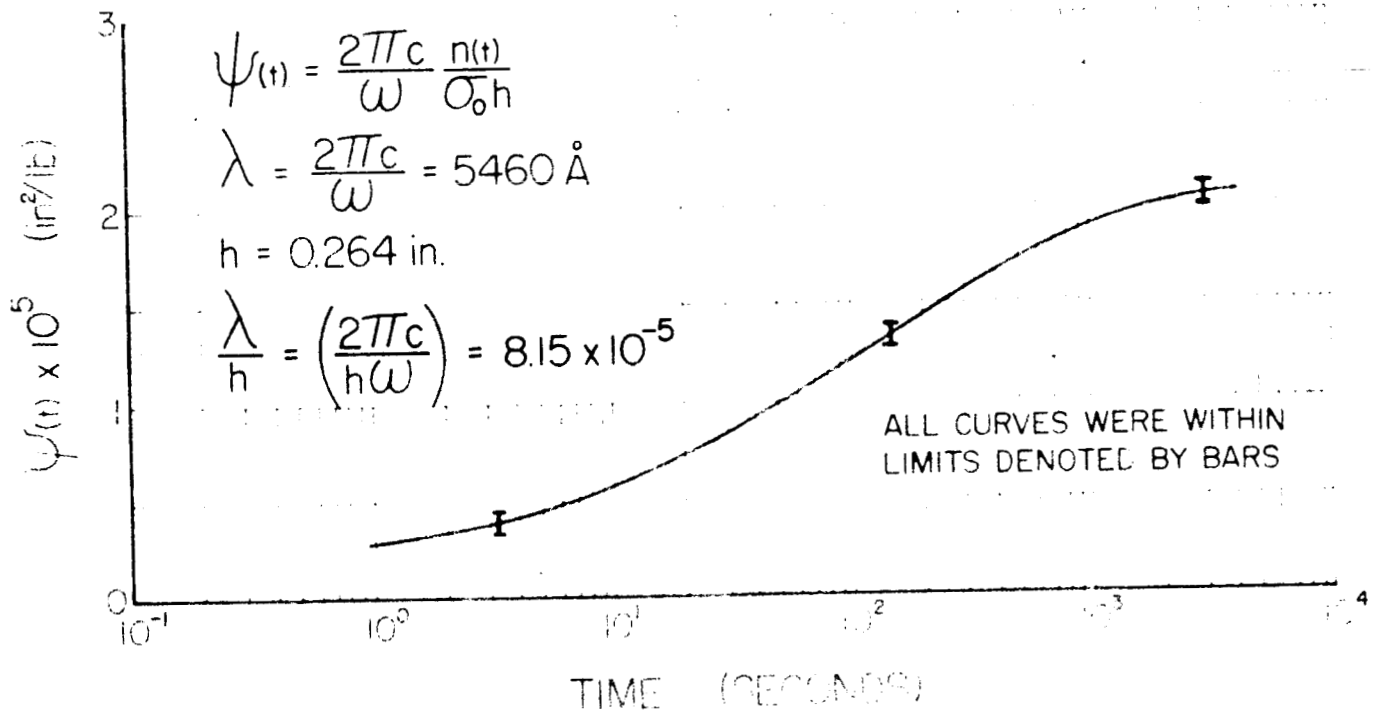
Fig. 7.1. Optical Creep Compliance. Mix A.

49
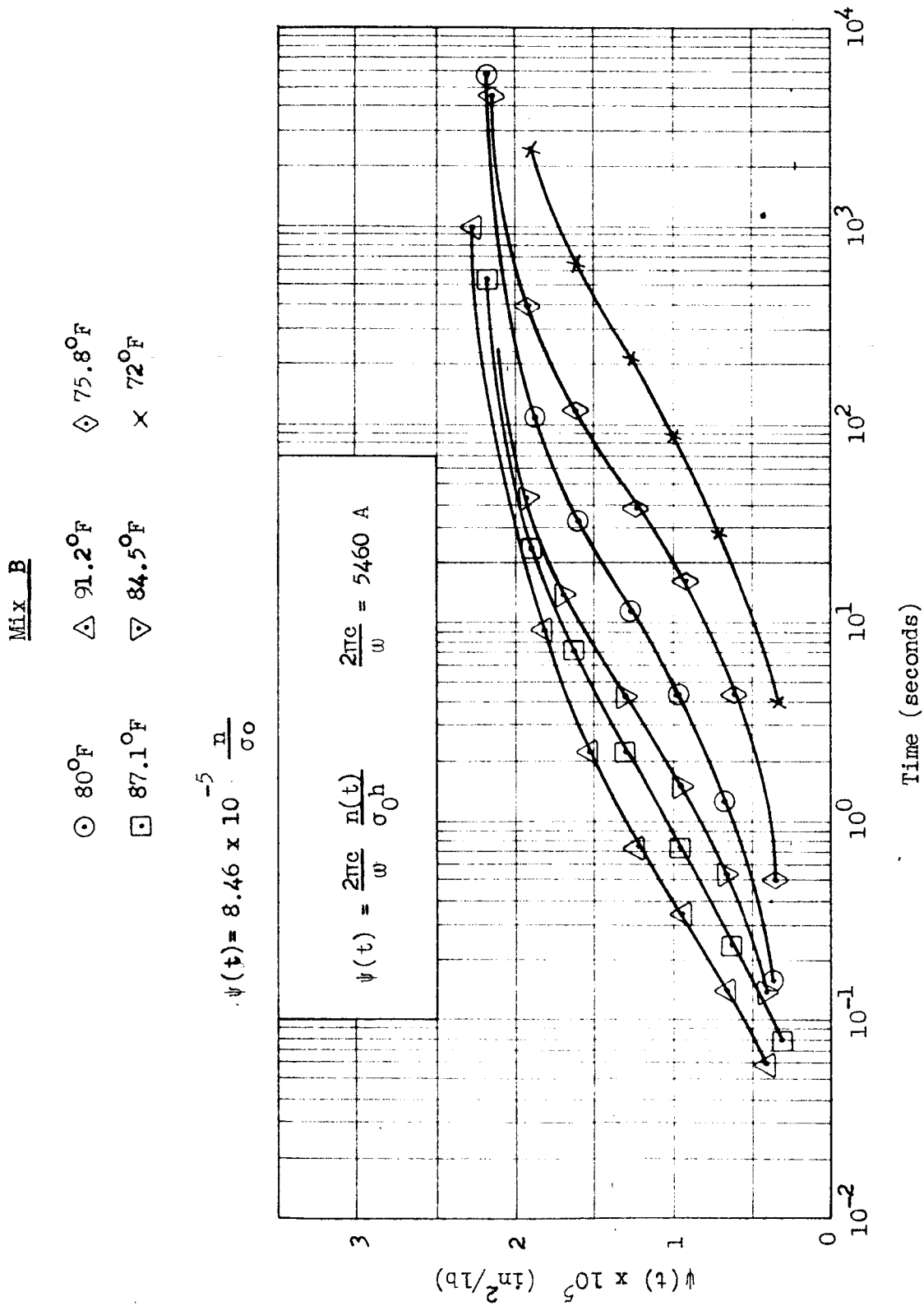
Fig. 7.2. Optical Creep Function. Mix B.

$$D(t) = \frac{\varepsilon_x(t)}{\sigma_0} \qquad 4.1\,\text{psi} < \sigma_0 < 13.6\,\text{psi}$$

ALL CURVES WERE WITHIN LIMITS
DENOTED BY BARS

TIME (SECONDS)

Fig. 7.3. Tensil —Creep Compliance. Mix A.

$$\mathcal{V}(t) = -\frac{\epsilon_y(t)}{\epsilon_x(t)}$$

ALL CURVES WERE WITHIN LIMITS
DENOTED BY BARS

TIME (SECONDS)
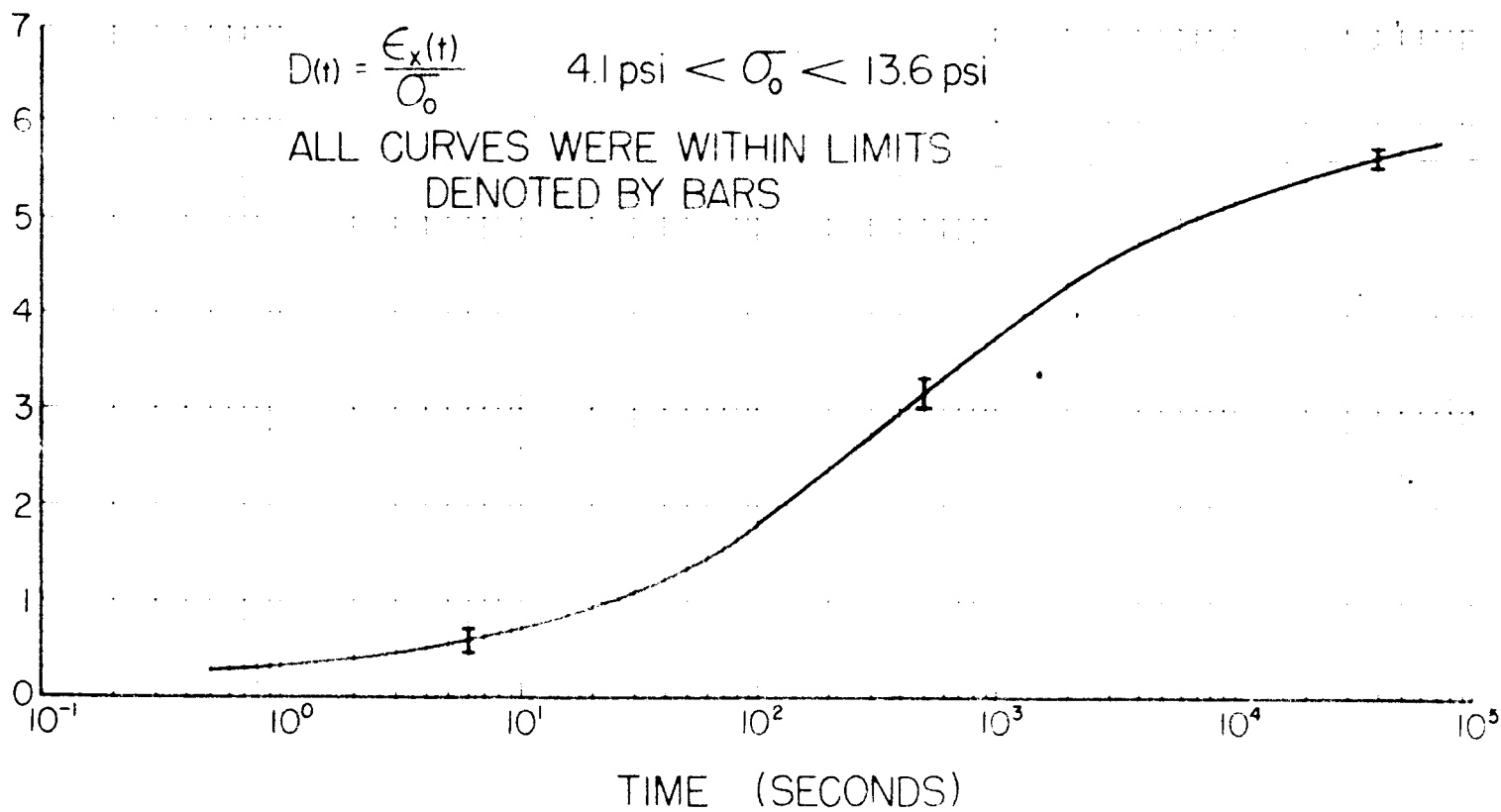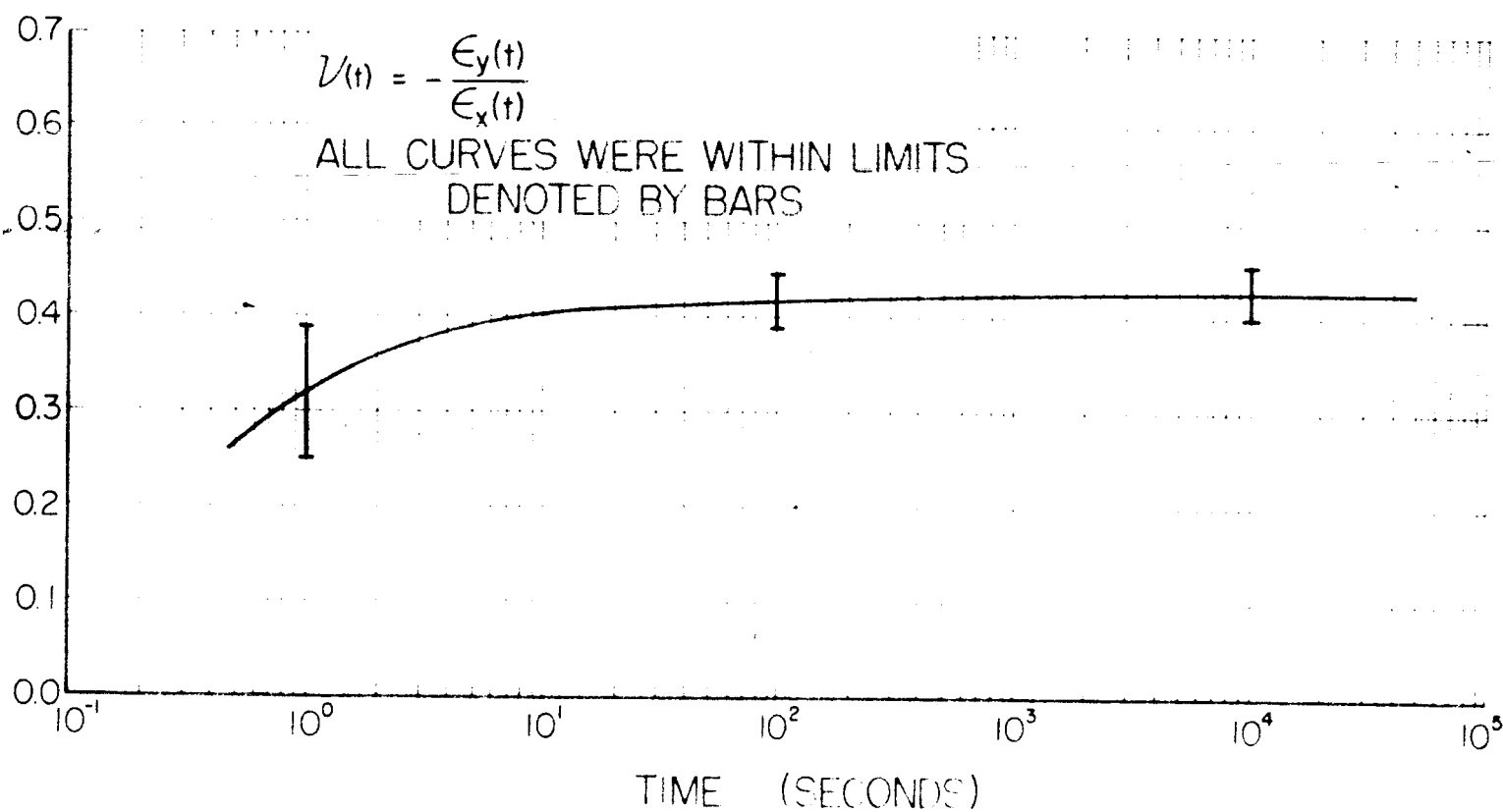
Fig. 7.4. Transverse Contraction Ratio. Mix A.

$$J(t) = 2D(t)\left[1 + \mathcal{V}(t)\right]$$

$$---- \mathcal{V}(t) = \mathcal{V}(\infty)$$

TIME   (SECONDS)
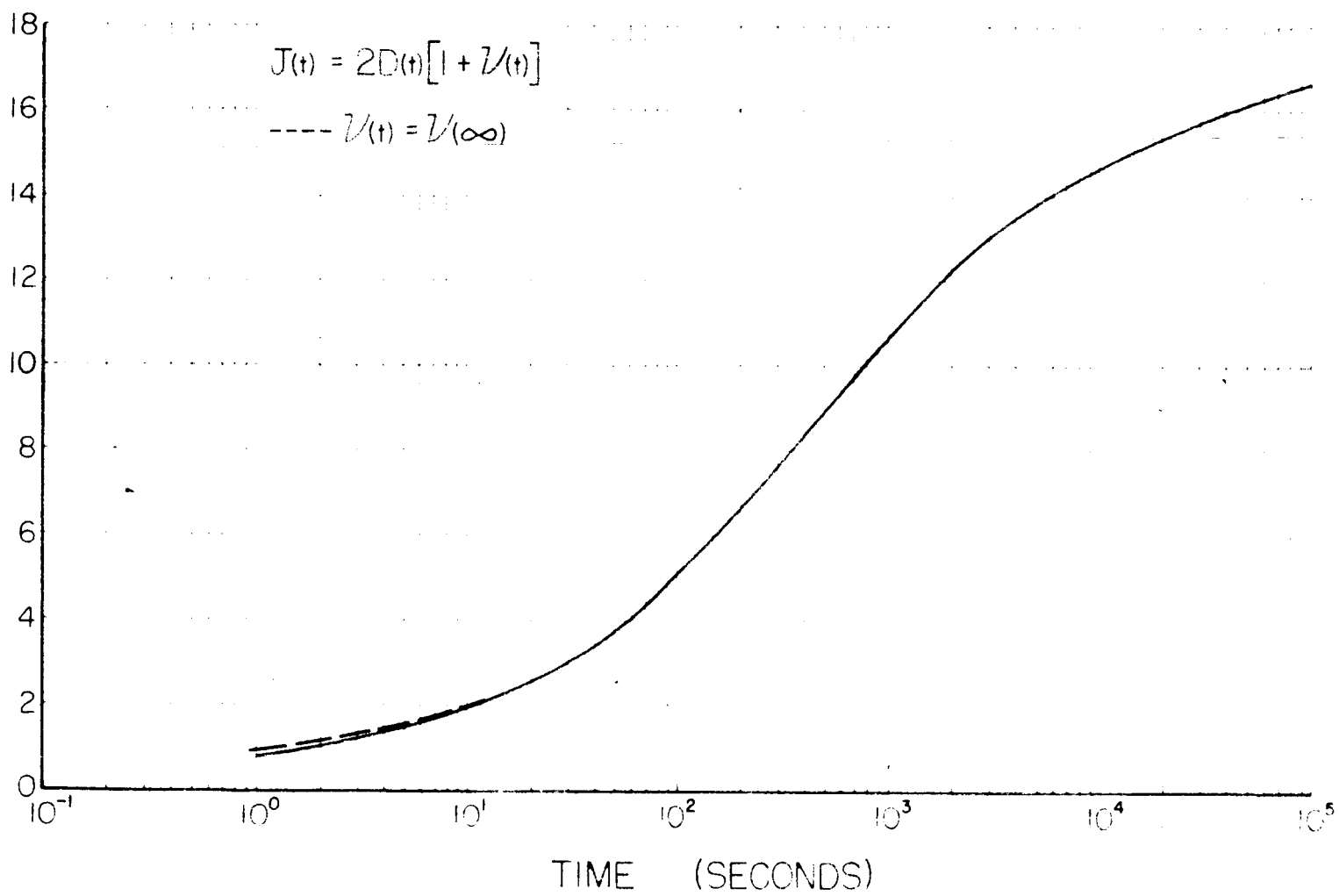
Fig. 7.5.   Shear-Creep Compliance (Calculated). Mix A.
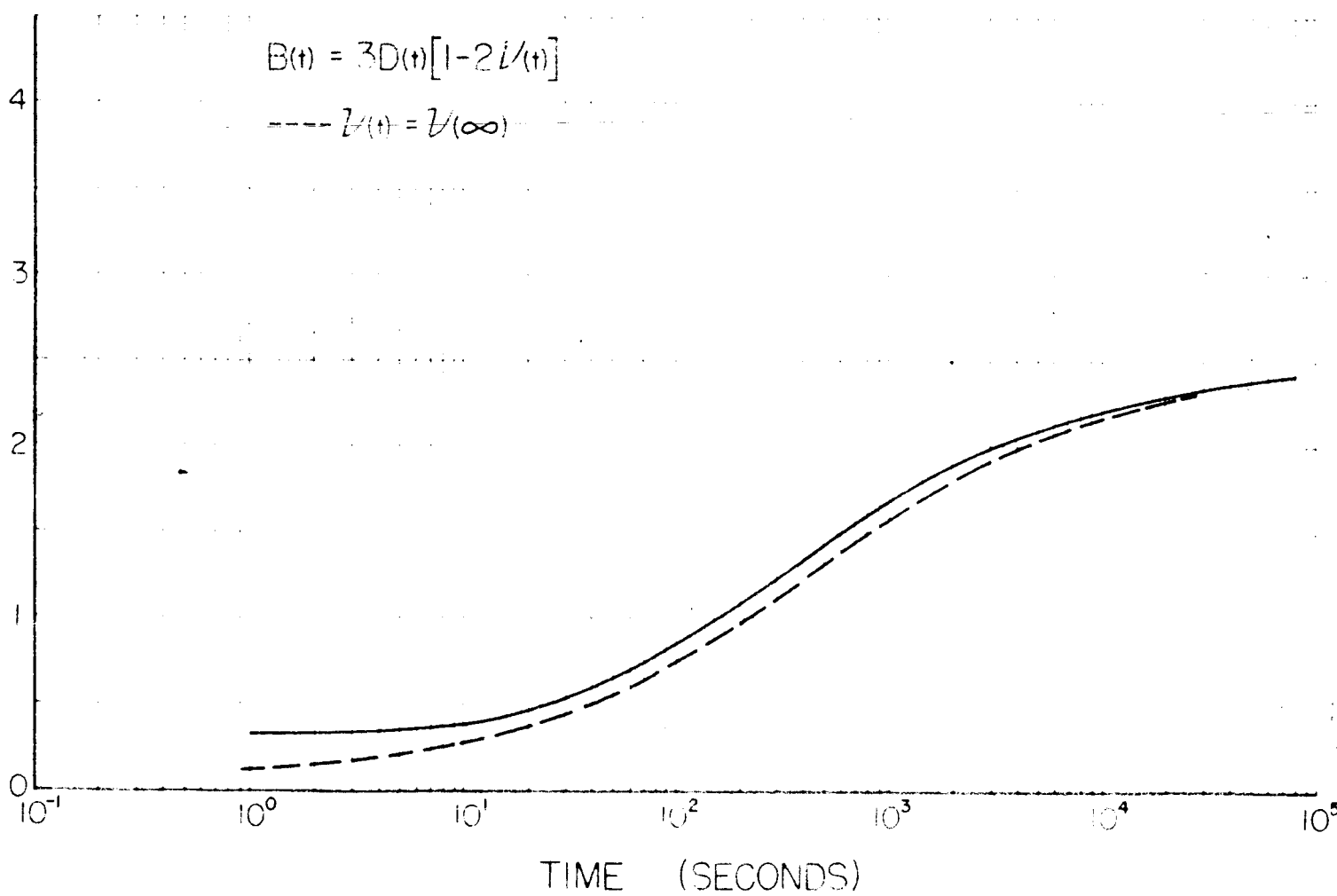
Fig. 7.6. Bulk-Creep Compliance (Calculated). Mix A.
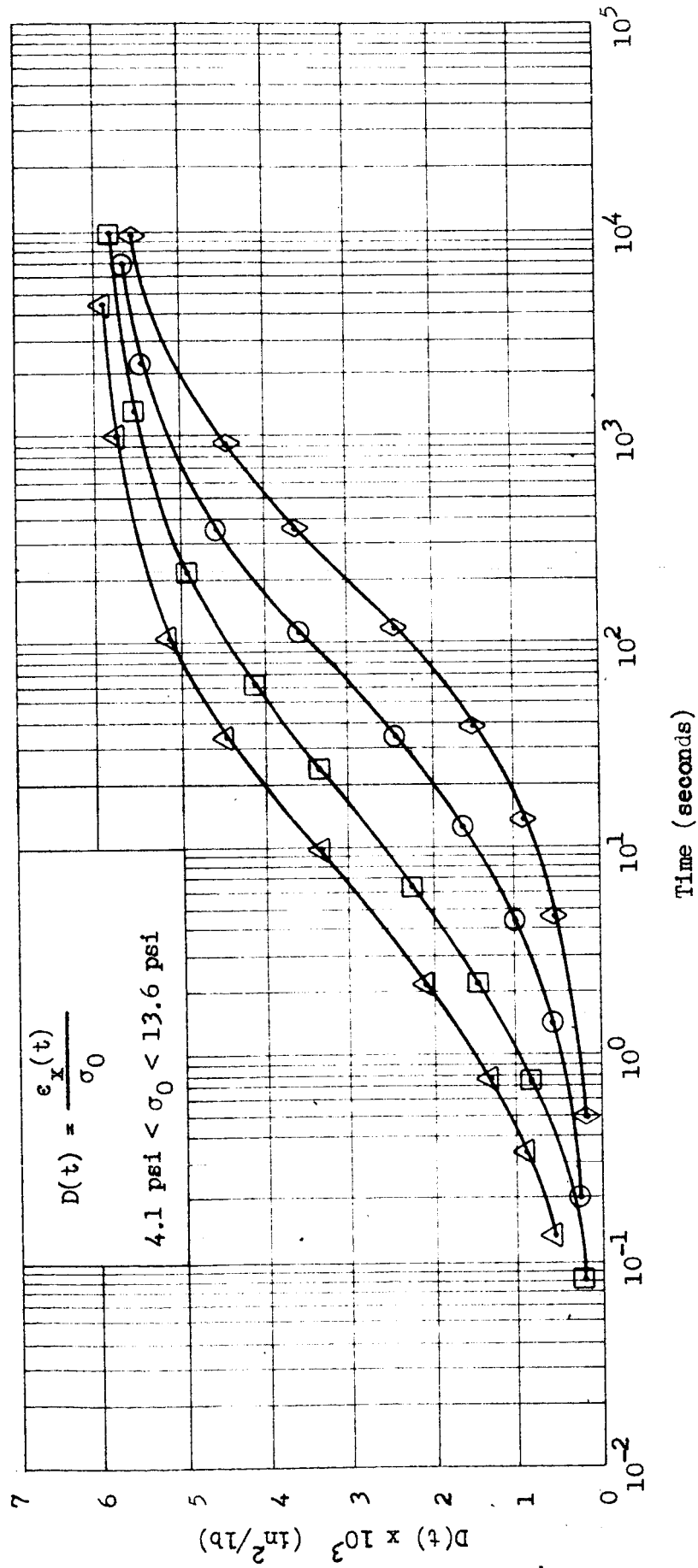
Fig. 7.7. Tensile Creep Compliance. Mix B.

Mix B

⊙ 80°F   △ 91.2°F

☐ 87.1°F   ◇ 75.8°F

$$D(t) = \frac{\varepsilon_x(t)}{\sigma_0}$$

4.1 psi $< \sigma_0 <$ 13.6 psi

Time (seconds)

$D(t) \times 10^3$ (in²/lb)
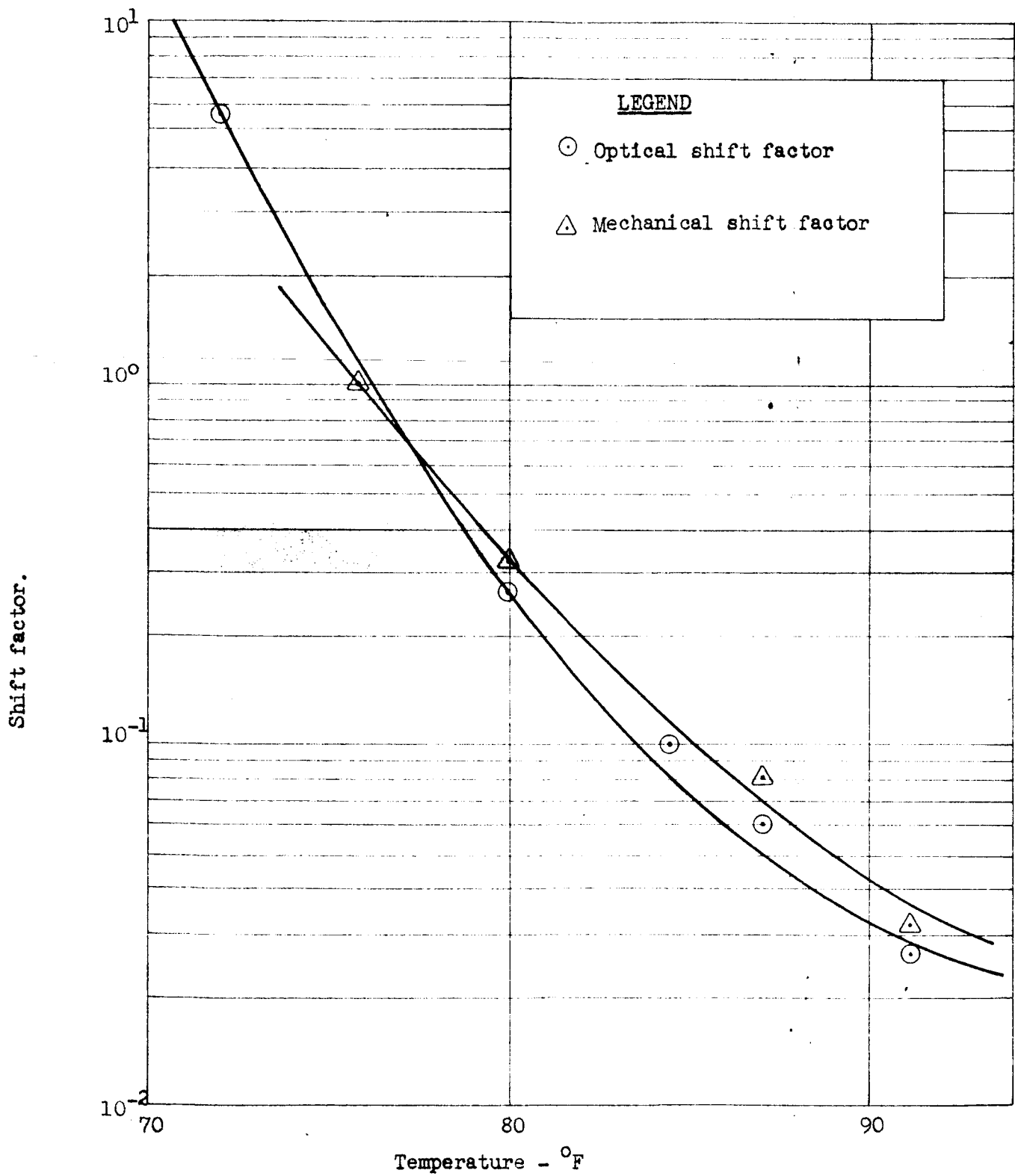
Fig. 7.8. Mechanical and optical shift factors. Mix B

Fig. 7.9. Optical Creep Compliance. Mix A.

$\Phi(t)$ Stress at Constant Fringe Order

$\psi(0) = 0.25 \times 10^{-5}$ in^2/lb

Mix A

$\dfrac{\Phi(t)}{\Phi(o)}$

Time (seconds)
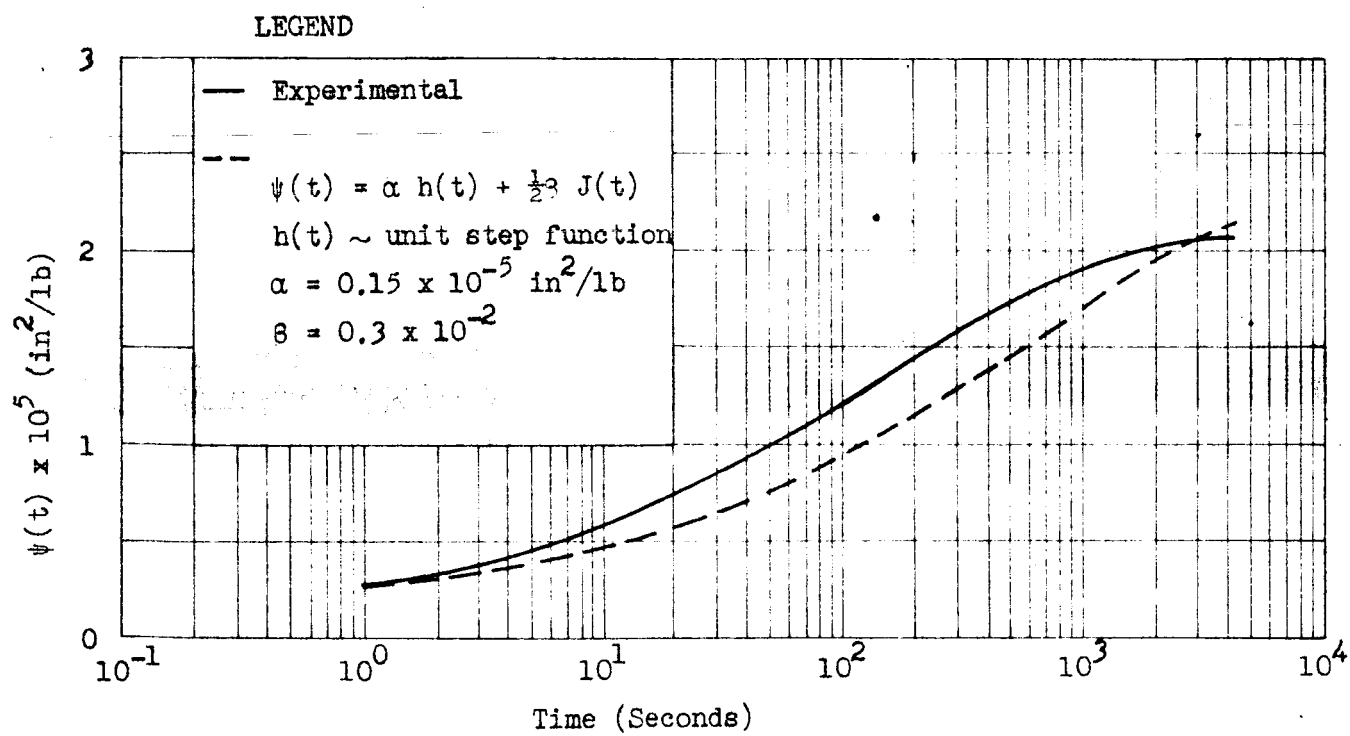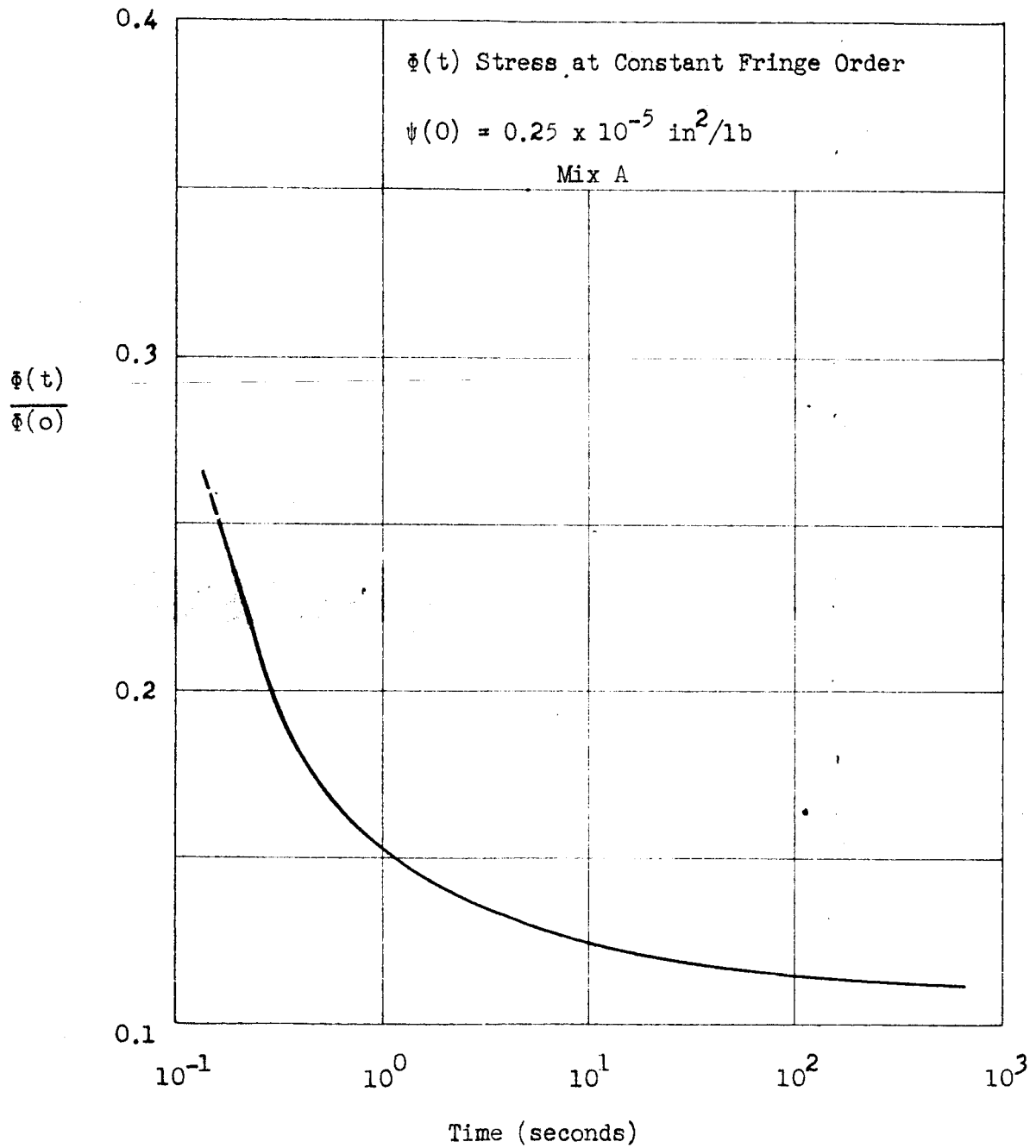
Fig. 7.10. Inverse Optical Creep Function.
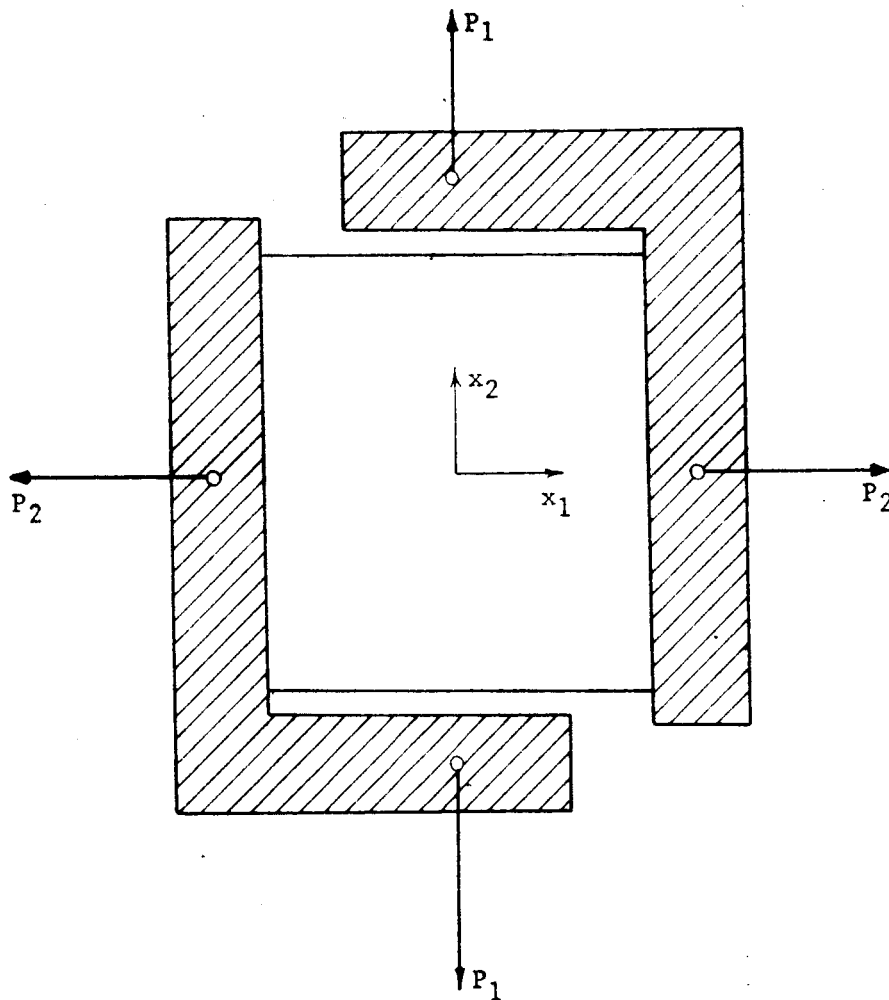
TEST   I

Fig. 8.1.   Combined Shear and Tension
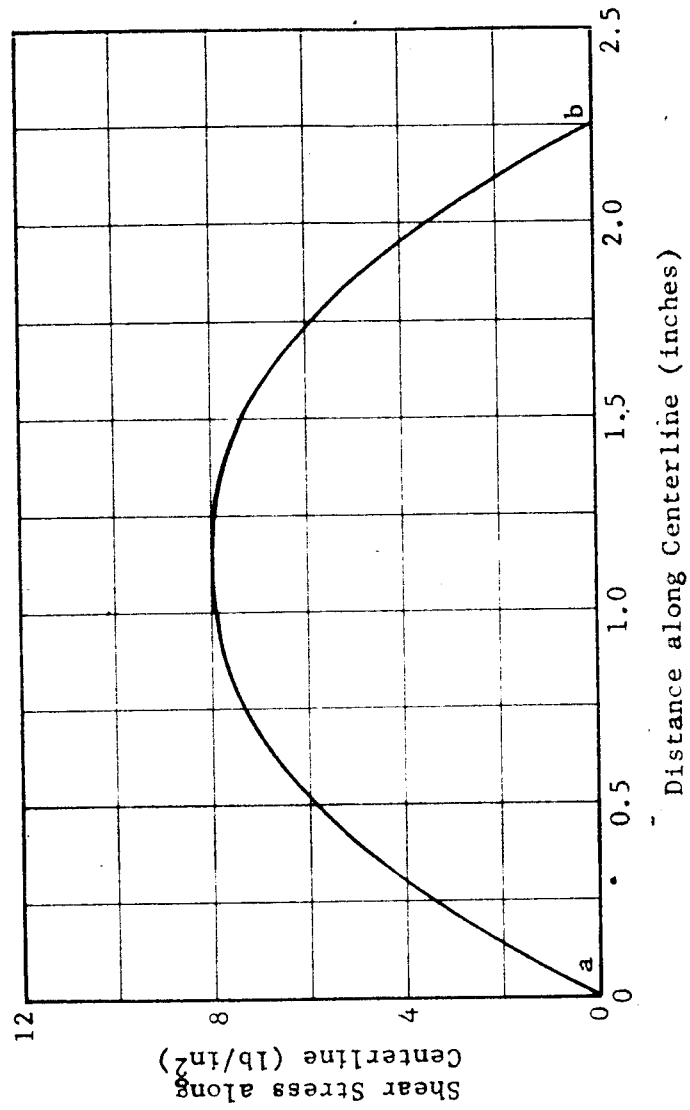
Fig. 8.2. Shear Stress
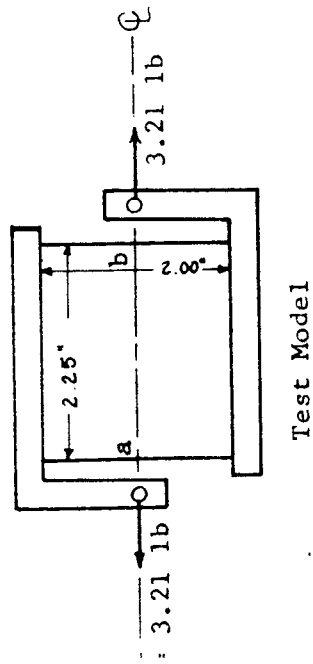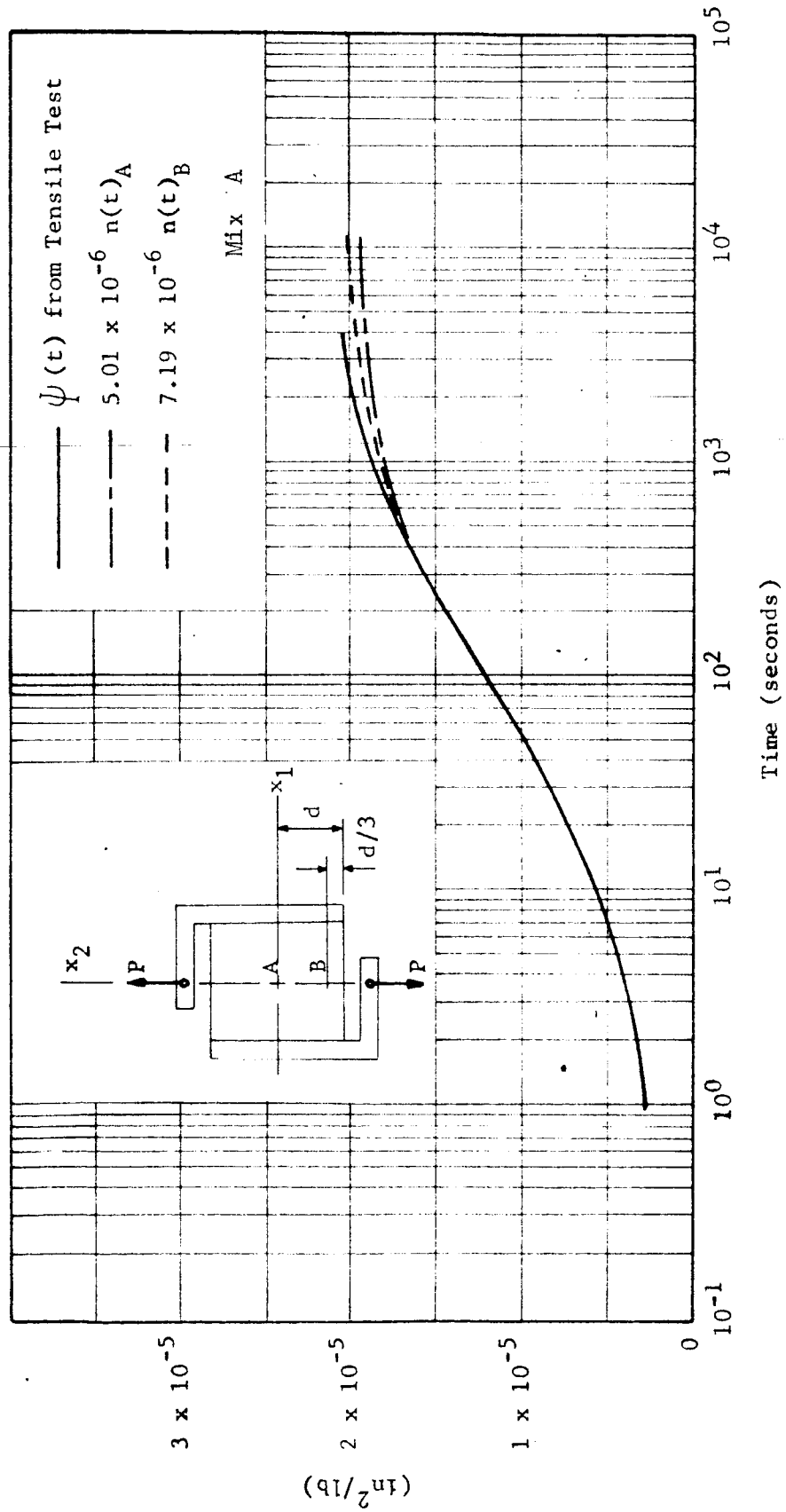
Fig. 8.3. Fringe Order in Shear Test.
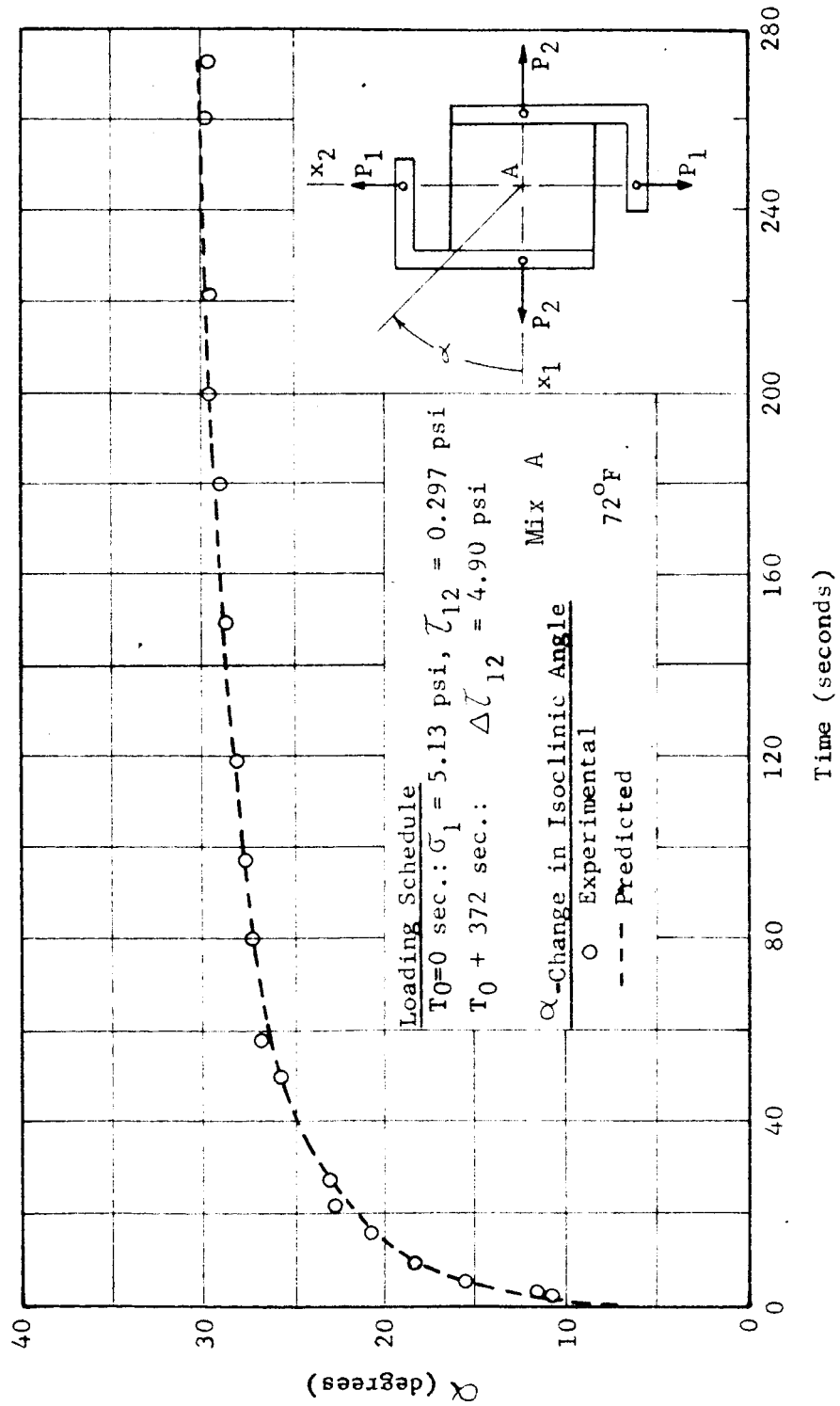
Fig. 8.4. Isoclinic Angle in Tension—Shear Test.

1/4R

0.500

2.200

5.400"
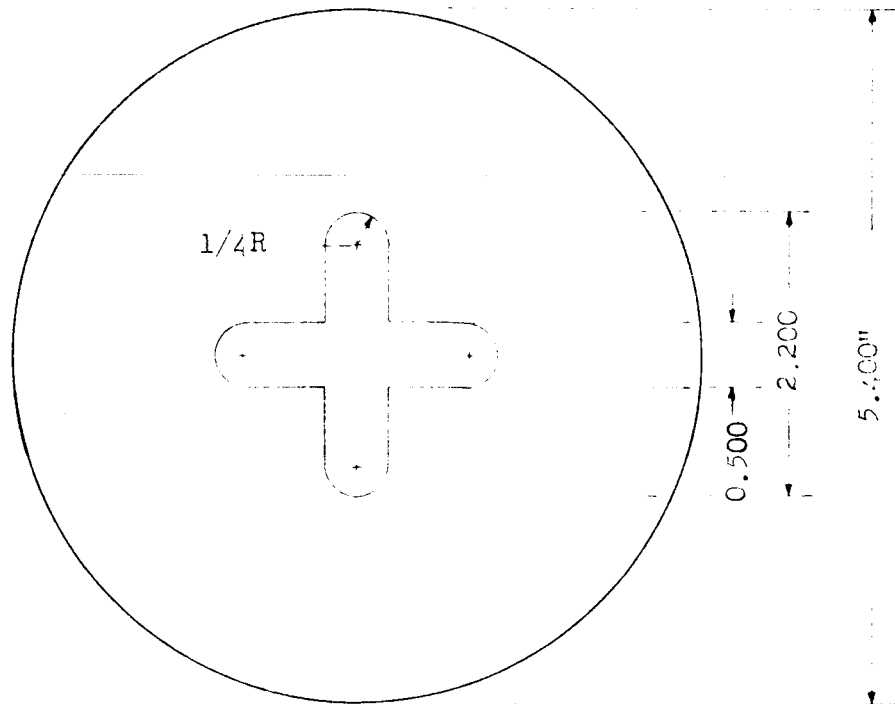
Fig. 9.1. Star Grain Model.
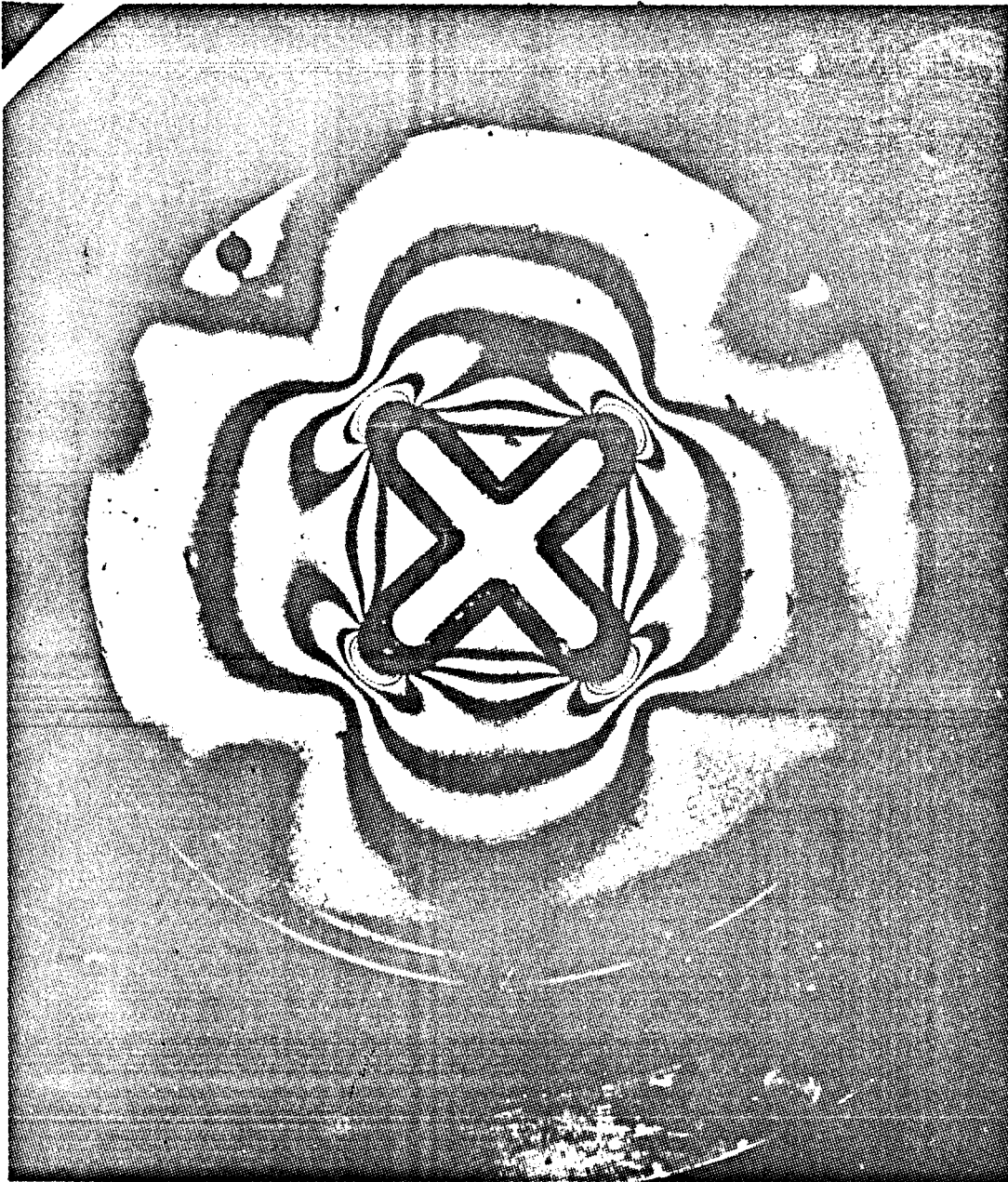
Figure 9.2: Isothermal pressurized grain
             Model 6300 seconds after loading
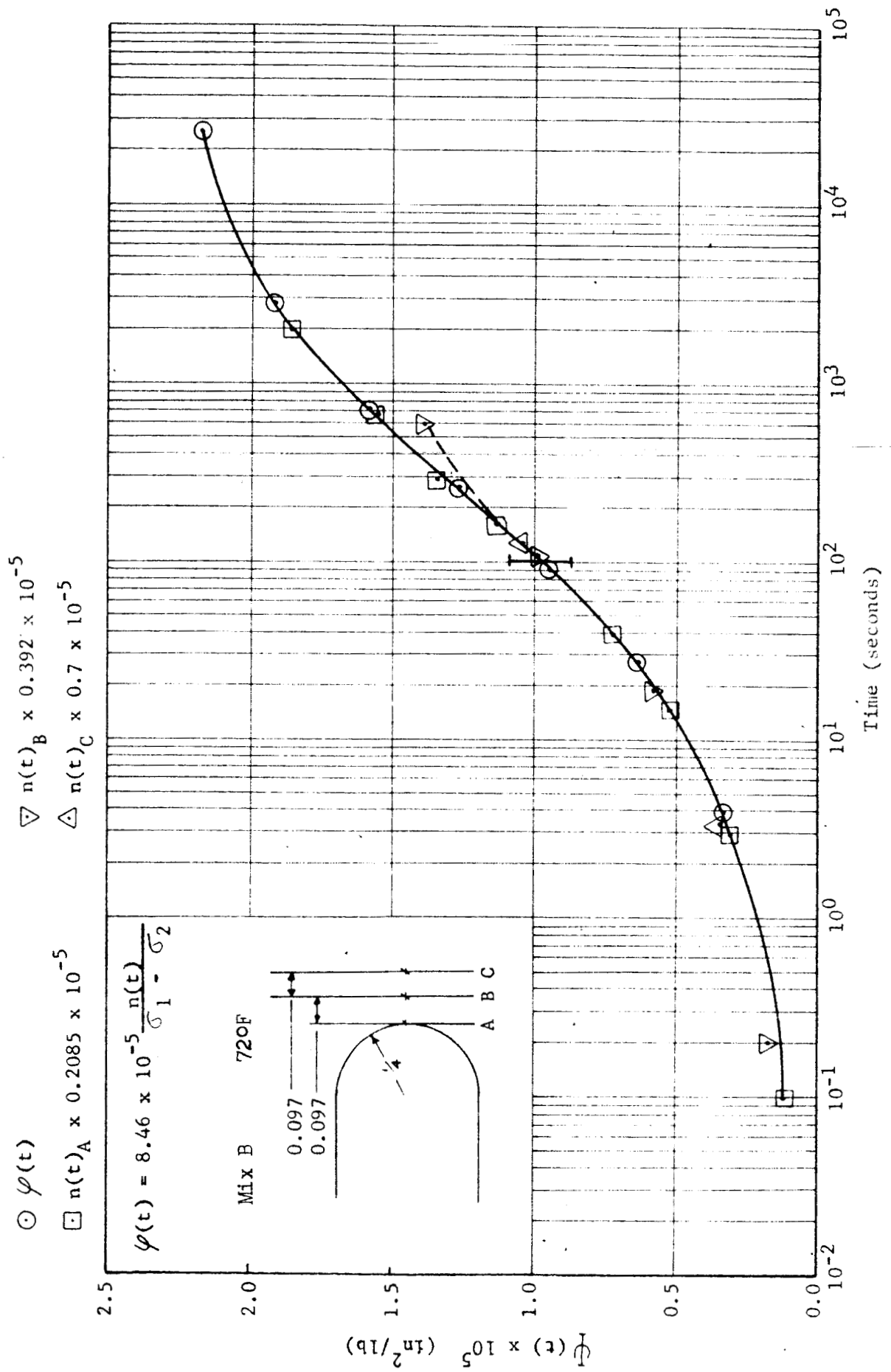
Fig. 9.3. Fringe Order at Uniform Temperature.
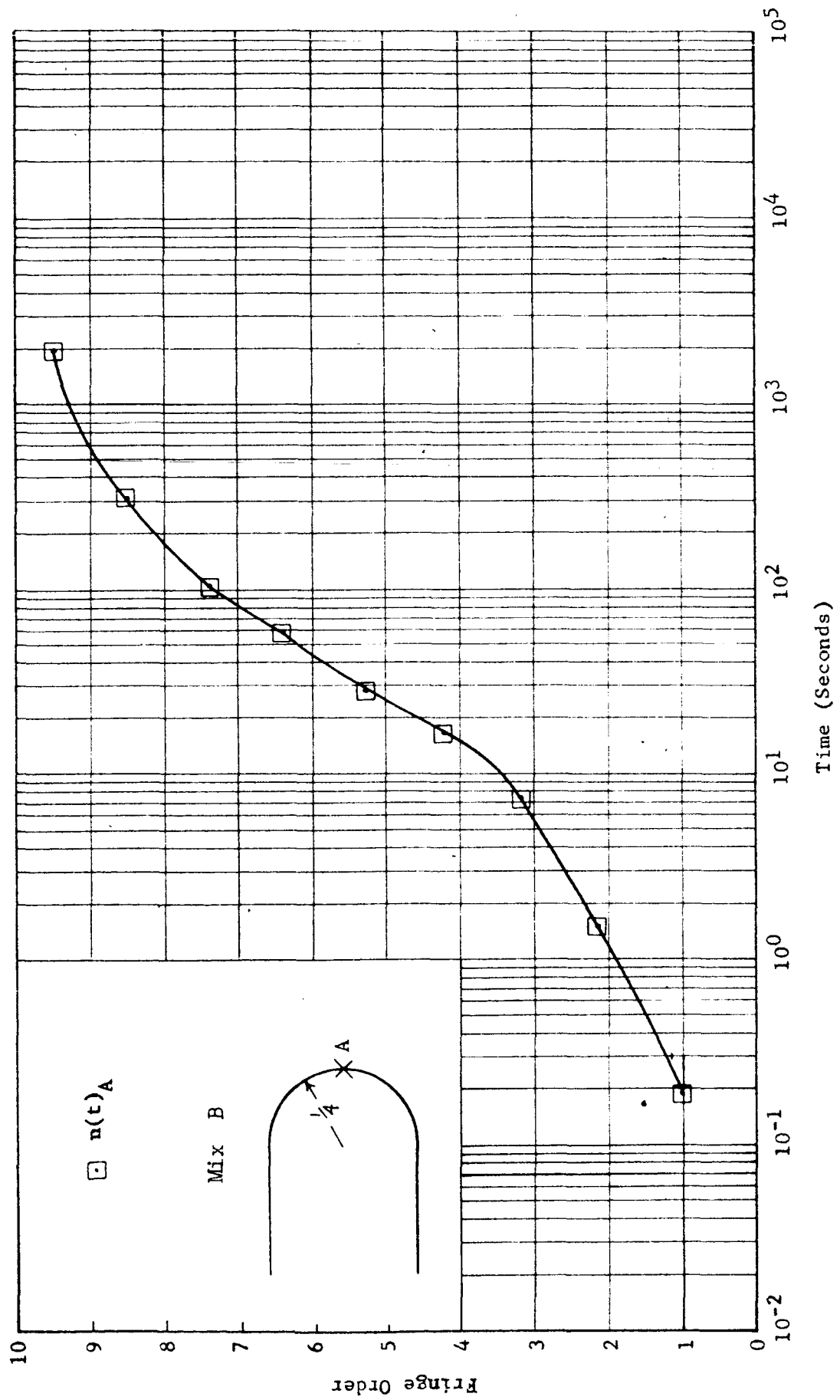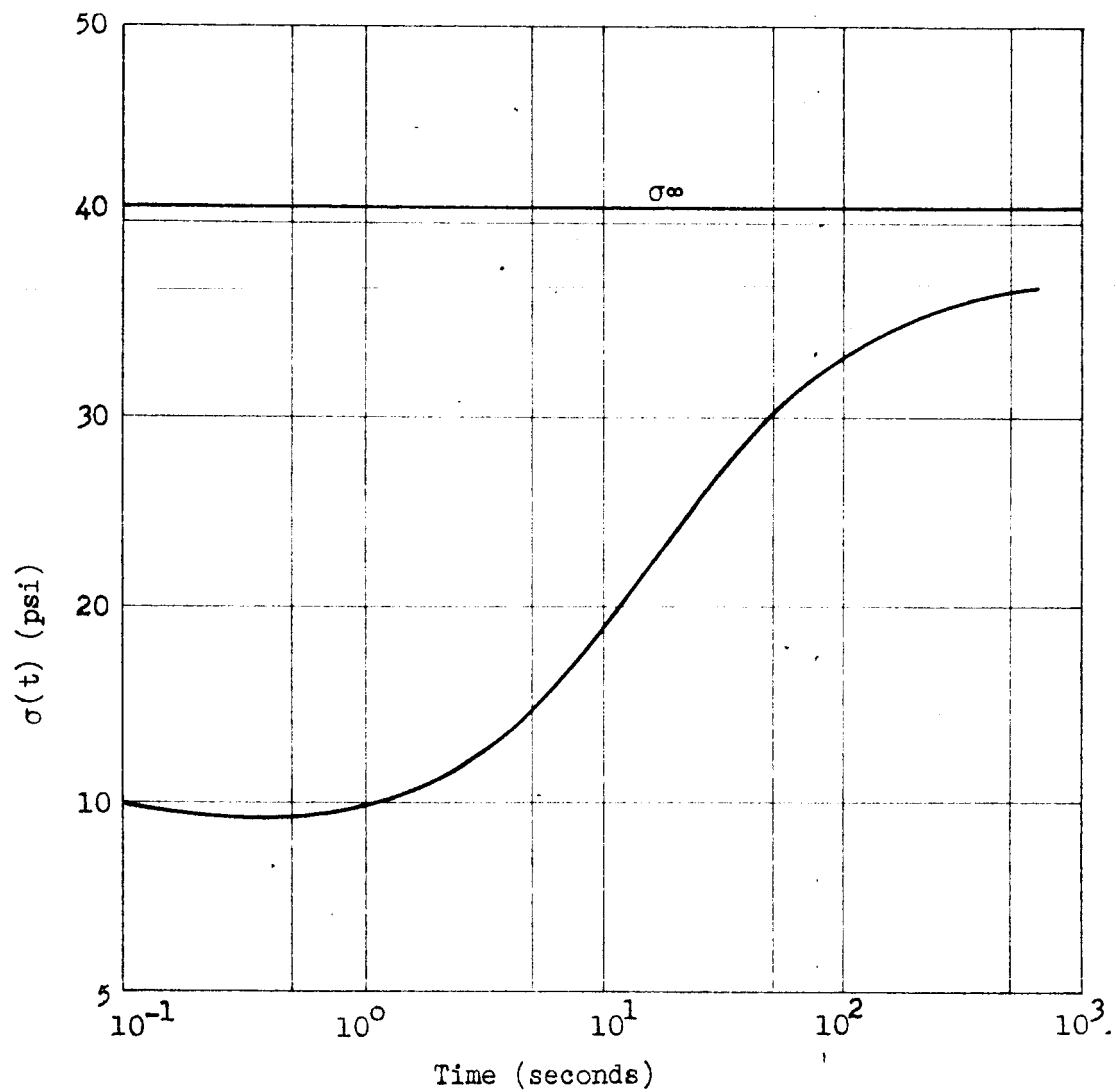
Fig. 9.4. Fringe Order, Heated Model.

Fig. 9.5. Stress at Star Root (point A), Heated Model.

APPENDICES

APPENDIX A.1.

CALCULATION OF RELAXATION MODULUS FROM CREEP COMPLIANCE

BY NUMERICAL METHODS

1. Introduction:

Most of the problems concerning stress distribution in linear visco-elastic bodies are often solved by assuming that the behavior of the material under stress can be approximated by a suitable combination of linear viscous and elastic elements (dashpots and springs). This method leads to the problem of solving a differential equation of the form:

$$\sum_{i=o}^{m} p_i \frac{d^i}{dt^i} \sigma(t) = \sum_{i=o}^{n} q_i \frac{d^i}{dt^i} \gamma(t) \qquad (A.1-1)$$

where $\sigma(t)$ is a stress component

$\gamma(t)$ is the corresponding strain component

p_i and q_i are material constants depending on the nature of the springs and dashpots used and m and n are integers whose values depend on the number of springs and dashpots and the way they are combined.

This method is simple if we can approximate the behavior of the material under consideration with a small number of elements. However, for many materials any realistic approximation of their stress-strain relation by the above method requires a large number of elements resulting in a differential equation of high order. The solution of such an equation becomes

almost impossible beyond a certain stage and hence the above method of representation of mechanical behavior is of limited use in stress analysis problems.

Another method which is much more general is to represent the stress-strain relations by Convolution integrals following Boltzmann's Super-position Principle. According to this, the stress-strain relation of a linear viscoelastic material can be written as.$^{(1.1)^*}$.

$$\sigma(t) = \int_{-\infty}^{t} E(t-\xi)\ \dot\gamma(\xi)\ d\xi \qquad (A.1-2a)$$

or

$$\gamma(t) = \int_{-\infty}^{t} D(t-\xi)\ \dot\sigma(\xi)\ d\xi \qquad (A.1-2b)$$

where $E(t)$ is the relaxation modulus of the material at time t. $D(t)$ is the creep compliance of the material at time t and the superposed dot represents differentiation with respect to time. Most of the problems are concerned with materials which were in stress free state prior to time t=o and in such cases the lower limit of integrals in (A.1-2a) and (A.1-2b) is replaced by zero. The relaxation modulus and creep compliance are continuous functions of time which characterize the particular viscoelastic material under consideration and hence should be evaluated experimentally. However, as they are not independent as shown in the next section, the measurement of one of the functions should suffice for the calculation of the other. Suitable numerical techniques are developed for the calculation of creep compliance from measured data of relaxation modulus in the previous

---

*Number in brackts refers to the references at the end of this appendix.

literature,[1,2] but no such methods are available for the calculation of relaxation modulus from data on creep compliance. Such a numerical method is very desirable as it is easier to perform creep tests and thus measure creep compliance at various times rather than the measurement of relaxation modulus. The aim of this discussion is towards such a goal.

2. Basic Theory:

Taking Laplace transform of (A.1-2a) and (A.1-2b) one obtains.

$$\overline{\sigma} = s \, \overline{\gamma} \, \overline{E} \tag{A.1-3a}$$

and

$$\overline{\gamma} = s \, \overline{\sigma} \, \overline{D} \tag{A.1-3b}$$

where the superposed bar on a variable represents the Laplace transform of that variable and s is the parameter used in performing the transformation. Multiplication of (A.1-3a) and (A.1-3b) results in

$$\overline{E} \, \overline{D} = 1/s^2 \tag{A.1-4}$$

Taking the inverse Laplace transform of (A.1-4) and assuming that the material is in stress free state prior to t = o, we get

$$\int_0^t E(t-\tau) \, D(\tau) \, d\tau = t \tag{A.1-5a}$$

or

$$\int_0^t D(t-\tau) \, E(\tau) \, d\tau = t \tag{A.1-5b}$$

The above equations are the fundamental relations between the creep compliance and the relaxation modulus of the material and hence can be used to calculate one of the above functions provided the other is known for all times starting with time zero. Any analytical solution of the above equation requires the creep compliance to be a simple function of time. But for many materials, any realistic approximation of the creep

compliance by simple functions is not possible and hence one must resort to numerical methods for solving either (A.1-5a) or (A.1-5b). Although the numerical method has the advantage of requiring values of the creep compliance at only a finite number of discrete times, it does have diffi-culties with accumulation of error as time increased. In the next section an attempt at a numerical method of evaluation of relaxation modulus from creep data is presented using equation (A.1-5b).

3. Numerical Method:

Several creep tests have been performed on viscoelastic models. The results are presented in Fig. A.1.1. All the data fell between the two broken line curves. The continuous curve shown is taken to be the actual creep curve. Additional information concerning these tests is presented in reference 1.3.

Suppose that the relaxation modulus at time t = T is desired, i.e. $E(T)$. The interval $[0,T]$ is divided into K subintervals of arbitrary magnitude with $t_1 = 0$ and $t_{K+1} = T$. Indicate $D(t_i)$, $E(t_i)$ etc. by $D(i)$, $E(i)$, etc. Using this notation (A.1-5b) can be written as:

$$t_{K+1} = \int_0^{t_{K+1}} D(t_{K+1} - \tau)\, E(\tau)\, d\tau$$

$$= \sum_{i=1}^{K} \int_{t_i}^{t_{i+1}} D(t_{K+1} - \tau)\, E(\tau)\, d\tau \qquad \text{(A.1-6)}$$

In each interval let us approximate

$$\int_{t_i}^{t_{i+1}} D(t_{K+1} - \tau)\, E(\tau)\, d\tau \simeq D(t_{K+1} - t_i)\, E(t_i)\, (t_{i+1} - t_i) \qquad \text{(A.1-7)}$$

so $\qquad$ $t_{K+1} \simeq \sum_{i+1}^{K} D(T_{K+1} - t_i)\ E(t_i)\ (t_{i+1} - t_i)$

$$\simeq D(t_{K+1} - t_K)\ E(t_K)\ (t_{K+1} - t_K) \qquad (A.1-8)$$

$$+ \sum_{i=1}^{K-1} D(t_{K+1} - t_i)\ E(t_i)\ (t_{i+1} - t_i)$$

Rearranging (A.1-8) we get

$$D(t_{K+1} - t_K)\ (t_{K+1} - t_K)\ E(K) = t_{K+1} -$$
$$\sum_{i=1}^{K-1} D(t_{K+1} - t_i)\ E(i)\ (t_{i+1} - t_i).$$

Hence

$$E(K) = \frac{t_{K+1} - \sum_{i=1}^{K-1} D(t_{K+1} - t_i) \cdot (t_{i+1} - t_i)\ E(i)}{D(t_{K+1} - t_K) \cdot (t_{K+1} - t_K)} \qquad (A.1-9)$$

This is the fundamental relation used for the evaluation of the relaxation modulus at various times. Notice that when K = 1, the above formula becomes

$$E(1) = \frac{1}{D(2)} \qquad (A.1-10)$$

and the number of output values is one less than the number of input values, ie. when $\Gamma(t)$ is given at (K 1) discrete times say $D(1)$, $D(2)$ .... $D(K+1)$ we can calculate only K values of E at times t_1, t_2, ... t_K.

Suppose there is a certain amount of error in the calculation of $E(K-1)$ due either to faulty data or to numerical rounding off. If the influence of this error is to be reduced, the coefficient of $E(K-1)$ should be less than 1. This value is indicated by C_{K-1}^K and is given by.

$$C_{K-1}^K = \frac{D(t_{K+1} - t_{K-1})}{D(t_{K+1} - t_K)} \cdot \frac{t_K - t_{K-1}}{t_{K+1} - t_K} \qquad (A.1-11)$$

Hence we should have

$$\frac{D(t_{K+1} - t_{K-1})}{D(t_{K+1} - t_K)} \cdot \frac{t_K - t_{K-1}}{t_{K+1} - t_K} < 1$$

or

$$(t_{K+1} - t_K) > \frac{D(t_{K+1} - t_{K-1})}{D(t_{K+1} - t_K)} \cdot (t_K - t_{K-1}) \qquad (A.1-12)$$

However $D(t)$ is an increasing function of time and $(t_{K+1} - t_{K-1}) > (t_{K+1} - t_K)$. This implies that

$$\frac{D(t_{K+1} - t_{K-1})}{D(t_{K+1} - t_K)} > 1$$

In order to reduce the error in the calculation of $E(K)$ due to the errors in $E(K-1)$, $E(K-2)$ etc. one should have

$$\frac{t_{K+1} - t_K}{t_K - t_{K-1}} > \frac{D(t_{K+1} - t_{K-1})}{D(t_{K+1} - t_K)} > 1 \qquad (A.1-13)$$

that is one should take each interval to be larger than the previous one and the size of the intervals in any individual calculation should be

decided by the inequality (A.1-13). The example given later in this
section is carried out on the basis of the above criteria.

4. Further Error Analysis:

Hopkins and Hamming[1,2] used similar methods of numerical integra-
tion in order to find creep function from measured values of relaxation
modulus and concluded that the error should gradually decrease on the
basis of the above criteria. Lee and Rogers[1,4] used similar criteria
and concluded that the error decreases rapidly in the above type of
numerical integration. However, careful observation shows that this is
not always the case and that one should go further into an error analysis
in order to have a proper subdivision of the time interval which insures
gradual error reduction. For the time being let no physical meaning be
specified to either $D(t)$ or $E(t)$. Calculate $E(t)$ from the known values
of $D(t)$ which are related by the approximate expression (A.1-2). Let
$E(K)$ and $\widetilde{E}(K) = (1 + \epsilon_K) E(K)$ be the computed and actual values of $E(t_K)$.
Then

$$\text{Error in } E(K) = \epsilon_K \; E(K) \tag{A.1-14}$$

Let the error which would occur in $E(K+1)$ be $\epsilon_{K+1} E(K+1)$. On the basis
of previous analysis one may write

$$\epsilon_{K+1} \; E(K+1) = C_K^{K+1} \; \epsilon_K \; E(K) + \Delta_{K-1} \tag{A.1-15}$$

where Δ_{K-1} is the error in calculated value of $E(K+1)$ due to errors in
$E(K-1)$, $E(K-2)$, ...$E(1)$.

Let $\quad C_K^{K+1} \equiv (1 - \alpha)$ \hfill (A.1-16)

Then

$$\frac{\varepsilon_{K+1} \, E(K+1)}{\varepsilon_K \, E(K)} = 1 - \alpha + \frac{\Lambda_{K-1}}{\varepsilon_K \, E(K)} \tag{A.1-17}$$

Equation A.1-17 shows that the error gradually decreases only if

$$\alpha > \frac{\Lambda_{K-1}}{\varepsilon_K \, E(K)} \tag{A.1-18}$$

But

$$\alpha = 1 - C_K^{K+1} = 1 - \frac{D(t_{K+2} - t_K)}{D(t_{K+2} - t_{K+1})} \cdot \frac{(t_{K+1} - t_K)}{(t_{K+2} - t_{K+1})} \tag{A.1-19}$$

Hence the criteria for the gradual reduction of the error is

$$1 - \frac{D(t_{K+2} - t_K)}{D(t_{K+2} - t_{K+1})} \cdot \frac{(t_{K+1} - t_K)}{(t_{K+2} - t_{K+1})} > \frac{\Lambda_{K-1}}{\varepsilon_K \, E(K)} \tag{A.1-20}$$

Two possible cases exist:

Case 1: $D(t)$ represents creep compliance. This is the case with which

this section is concerned. In this case $D(t)$ is an increasing

function of time and

$$\frac{D(t_{K+2} - t_K)}{D(t_{K+2} - t_{K+1})} > 1 \tag{A.1-21}$$

<u>Case 2</u>: D(t) **represents relaxation modulus.** This case corresponds to
that considered in references 1.2 and 1.4 . In this case D(t)
is a decreasing function of time and

$$\frac{D(t_{K+2}- t_K)}{D(t_{K+2}- t_{K+1})} \quad < \quad 1 \qquad\qquad (A.1\text{-}22)$$

If the intervals are gradually increasing, the second term on the left side
of (A.1-20) is much less than unity and the inequality is satisfied, except
in extreme cases. This is the case in the problems solved in references
(1.2) and (1.4).

In the first case, however, the second term on the left side of (A.1-20)
is not much less than unity, as one of factor in that term is much greater
than unity, and the other much less than one. Hence unless proper sub-
division of [0,T] is made, the inequality (A.1-20) cannot be satisfied
and a possibility of increasing error exists for many types of partitions
of the interval [0,T].

5. Data Reduction:

From Fig. A.1.1 it is seen that the data for short times is not avail-
able (particularly D(o)). Unfortunately, this short time data plays an
important role in the calculations as it is involved in the calculation of
E at every subsequent time. From the above discussion it is seen that the
accuracy of the calculated values of E depend, to a large extent, on the
accuracy of short time values of D; which are either not available or
available only as an approximation. Hence a best estimate must be made
for the short time data.

D(t) is an increasing function of time with continuously decreasing derivative. This fact is used as a guide in estimating the short time data. The original experimental data is given as a graph between D(t) and log t. It is very difficult to determine on this scale whether D(t) is increasing or decreasing. Hence the short time data is replotted (Fig. A.1.2) as a graph of D(t) versus t. A smooth curve with continuously decreasing slope is drawn passing through most of the data points and this curve is extrapolated to t = o. This curve is then taken as the correct representation of the short time data.

6. An Example:
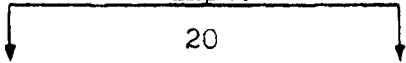
A Fortran program has been written for the calculation of relaxation modulus from creep compliance as given by equation (A.1-9). A copy of this program is presented in Table A.1-1. Taking creep compliance data from Figures A.1.1 and A.1.2 the relaxation modulus has been calculated for times up to 20,000 seconds. Since the results and data are interchangeable in equation (A.1-9) the creep compliance has been calculated using the above calculated values of relaxation modulus as the input data. The results of both these calculations are shown in Tables A.1-2 and A.1-3. The calculated values of the relaxation modulus are shown plotted versus log t in Fig. A.1.3.

References:

1.1.   A. J. Stavaman and F. Schwarzl: "Linear Deformation Behavior of
       High Polymers." Die Physik der Hock Polymeren. P. 1-125. Ed.
       by H. Stuart, Springer-Verlag, Berlin, 1956.

1.2.   I. L. Hopkins and R. W. Hamming: "On Creep and Relaxation ."
       Journal of Applies Physics. P. 906-909, Vol. 28, No. 8. 1957

1.3.   E. H. Dill and C. Fowlkes: "Photoviscoelastic Experiments I."
       The Trend in Engineering. P. 5-10, Vol. 16, No. 3. 1964.
       The University of Washington.

1.4.   E. H. Lee and T. G. Rogers: "Solutions of Viscoelastic Stress
       Analysis Problems Using Measured Creep or Relaxation Function."
       Journal of Applied Mechanics. P. 127-133, March, 1963.

TABLE A.1-2
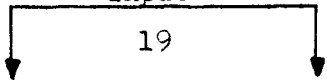
Input data for mechanical relaxation from mechanical creep

Time (sec.)	Creep D(t)/D(o)	Mechanical Relaxation
	Input 20	Output
0.0	1.0	0.8
1.0	1.25	0.640
2.0	1.50	0.526869
3.5	1.75	0.411094
6.0	2.10	0.322320
10.0	2.55	0.235700
20.0	3.30	0.197657
35.0	4.10	0.161736
60.0	4.95	0.137943
100.0	5.90	0.110897
200.0	7.35	0.102139
350.0	8.60	0.092821
600.0	9.55	0.086904
1000.0	10.50	0.079325
2000.0	11.60	0.077144
3500.0	12.5	0.073678
6000.0	12.95	0.072718
10000.0	13.30	0.071856
20000.0	13.6	0.072256
35000.0	13.75	

$$D(0) = 0.4 \times 10^{-3} \ \text{in}^2/\text{lb}.$$

TABLE A.1-3

Input data for mechanical creep from calculated mechanical relaxation.

Time (sec.)	Relaxation Input	Creep Output
	19	$E(t)$ x 0.4 x 10^{-3} lb/in^2
0.0	0.8	1.562500
1.0	0.640	1.838699
2.0	0.526869	2.239464
3.5	0.411094	2.881257
6.0	0.322320	3.799231
10.0	0.235700	5.838305
20.0	0.197657	5.889435
35.0	0.161786	7.189413
60.0	0.137943	8.698941
100.0	0.110897	11.320508
200.0	0.102139	10.686227
350.0	0.092821	11.721610
600.0	0.086904	12.728606
1000.0	0.079325	13.942489
2000.0	0.088144	13.511937
3500.0	0.073678	13.982328
6000.0	0.072718	14.177561
10000.0	0.071856	14.052345
20000.0	0.072256	

Fig. A.1.1. TENSILE CREEP COMPLIANCE

Experimental Curves all fell within the
dashed Curves and were smooth

T = 21°C

D(t) x 10⁻⁵ in²/lb

Time (seconds)

Fig. A.1.2. TENSILE CREEP COMPLIANCE

(Expanded Portion of Fig. A.1.1.)
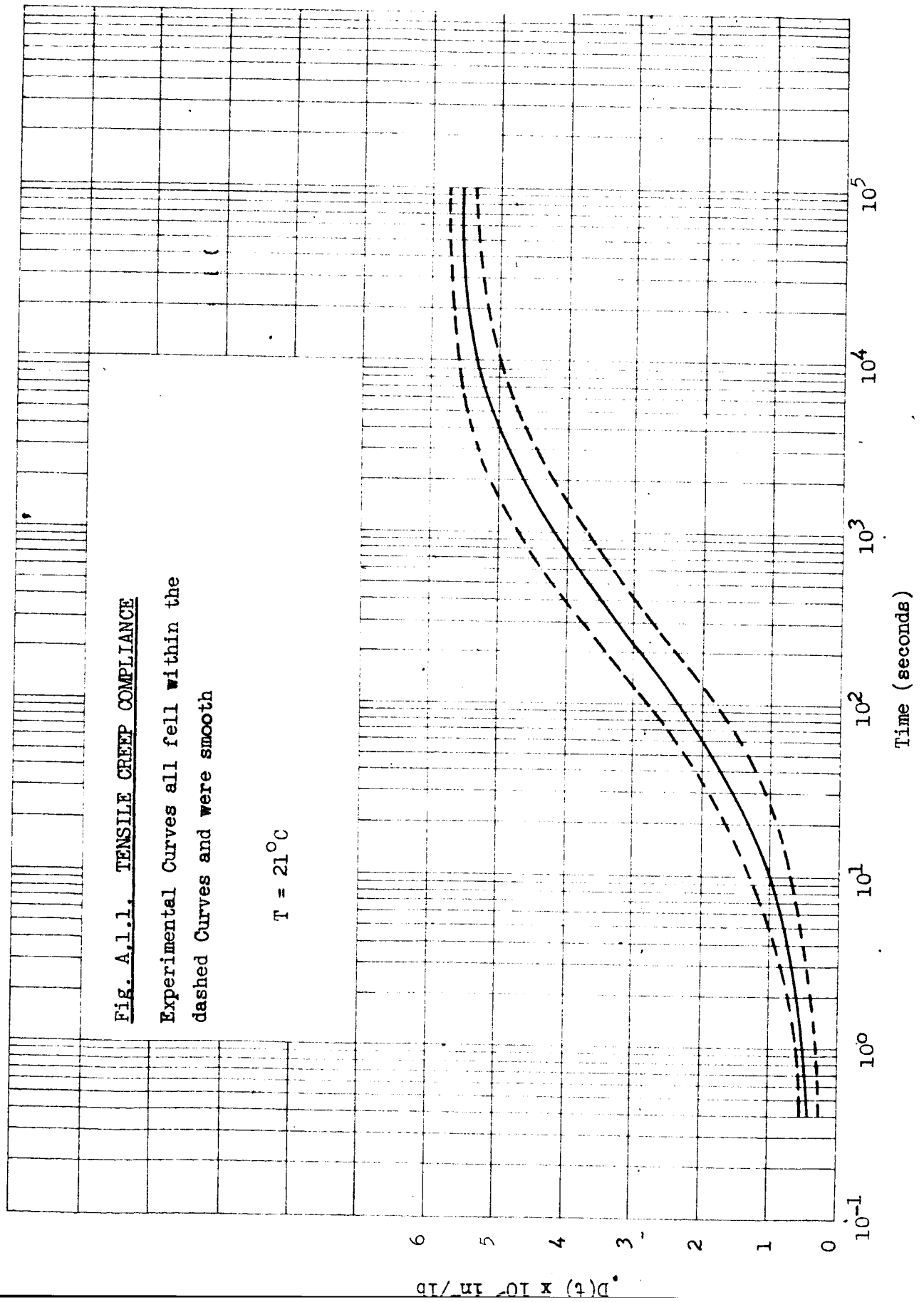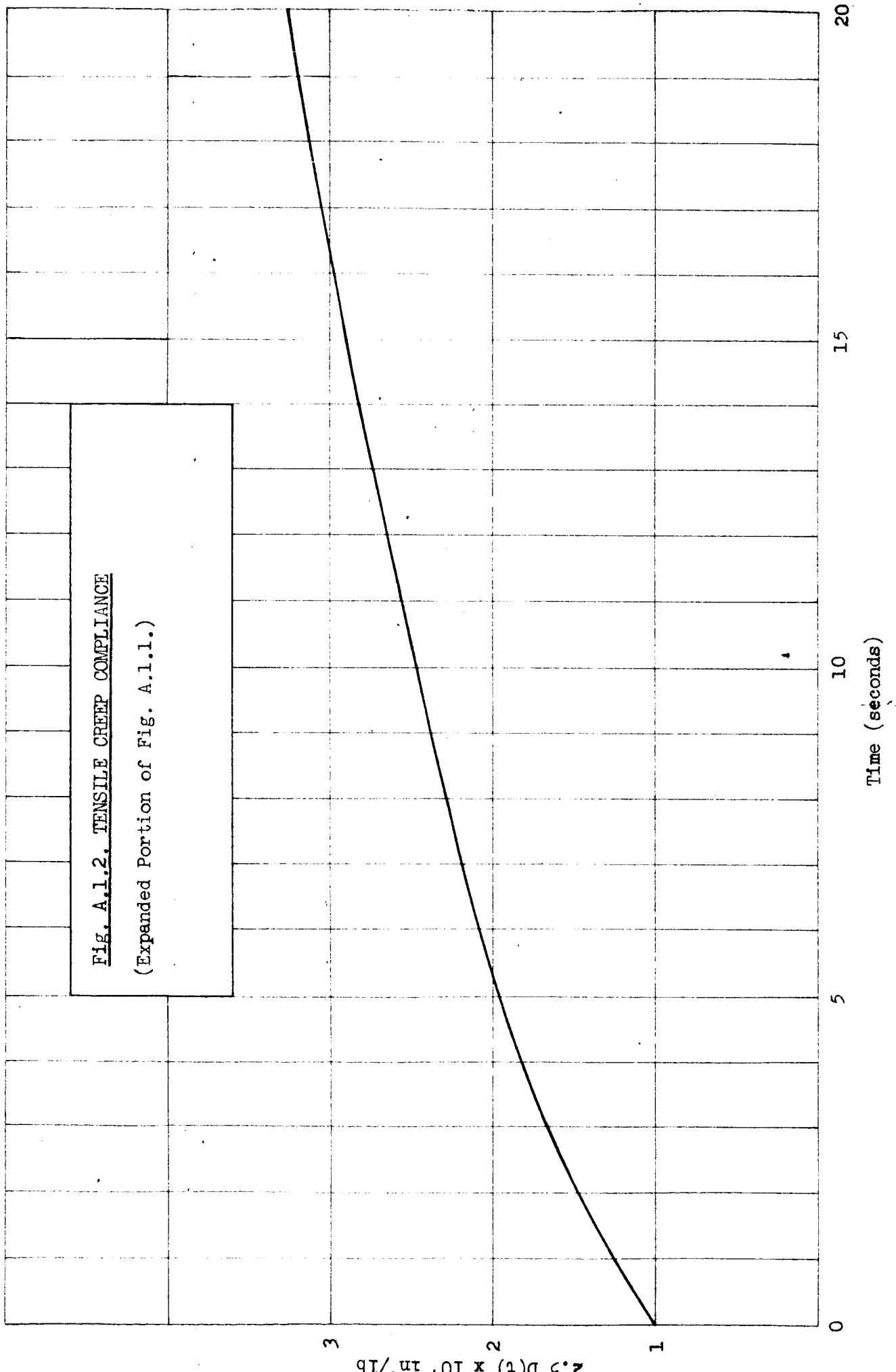
Fig. A.1.3. CALCULATED RELAXATION MODULUS

$E(0) = 2.5 \times 10^3$ 16/in^2
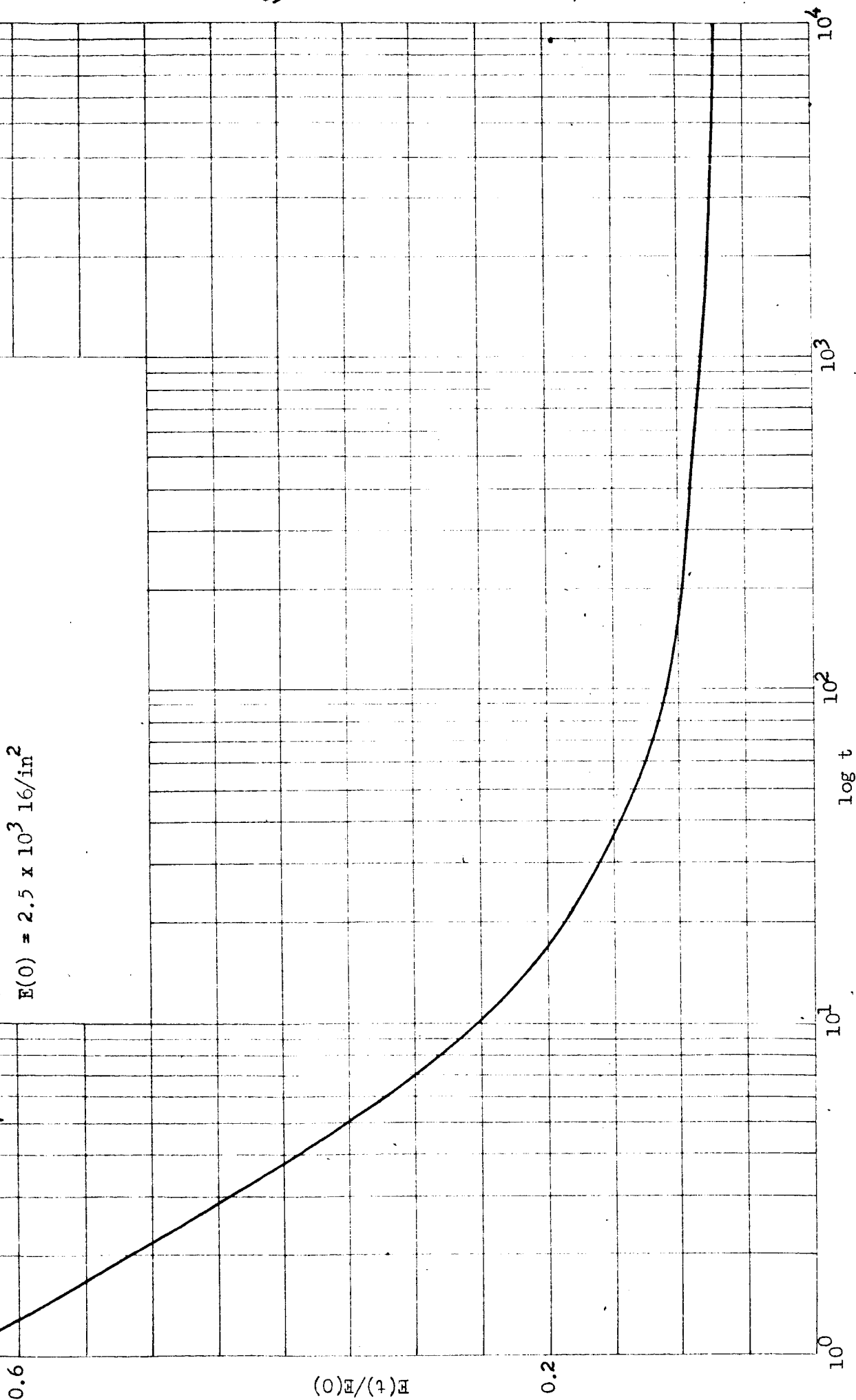
APPENDIX A.2.

Preparation of Model Material

The model material must be transparent, exhibit birefringence dependent upon the mechanical state and have viscoelastic properties similar to those of the prototype. The first phase of the development of a model material consisted of mixing 25 test batches of epoxy and polyester resins and silicone rubbers with various plasticizers and hardeners. The more promising candidates were selected from the 25 original mixes and were cast into sheets. Tensile specimens were cut from the sheets and creep tests were performed to determine the best model material.

Commercial flexible polyester (Reichold Chemicals Inc. #8151) and with 1% MEK Peroxide is a useable model material; however it has low birefringence and relatively high absorbtivity. The main disadvantage of this material is the difficulty of mixing reproducible batches.

An epoxy (CIBA, Araldite 502) plasticized with varying amounts of Di-n-butyl Phthalate and cured with CIBA, Araldite 151 produces a low-modulus, transparent viscoelastic material. The birefringence of this material is not as high as the material used for subsequent experiments.

Mixtures of CIBA, Araldite 502 and 508 cured with 10% TETA are birefringent but have a high modulus and a very short relaxation time.

The material selected was an epoxy mixture made from components manufactured by the CIBA Co. Three components are used: Araldite 502, a rigid epoxy used for photoelastic testing and as a structural adhesive, Araldite 508, an epoxy flexibilizer and Araldite 963, an amine hardener. This material

was selected because of its high birefringence and because its relaxation time could be varied over a wide range by simply varying the proportion of flexibilizer used in the mix.

If Araldite 6010 is substituted for Araldite 508 a final material is obtained which is of slightly higher modulus for the same proportions and has nearly identical birefringence.

Tests were made to determine the amount of permanent viscous flow in the material. Creep tests were performed on tensile specimens at the maximum level of stress used in subsequent model testing. The specimens were then removed from the creep test apparatus and allowed to relax for several days. Measurements of the initial and final lengths of the specimens showed that the permanent strain due to viscous flow was less than 0.1%.

A mold was prepared to cast sheets of the material 1/4 inch thick and two square feet in area. Sheets of plate glass were used for the two faces of the mold, 1/4 inch surgical tubing formed a gasket between the sheets on 3 sides, the thickness being controlled by 1/4 inch spacers placed between the glass faces and outside of the gasket.

This epoxy formulation is a very tenacious adhesive and care must be taken to completely cover all surfaces exposed to the epoxy with a release agent. To insure mold removal the surfaces must first be cleaned with a solvent, three light coats of a Carnuba-base wax are then applied. allowing each coat to partially dry and polishing it before application of the next coat. Finally all surfaces are sprayed with a polyvinyl alcohol solution which when properly applied and dried forms a smooth water soluble film.

Some experimenting was required to evolve a spraying technique which would give a glassy smooth surface. The Carnuba base wax and the polyvinyl alcohol solutions are available through most commercial fiberglass supply houses.

At room temperature the viscosity of the uncatalyzed resin components is such that small air bubbles will become trapped in the mixture while stirring, resulting in a poor casting. If the mixture is placed in a vacuum some bubbles will be drawn out but the mixture will catalyze before all of the bubbles are gone. If the resin components are heated to $130^{O}F$ prior to mixing the viscosity is lowered sufficiently to allow entrained air to float off before solidification. This approach has been used to cast a number of very successful sheets of model material. Heating the components reduces the pot life of the mixture to less than five minutes after the hardener is added. Final mixing and pouring into the mold must be done quickly. A paddle mounted at the end of a rod and driven by a slow speed drill motor facilitates mixing.

The resin is cured in an oven for 12 hours while the temperature is maintained at $160 \pm 5^{O}F$. The mold is taken from the oven and the clamps removed. The rubber-tube gasket is stripped off and a razor blade is used to cut around the edges between the cast sheet and the glass. Wooden wedges are slowly pressed between the edges of the glass faces while the sheet is held under running water.

Careful prying will remove the mold after about five or ten minutes. The newly cast sheet is then washed to remove the mold release agent and placed on a flat paper or teflon coated surface to relax to equilibrium.

After the sheet has relaxed for a day models and specimens may be laid out on the sheet. These shapes are then cut from the sheet on a band saw at high speed with a skip-tooth blade.

Machining accurate models from this material presents some problems. If the material is clamped lightly in a vice or a chuck it relaxes and becomes loose. If the vice or chuck is tightened enough to hold the part, the part becomes distorted so that a flat surface or a square edge after removal from the jig is no longer flat or square. Another difficulty appears when a deep cut is made. During a deep cut the tool mashes the material under it slightly so that after relaxation the part is larger than expected.

These peculiarities have been dealt with by using double-sided adhesive tape to hold the model to the face plate for turning operations and by taping the jaws and bottom of the vice for milling operations. If sharp corners are required, the model may be taped on both faces and sandwiched between 1/8 inch plexiglas, the sandwich being then taped on both edges and very lightly clamped in a vice. If a particular dimension is desired, it should be approached slowly with fine cuts. When the machine has reached the final setting, the specimen is allowed to relax for 15 to 30 minutes and the last cut is made at the same machine setting. This process can be repeated if extreme accuracy is required.

Flat surfaces and edges are cut with a sharp fly cutter running at high speed. Circular section can be turned in a lathe at high speed using a sharp pointed tool with about 35°. Holes may be drilled if the model is sandwiched between plexiglas and the drill is sharp and turned at high speed.

For some models it is helpful to cool the model in a refrigerator immediately before machining. The material is quite stiff at $40^{\circ}F$.

The models used to date in the project have been machined dry. If a

coolant is to be used experiments should be made on small scrap pieces to test if the coolant accelerates the growth of edge fringes. Water, for example, will considerably accelerate the growth of edge fringes.

Finished models stored at normal room conditions will be useable for several weeks or more before edge fringes become excessive. Carnuba wax, acetone, n-heptane, methylenedichloride and water will accelerate edge fringe growth, a dessicating atmosphere will retard edge fringe growth. The models reported have all been stored at room conditions.

APPENDIX A.3.

Calibration of Model Material

The photoviscoelastic material is calibrated in a tensile creep test. A typical tensile specimen 1/4" thick by 0.6" wide by 6" long is shown in Fig. A.3.1. Usually six or eight calibration specimens are cut from each sheet of model material. Experiments have shown that specimens cut from different locations and orientations in the sheet yield the same creep behavior.

The entire batch of specimens may be stacked on edge and milled to a uniform width in one set up with a fly cutter. Aluminum tabs are bonded to each end of each specimen with Eastman 910 and the specimens are placed on edge on a flat surface to relax before testing. By having six or eight specimens any one specimen has enough time to relax between tests while the other specimens are tested.

Two creep calibration jigs are shown in Figures A.3.2 and A.3.3. In both jigs the load is applied to the specimen by releasing a weight and total specimen deformation is measured with a differential transformer. The load is measured with a beam instrumented with strain gages. The load cell output allows one to see in detail the shape of the input-load step in creep testing and records the load relaxation in relaxation testing. The time interval during loading is approximately 0.2 seconds. A calibrated clip gage bent from a 0.010 inch thick strip of aluminum and instrumented with strain gages is used to measure the changing width of the specimen as it creeps. This measurement allows Poisson's ratio to be computed.

All strain gages and differential transformers are powered and their outputs recorded on a 6-channel Brush recorder with a calibrated time base.

The fringe growth is also automatically recorded. The output of a mercury-arc lamp is filtered with a Wratten 77A filter which passes the green line (5460 $\overset{o}{A}$) of mercury. This light is passed through a polarizer (Polaroid) through the creep test specimen, through a second polarizer with axis at right angles to the first and then into a photomultiplier tube. The output of the photomultiplier tube shows the periodic increasing and decreasing of light intensity. The maximums and minimums of this curve are well defined and represent increasing half fringe orders.

Both creep test jigs have electric resistance heaters which are automatically controlled to maintain a set temperature $\pm$ 0.2^{o}F over the range from room temperature to 150°F. Circulating fans within the test chambers insure a uniform temperature. One creep test jig, Figure 4.3.2. is equipped with a well insulated test chamber and four thermoelectric cooling plates. The plates are powered with 12V, 100A d.c. and controlled to maintain a set temperature $\pm$ 0.2^{o}F from room temperature to 30°F below room temperature.

The glass transition temperature for the model material is in the region of room temperature. Small changes in temperature (5°F) cause marked changes in mechanical behavior. At 130 to 150°F the relaxation time is very short and the material is rubbery while at 32°F it is quite rigid.
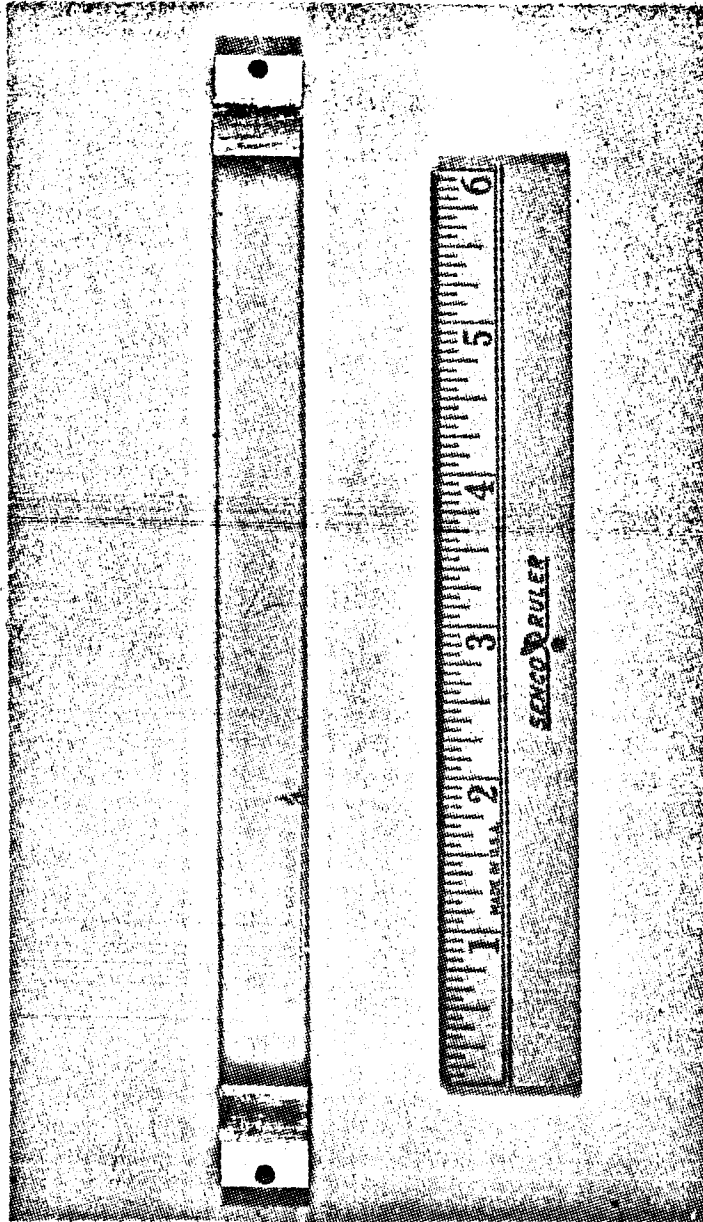
Figure A.3.1: Tensile Creep Specimen
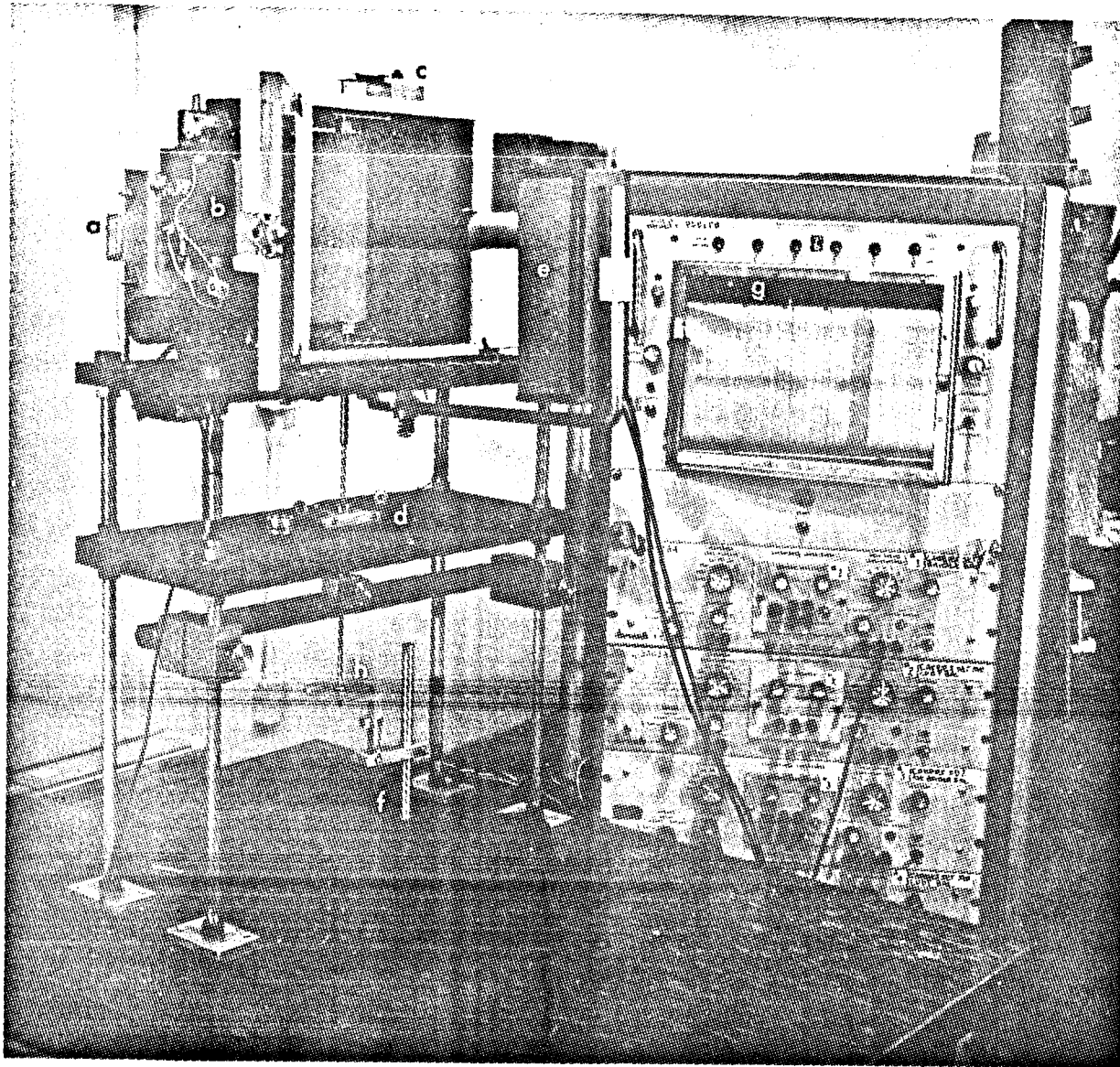
(a) light source, filtered Hg arc
(b) temperature controller
(c) load cell
(d) differential transformer
(e) photomultiplier tube
(f) calibrator
(g) brush recorder
(h) weight pan

Figure A.3.2: Tensile calibration bench
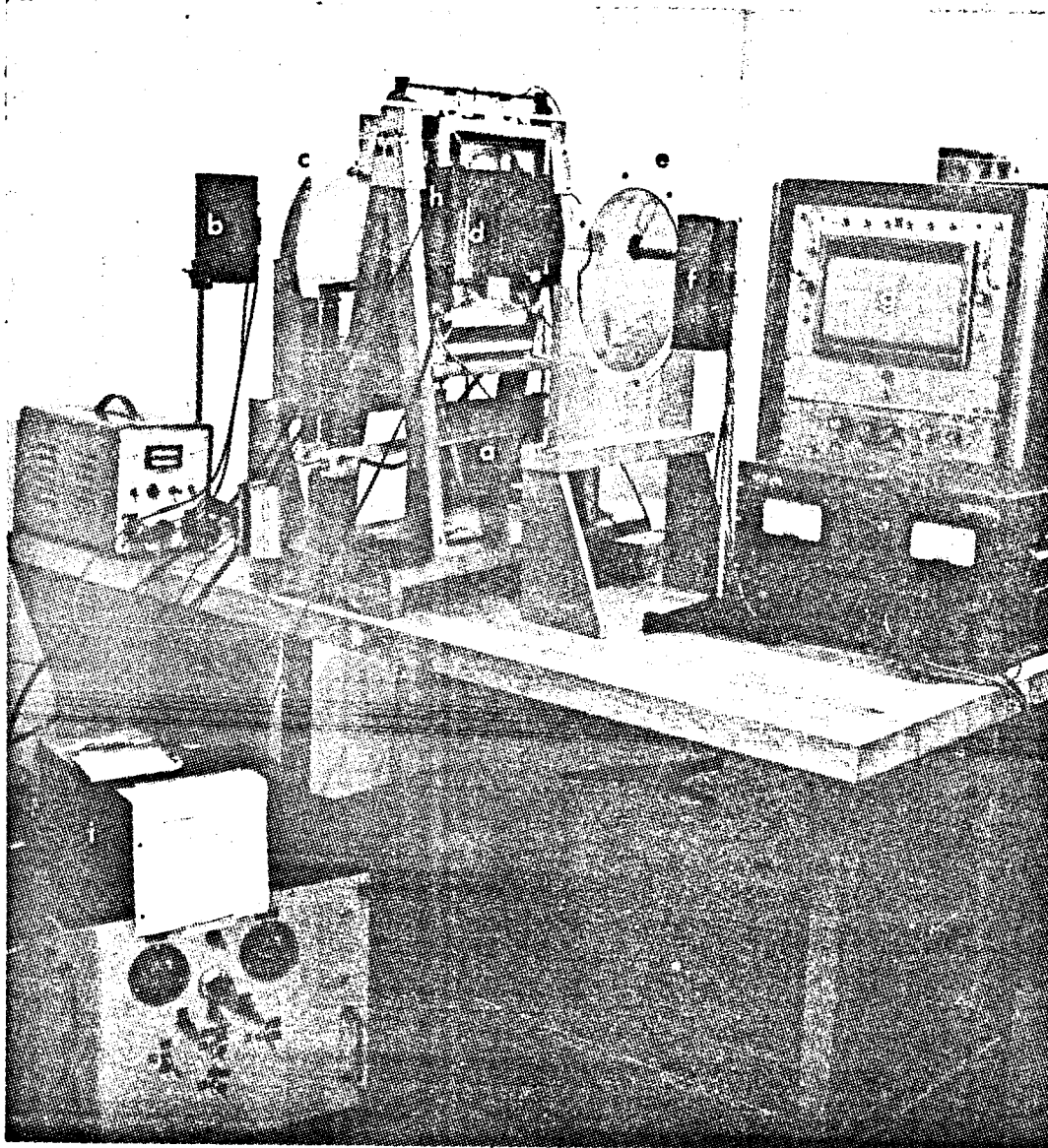
(a) loading frame
(b) light source, filtered Hg arc
(c) Polarizer and 1/4 λ plate
(d) tensile specimen
(e) analyzer and 1/4 λ plate
(f) photomultiplier tube
(g) brush recorder
(h) thermoelectric coolers
(i) power supply and control for
    coolers

Figure A.3.3:   Tensile Calibration Bench

Thermal Properties

The coefficient of thermal expansion was measured in the jig shown in Figure A.4.1. The specimen rests on a Teflon coated surface of the jig and one end is bonded to the jig. A metal tab is bonded to the free end of the specimen and a fine wire soldered to the tab leads to one terminal of an ohmmeter. The ohmmeter registers a short circuit when the micrometer is brought to touch the free end of the specimen. By using this system the micrometer measurements may be repeated to within ± 0.0002. Such accuracy cannot be obtained by mechanical feel due to the low modulus of the model material.

The jig was placed in an oven, allowed to come to equilibrium at several temperatures and changes of length were measured. The hysteresis was determined by approaching a given temperature from above and below and was small. The temperature was varied between 70 and 110°F and the coefficient of thermal expansion was calculated to be $1.01 \times 10^{-4} \frac{in}{in-°F} \pm 5\%$. Correction was made for the expansion of the measuring jig.

The coefficient of thermal diffusivity was calculated by measuring the temperature history at the centers of two slugs immersed in a constant temperature bath. The temperatures were measured with iron-constantan thermocouples cast into the slugs. The constant temperature bath was water in a large laboratory thermos bottle.

The slugs and the bath were allowed to reach their separate equilibrium temperatures as determined by the thermocouple readings. The slugs were then immersed in the bath and stirred vigorously. The temperature history being recorded on a calibrated, self-balancing potentiometer. A rectangular

and a cylindrical slug were each tested several times to insure re-
producibility. The thermal diffusivity was calculated for both geometries
at several points in the temperatures history and was 32.9×10^{-4} ft^2/hour
$\pm 4\%$.

The specific heat was determined by a calorimeter test and was
0.003 BTU/lb.$^{\circ}$F $\pm 8\%$. The density of the model material is 0.046 lb/cubic
inch. From these values the thermal conductivity was computed to be 0.131
BTU/hr. ft$^{\circ}$F $\pm 10\%$.
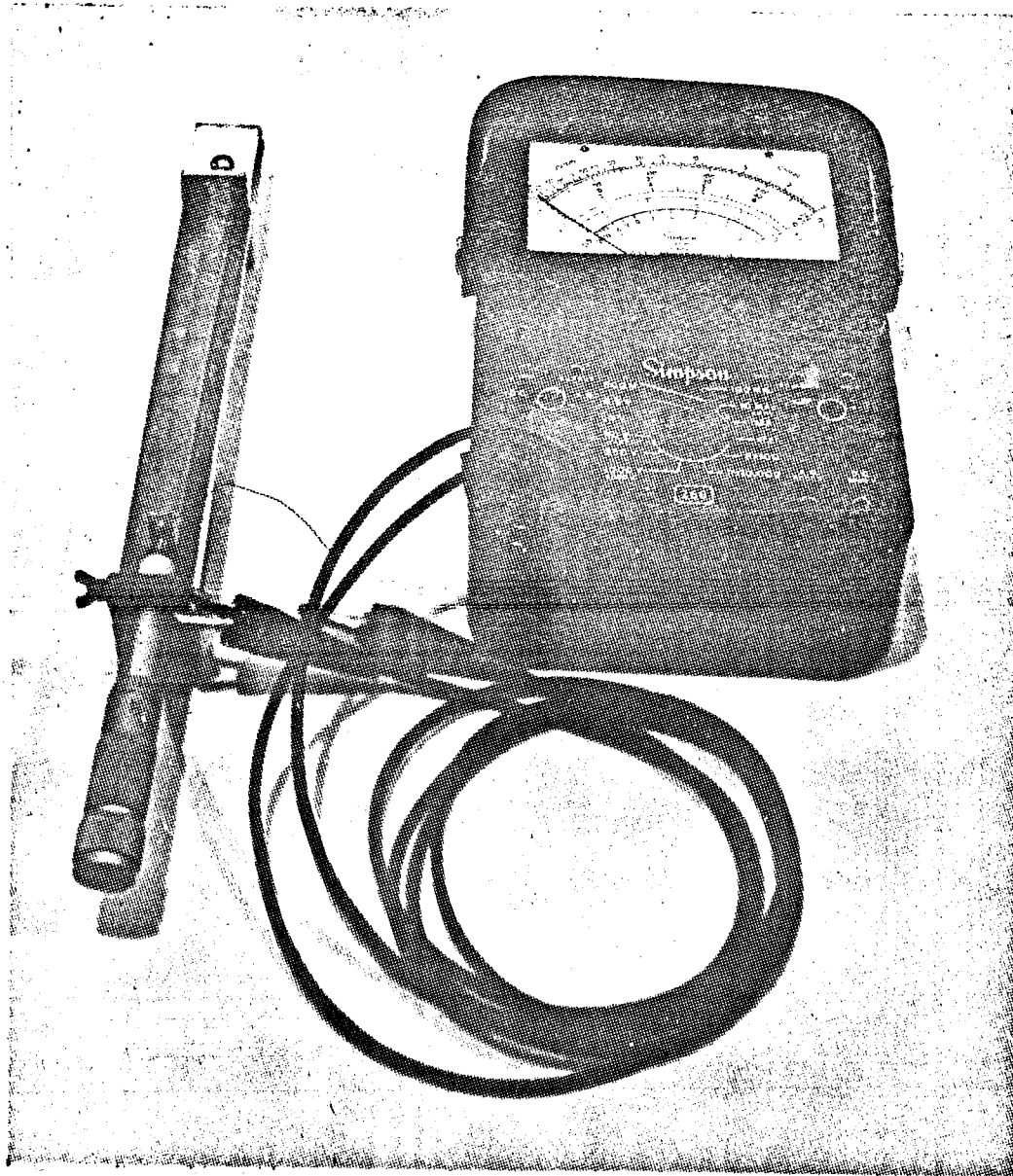
Figure A.4.1: Apparatus for Thermal Expansion Determination

Wave Speed

The speed of a weak pulse through various model materials was measured. This measurement was made in order to get the limiting value of the short-time modulus using the relationship (2.7-8.)

The specimen was a rectangular bar 1/4" x 1/2" x 6' long. A 1/16" thick aluminum tab was bonded to the driven end of the specimen and a wire attached to the tab and led to an oscilloscope. The pulse was generated by a rod swung on strings as a pendulum. Another wire led from the rod through a battery to the oscilloscope. When the striker rod hit the metal tab on the end of the specimen a trigger pulse was generated. A crystal pickup was bonded to the other end of the specimen with double-backed tape. The pickup and the specimen were positioned on a layer of foam rubber. This arrangement is shown in Figure A.5.1.

The output trace of the crystal pickup was photographed from the oscilloscope screen for a calibrated sweep rate, Figure A.5.2. The sweep was started when the striker hit the metal tab on one end of the specimen. The knee in the pickup output corresponds to the arrival of the pulse at the other end of the specimen. The interval between the start of the trace and the knee is thus the time required for the elastic pulse to traverse the specimen. Experiments were run with specimens of various lengths which showed that end effects were negligible.

The graphs in Figures A.5.3. and A.5.4. show the short-time modulus for varying amounts of flexibilizer and the dependence of short-time modulus on temperature in the mixture used for the reported models.
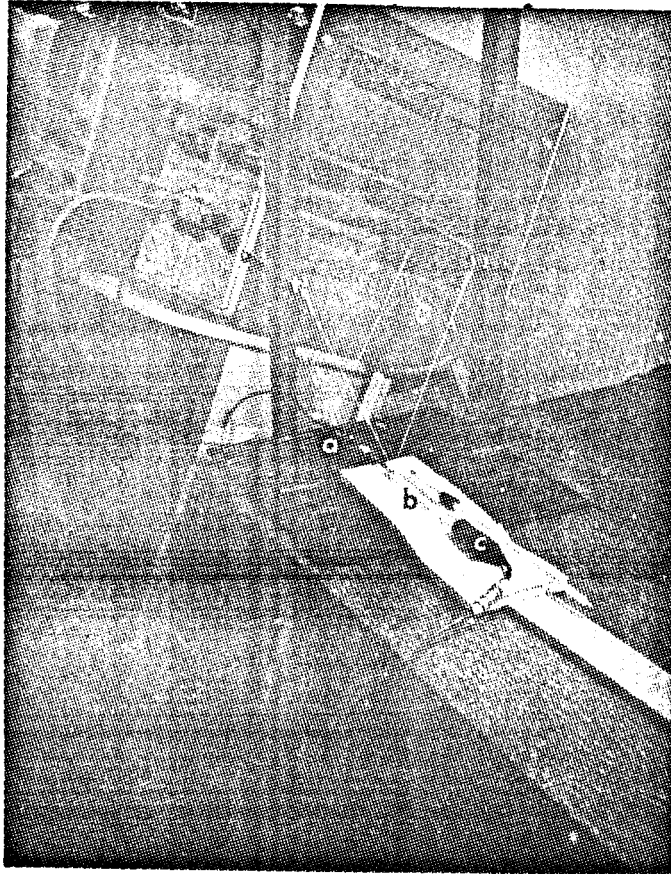
(a) striker and trigger
(b) model
(c) crystal pickup

Figure A.5.1:   Apparatus for measuring pulse speed
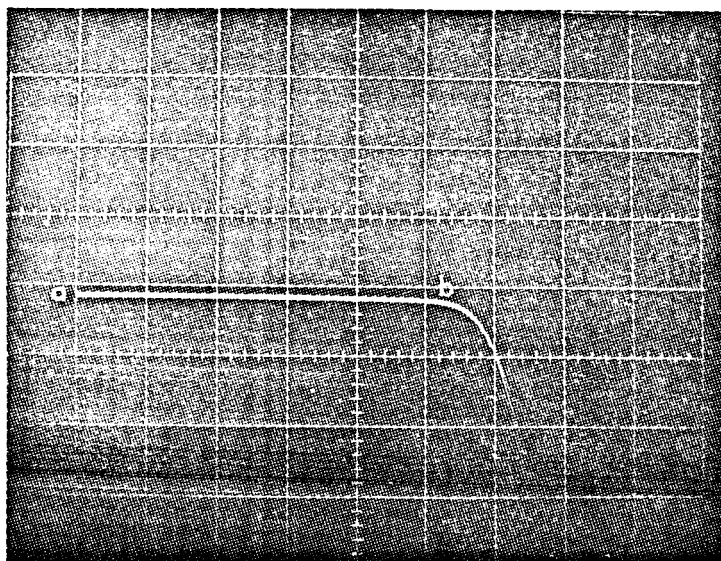
Temperature = 78°F
Sweep rate = 20 msec/cm

(a) initiation of pulse
(b) arrival of pulse

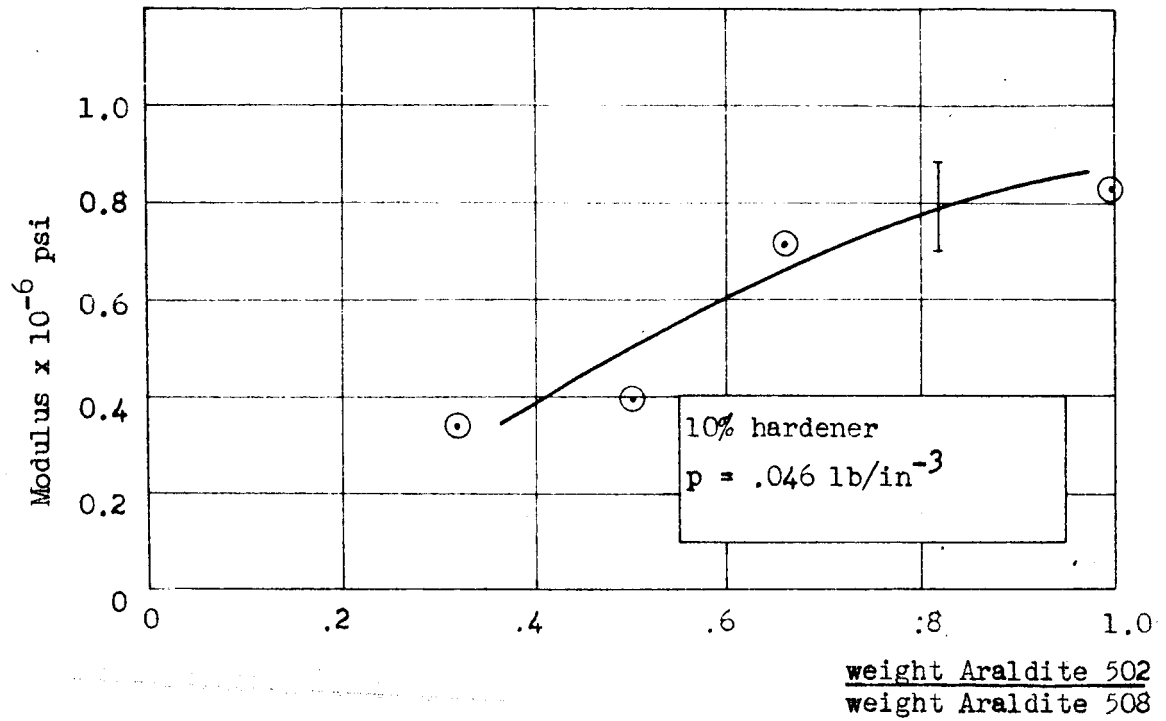Figure A.5.2: Oscillograph trace showing arrival of pulse
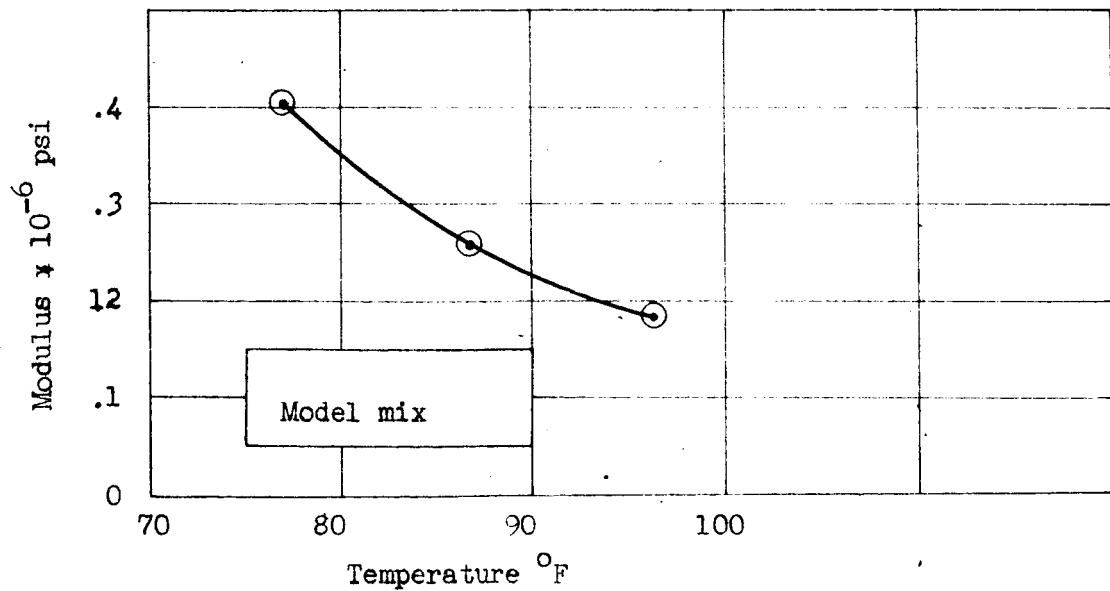
Fig. A.5.3.   Short-time modulus.

Fig. A.5.4.   Short-time modulus at various temperatures

APPENDIX A.6.

Rotating Elements Bench

The axes of principal stress at a point in some models change with time. During a test these changes may be determined by measuring the angle change of a polarizing axis as it is adjusted to keep the isoclinic fringe on the point and by knowing the fringe growth behavior from a tensile creep test. An equivalent method consists of rotating the polaroids continuously, while watching the point in question. As the isoclinic sweeps through the point during each revolution the angle is noted. This latter system is used in the rotating element bench.

The bench is shown in Figure A.6.1. Three light sources may be used: a point source, d.c. mercury arc with a Wratten 77A filter, a distributed source, a.c. mercury arc and a green fluorescent, diffused source. Condensing lenses are used with the point source light to get parallel beam through the specimen. The lenses are removed from the light path when the distributed light sources are used.

Each lens stand is fitted with a ball-bearing carrier to support the rotating polaroid around its outside edge. The polaroid is driven by a stepping solenoid through a positive drive, link chain. When the solenoid is pulsed the polaroid advanced 9°. The pulse rate is continuously adjustable from 5 pulses per second to 1 pulse per 2 minutes.

A 16 mm Cine Special camera is used to record the fringe patterns. Mounted next to the model and in the field of view of the camera is a digital timer with 1/10 second minimum reading. Incorporated in the timer is a numbered wheel driven by a small rotating solenoid which is

tied to the driver solenoids indicating the angle of the polarizing axes.

During the first minute after loading the camera is run at 16 frames per second to capture the rapidly changing fringe patterns. The frame rate is then reduced to 1 frame/second. As the fringe patterns approach equilibrium the frame rate is correspondingly reduced.

Loading Frame:

A model is mounted in grips in the loading frame and the upper grips are connected to a load cell through a universal joint. Two load cells of differing sensitivities are available. Four loading patterns may be used; constant load, constant strain, constant strain rate and sinusoidal strain.

Constant loads are applied by hanging weights on the specimens and constant strains are applied by using a heavy weight to force the loading mechanism against a present stop. Constant strain rate is applied to the model by driving the lower grips with a 220 volt, 3 phase motor operating through a gear change set. By changing the gears the strain rate may be varied between 0.0418 and 5.75 inches/minute. A spring loaded can and tappet mechanism supplies the sinusoidal strains, Figure A.6.2. The mechanism is driven by an electric motor through a Zeromax speed reducer. The frequency is continuously variable from 0 to 400 cycles/minute and the maximum amplitude may be varied between 0 and 0.2 inches, by inserting appropriate ca   All of the loading mechanisms are mounted in a rigid frame. Strains are measured with differential transformers and read out on a Brush recorder or an oscilloscope equipped with a camera.
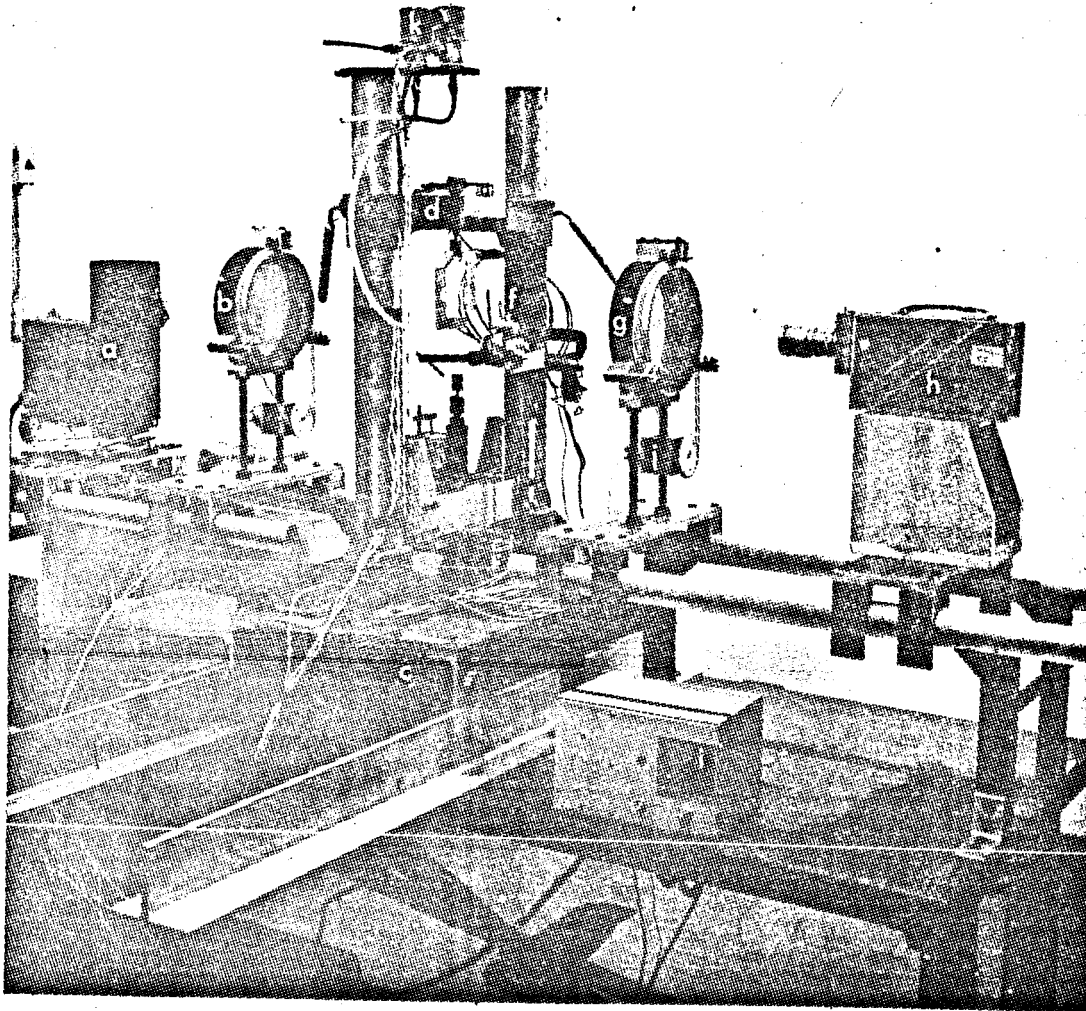
(a) light source, filtered Hg arc
(b) Polaroid, rotating
(c) loading frame
(d) load cell
(e) model
(f) timer and angle indicator
(g) Polaroid, rotating
(h) camera
(i) rotating Polaroid control and power supply
(j) drive solenoids
(k) solenoid valves for pressure loading

Figure A.6.1: Photoviscoelastic Bench
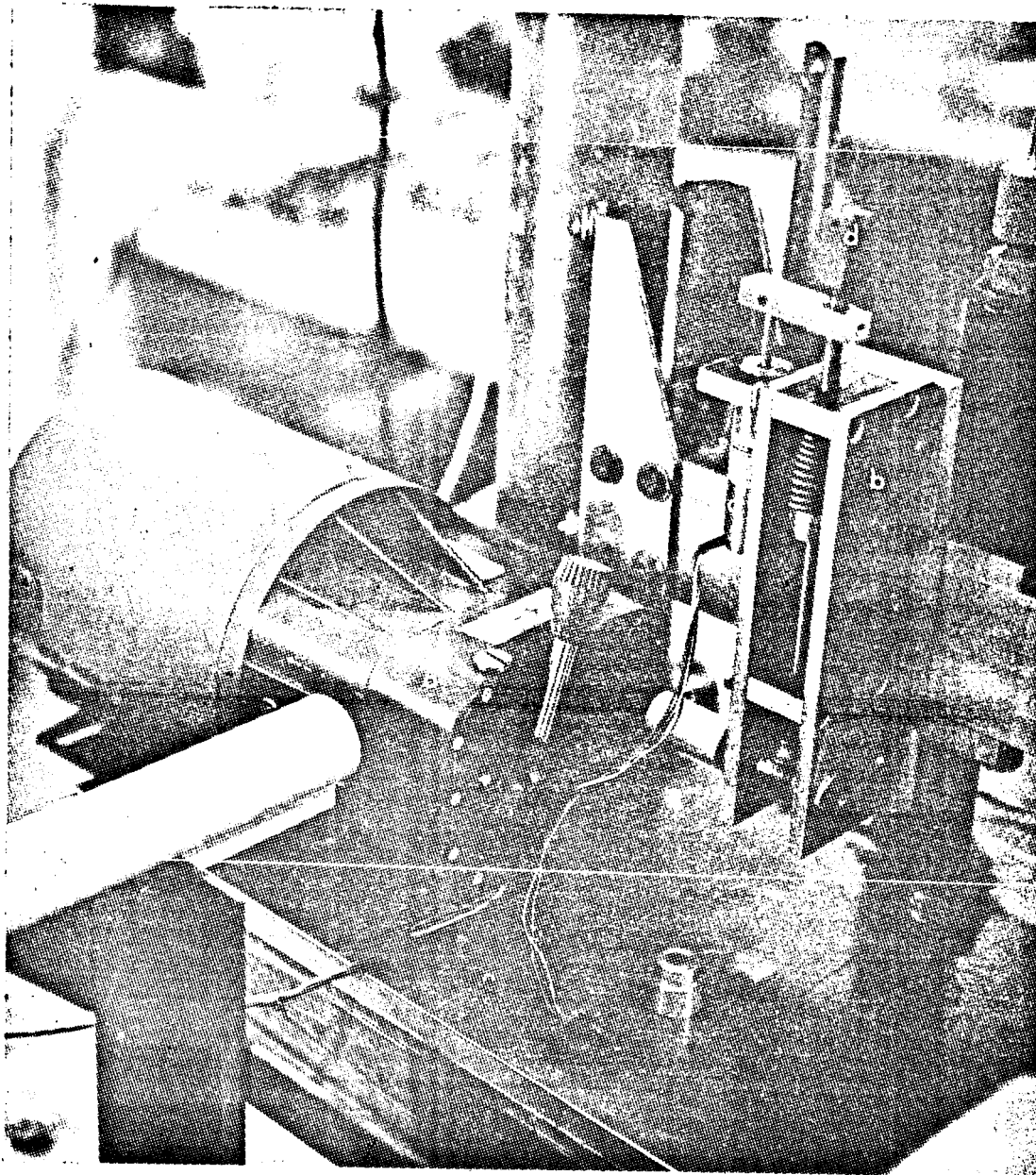
(a) variable speed drive
(b) cam and tappet
(c) differential transformer
(d) grip

Figure A.6.2: Oscillating loader

APPENDIX A.7.

Pressure Loading Device and Heater

Model: The model and tensile calibration specimens were cut from a 1/4" thick sheet of photoviscoelastic material. The model dimensions are shown in Fig. A.7.1. The shape chosen simulates a solid propellant motor with a four-point star perforation.

Loading Jig: A loading jig was built to apply a uniform pressure to the outside edge of the model. The jig is pictured in Figure A.7.2. Pressure is applied through a 0.010" thick laytex diaphragm. The diaphragm is designed to have enough slack to follow the model as it deforms without stretching thus maintaining uniform pressure.

The uniformity of the loading and the pressure efficiency of the diaphragm were determined with the elastic, Hysol 4485 specimens pictured in Figure A.7.3. Knowing the elasticity solution for the circular disc and the photoelastic fringe constant for the calibration model material one may calculate the effective pressure acting on the model. This compared to the gage reading of the air pressure acting on the diaphragm establishes the pressure efficiency of the jig. Non-uniformity in the pressure around the edges of the disc will cause the fringe pattern to depart from concentricity. A measure of this non-uniformity is the percent variation in fringe order around an imaginary concentric circle drawn on the model. A picture of a loaded calibration specimen is shown in Figure A.7.4. The pressure is uniform to within 10% and the jig efficiency (effective pressure/gage pressure) is 68%.

The model is sandwiched in the jig between two 1/4" Plexiglas guards. Polaroid is bonded to the model side of each guard. These guards serve to contain the thin laytex diaphragm and to prevent the low modulus model from buckling. A copious layer of thin oil separates the model from the guards. Calibration tests show that the friction is insignificant.

Tsts: An isothermal model was placed in the loading jig and loaded with a step input (approximately 0.1 sec rise time) of pressure which was maintained constant throughout the test. The changing fringe patterns were recorded on a 16 mm movie camera running at 16 frames per second. The apparatus is pictured in Figure A.7.5. The results of this test are discussed in the text.

In a second test the model was heated to an equilibrium temperature distribution. Heat was supplied by a star-shaped nichrome resistance heater

A preliminary test was run to determine the temperature distribution. A dummy model and guard of the same materials and dimensions of the test model and guard were placed in the loading jig. Holes 0.020" in diameter were drilled through the guard and into the model at several stations. These holes were filled with oil to minimize their effect on the temperature distribution. The model was heated to equilibrium with constant power input to the heater. A small iron-constantan thermocouple probe was placed sequentially into the holes to measure the temperature. Several tests showed that the temperature distribution could be repeated to within $\pm 1^{\circ}F$. The model and apparatus used for this test is shown in Figure A.7.6.

The test model was then placed in the jig and heated to equilibrium with the same heat input used for the temperature distribution determination. Two thermocouple wells were drilled in the test model to spot check the distribution. The model was then loaded as in the first test and the fringe patterns recorded with the 16 mm movie camera.

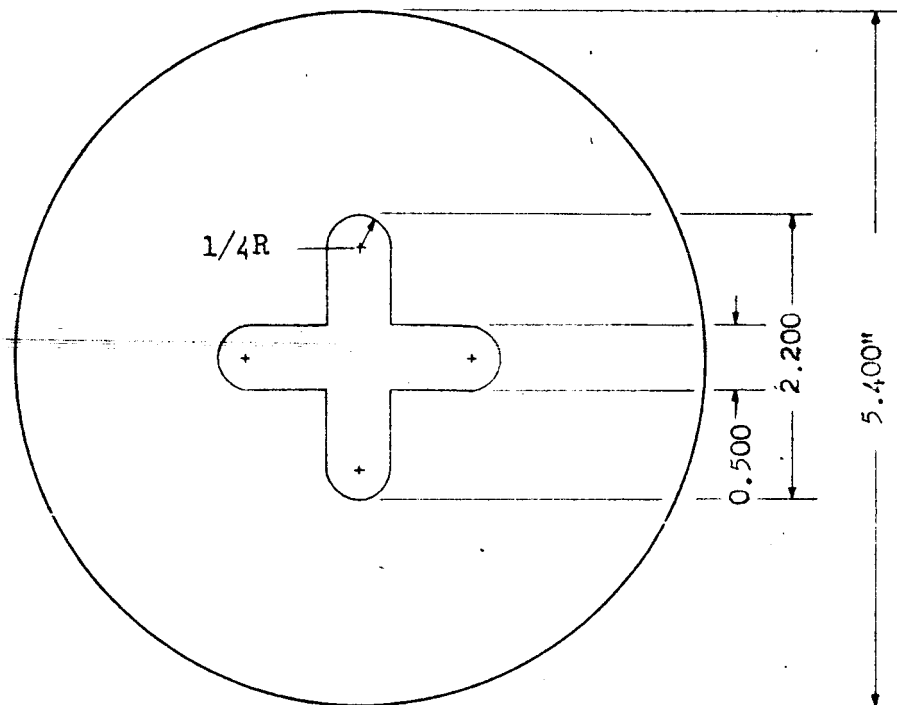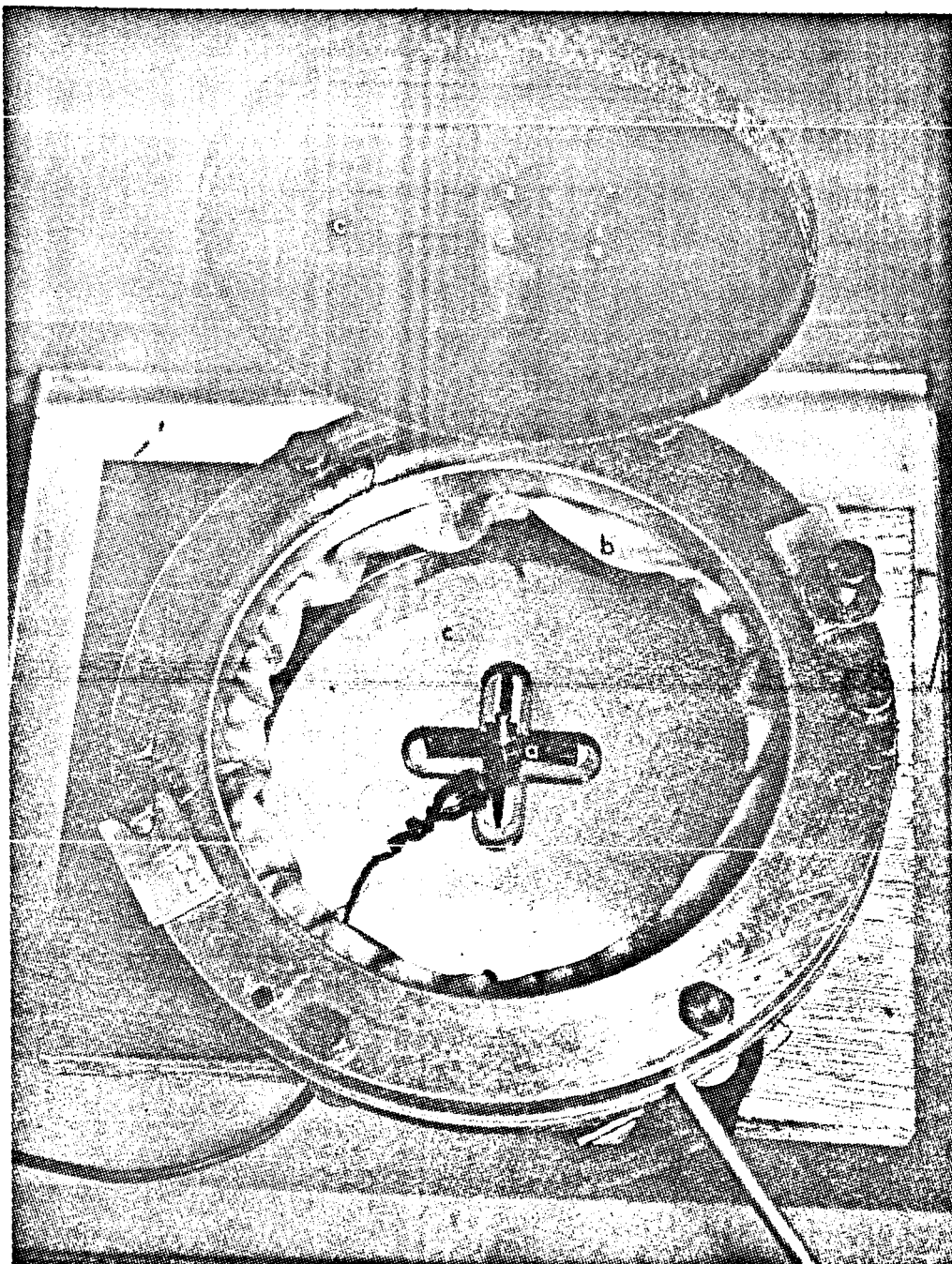The results of this test are discussed in the main body of the report.

Fig. 7.1.   Star Grain Model.

a) nichrome heater
b) laytex diaphragm
c) guards, (Polaroid laminated to plexiglas)

Fig. A.7.2. Pressure loading jig (model removed)
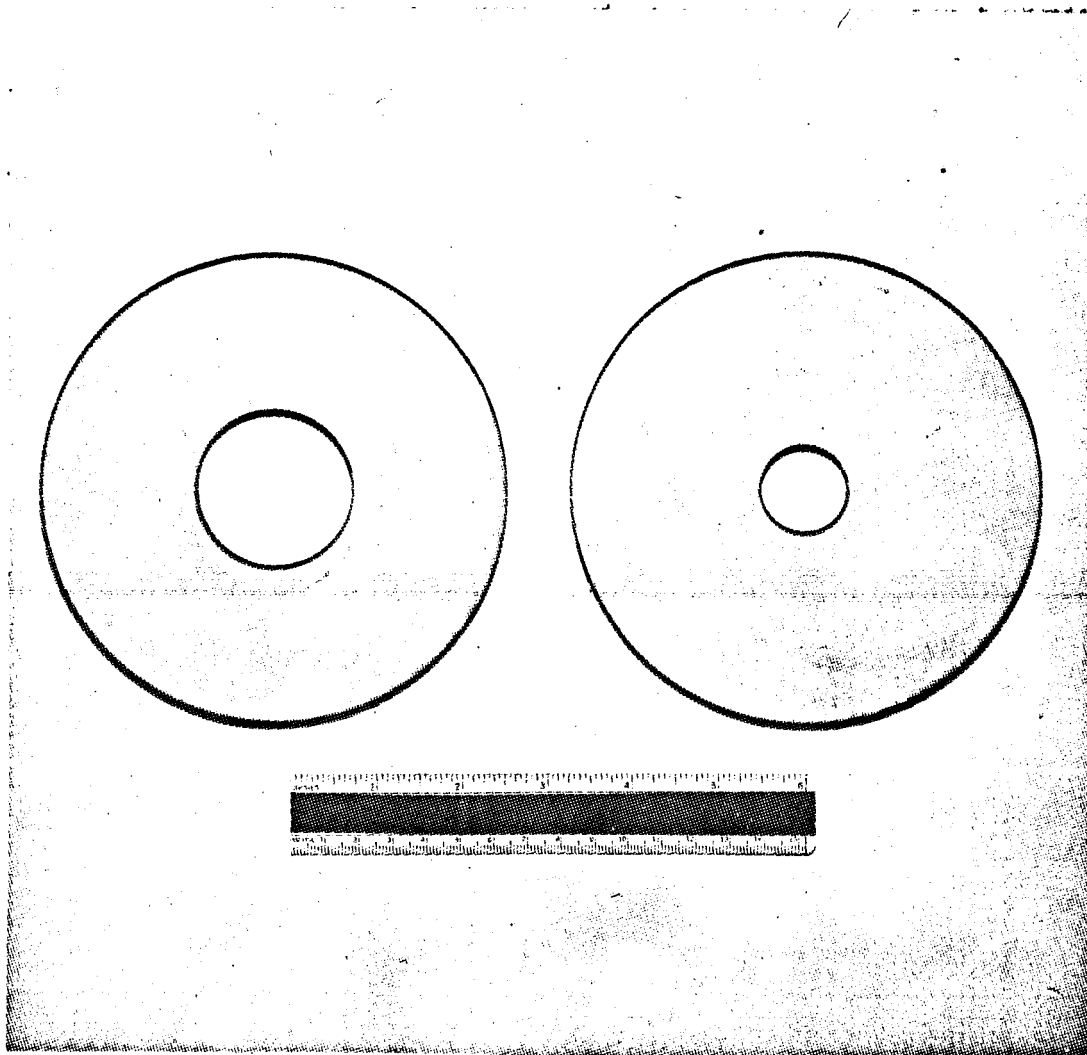
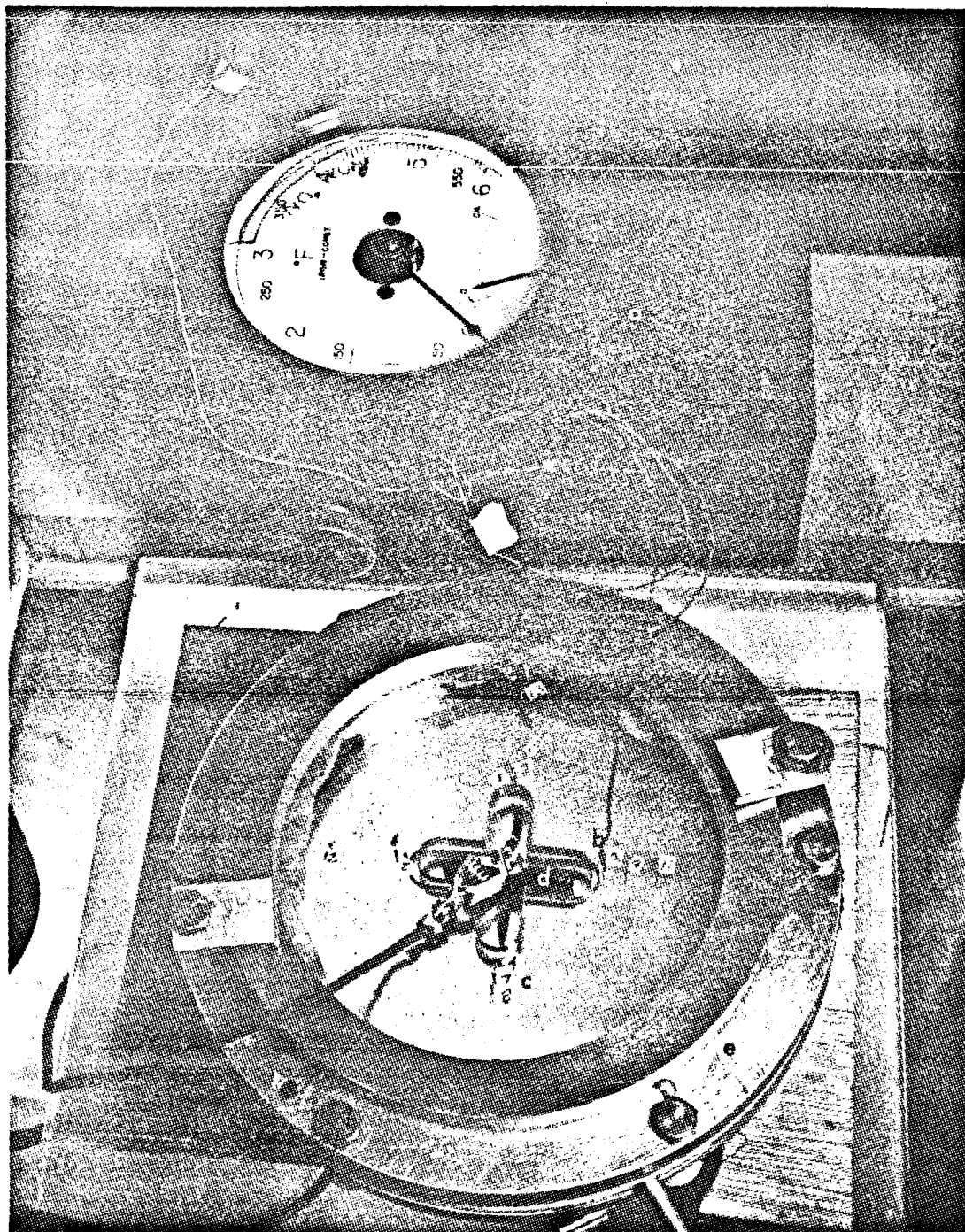Fig. A.7.3. Hysal 4485 calibration specimens
for calibrating pressure jig.
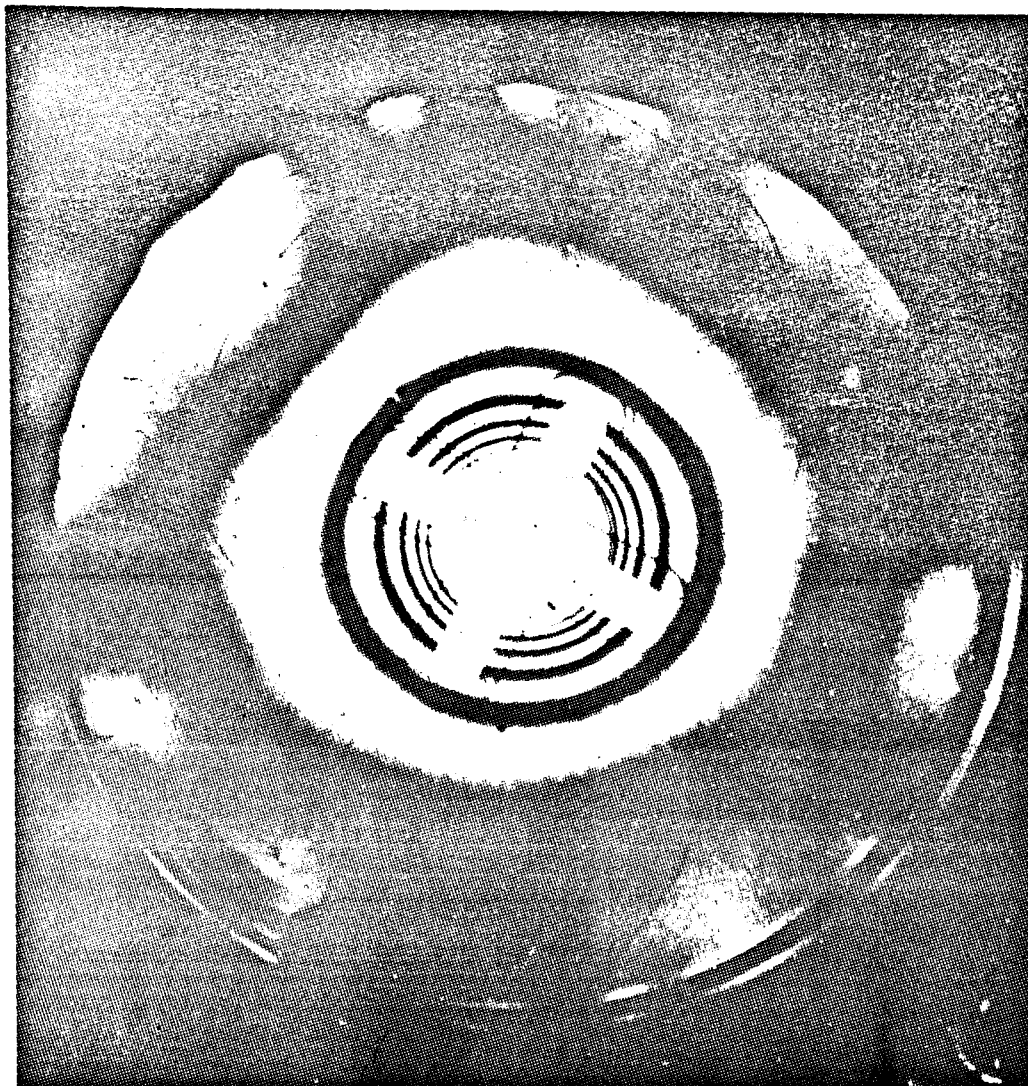
Fig. A.7.4. Pressure calibration specimen with circular
hole (star cutouts in Polaroid).
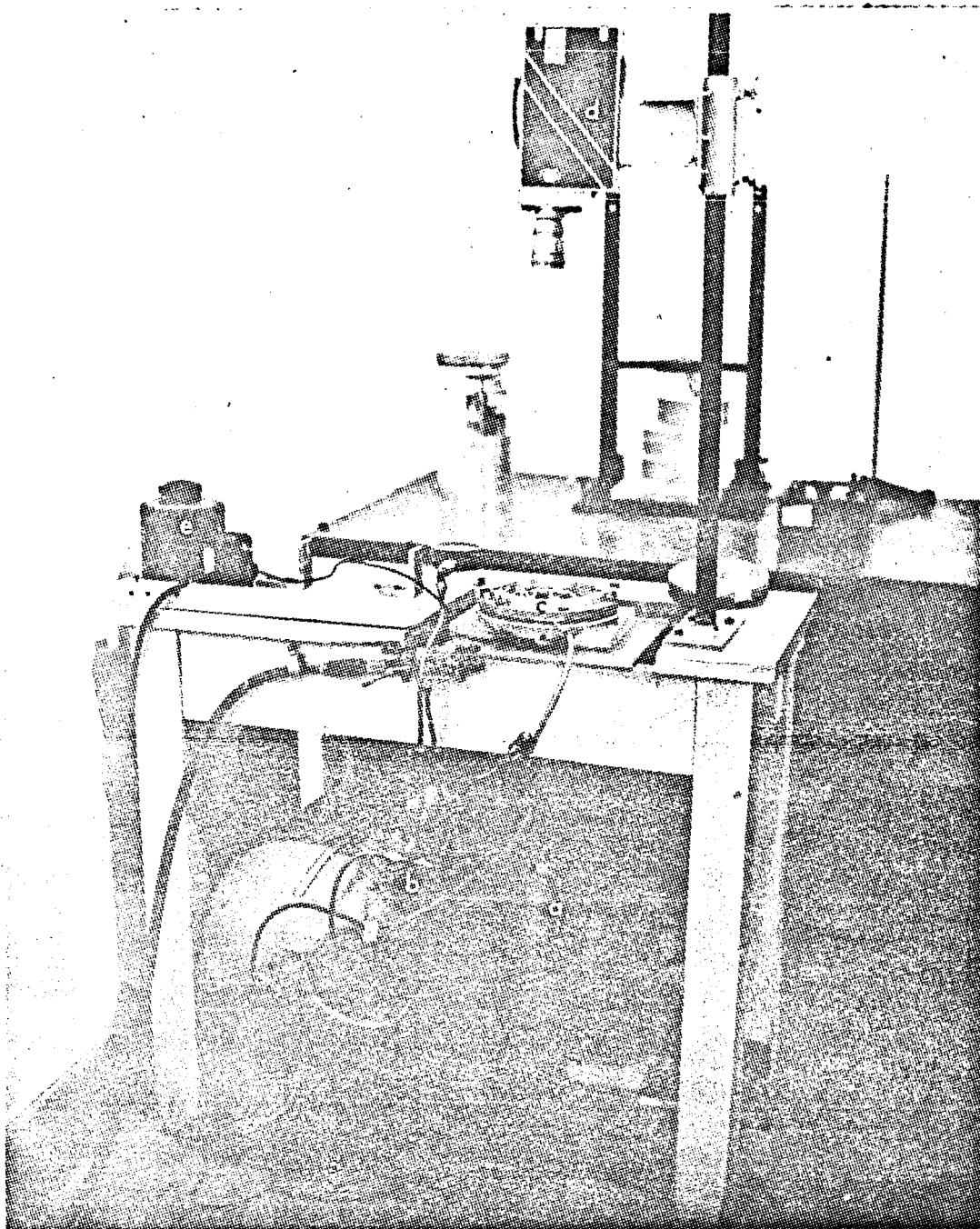
a)   light source, filtered Hg

b)   constant pressure air supply

c)   loading jig (Polaroids incorporated)

d)   camera

e)   heater variac

Fig. A.7.5.   Horizontal polariscope for heated model studies

a) Potentiometer

b) Thermocouple probe

c) measuring stations

d) heater

e) pressure loading jig

Fig. A.7.6. Apparatus for determining temperature distribution

APPENDIX A.8.

High Resolution Optical Bench

Introduction:

A high resolution optical bench has been designed and built. It was designed to be used primarily as a parallel beam polariscope. This type of polariscope lends itself more readily to solving problems where a high degree of precision is required. A general view of the polariscope is shown in Figure A.8.1, and the major elements of the bench are outlined. The desirable characteristics of this polariscope are: (1) the beam is collimated to a high degree, which is necessary in several methods of optical observations of physical phenomena. (2) the useable field is quite large (11" in diameter), (3) the field is more uniform than one obtained by other means.

This polariscope is meant to supplement the existing diffused light, and rotating element polariscopes described previously. Its purpose is to utilize methods of observation which are not possible with the others. For example, photoviscoelastic materials in general have low birefringent response which for most loading conditions results in a low fringe order with rather small fringe gradients. One method to improve an accuracy of observations under such conditions is to use a fringe multiplying device. This consists of two partially reflecting plane mirrors which are inserted on each side of the model to be tested. This results in a multiplication of the fringe pattern and hence significantly increases the accuracy. Such a device requires a parallel beam and the accuracy which can be obtained depends to an extent on the collimation of the beam.

In the following each system of this polariscope is described in detail. It would be well to note in passing that the uses of this optical bench

are not limited to its various uses as a polariscope. Other methods
of optical observations such as Moiré fringes are planned.

Optical System:

The primary characteristics of the high resolution optical bench
from an optics point of view are:

(a) It utilizes a point light source

(b) It has a parallel beam working section

(c) It has an eleven inch diameter usable working section.

(d) It utilizes multi-element collimating lenses to achieve
    these characteristics.

A schematic diagram showing the arrangement of the optical system
is shown in Figure A.8.2. The point light source is placed at the focal
point of the large collimating lens. This is multi-element 48" focal length,
F/6.3 aerial photography lens. These high quality lenses, which are the
heart of the optical bench, were obtained from government surplus. When
used in this manner an 11" diameter usable field can be obtained. The
beam is collimatical such that the deviations from a parallel beam are
less than 4 seconds of arc.

Within the parallel beam the light is linearly polarized by means
of an absorption type polarizing sheet. Next the light is passed through
a quarter-wave plate which generates circularly polarized light. Just
before the light enters the second collimating lens it passes through
secon quarter-wave plate and an analyzer. These elements are mounted
directly on the collimating lens, this arrangement is shown in Figure A.8.3.

The quarter-wave plates are designed for $5540 \pm 200°$A light and the polaroid sheets are relatively insensitive to changes in wave length over the visible range.

A focusing lens is placed at or near the focal point of the second collimating lens. This is used to change the size of the image that can be obtained on the viewing screen with a limited motion of this screen.

The viewing apparatus of course depends upon the type of experiment being conducted. At present it consists of the ground glass screen of an 8 x 10 view camera. This portion of the polariscope has been fitted with an optical bench to facilitate the mounting of other types of observation equipment. This may be seen in Figure A.8.3.

Illumination System:

In order to obtain accurate quantitative results in photoelastic experiments monochromatic light is required. This is achieved in this polariscope in the same manner as used in the other polariscopes described. A high pressure mercury arc lamp is used in conjunction with a narrow band filter. The lamp used is a PEK-109 its spectral output is shown in Figure A.8.4. It will be noted that the output is very rich in ultra-violet. The particular emission line used is the $5460°$A line. The quarter wave plates used were supplied by the Polaroid Corporation, and are designed to be operated at 5600 ± 200 A$°$. It will thus be noted that the quarter-wave plates are not perfectly matched to the light and would result in slightly elliptically polarized light in the working

section rather than the desired circularly polarized light. The effect of this is quite small and is compensated for by arranging the quarter-wave plate of the polarizer and analyzer perpendicular to each other. This reduces the effect to a second order one when compared to other optical imperfection in the system, for example, the finite size of the point light source (a 0.012" arc).

The characteristic of various types of filters used in this polariscope are shown in Figure A.8.5. In this particular use, it will be noted that the dielectric narrow band pass filter is superior for the following reasons: (1) the transmittance is higher and yields an increase in light intensity by a factor of 2.4 and (2) the shape of the transmission curve is more nearly center on the mercury line and its general shape is more symmetric.

Loading Devices:

At the present two types of loading devices have been built for use with this polariscope. Figure A.8.6. shows a straining frame of typical design which applies either tension or compression loads. Figure A.8.7 shows a pressure loading rig for use in applying a uniform pressure to the external surface of a circular disc. This pressure jig differs from the one described in Appendix A.7 in that this one is designed for use with material of a higher modulus of elasticity and lower birefringent response. Thus the operating pressure must be higher (100 psi) and the model deflections may be assumed to be small. In this device O-rings were used to provide a pressure seal against the model, thus allowing the pressure to be applied directly to the model. Nitrogen gas is used for the working medium. Also seen in Figure A.8.7 is a 6-place binary counting device which is used to number negatives.
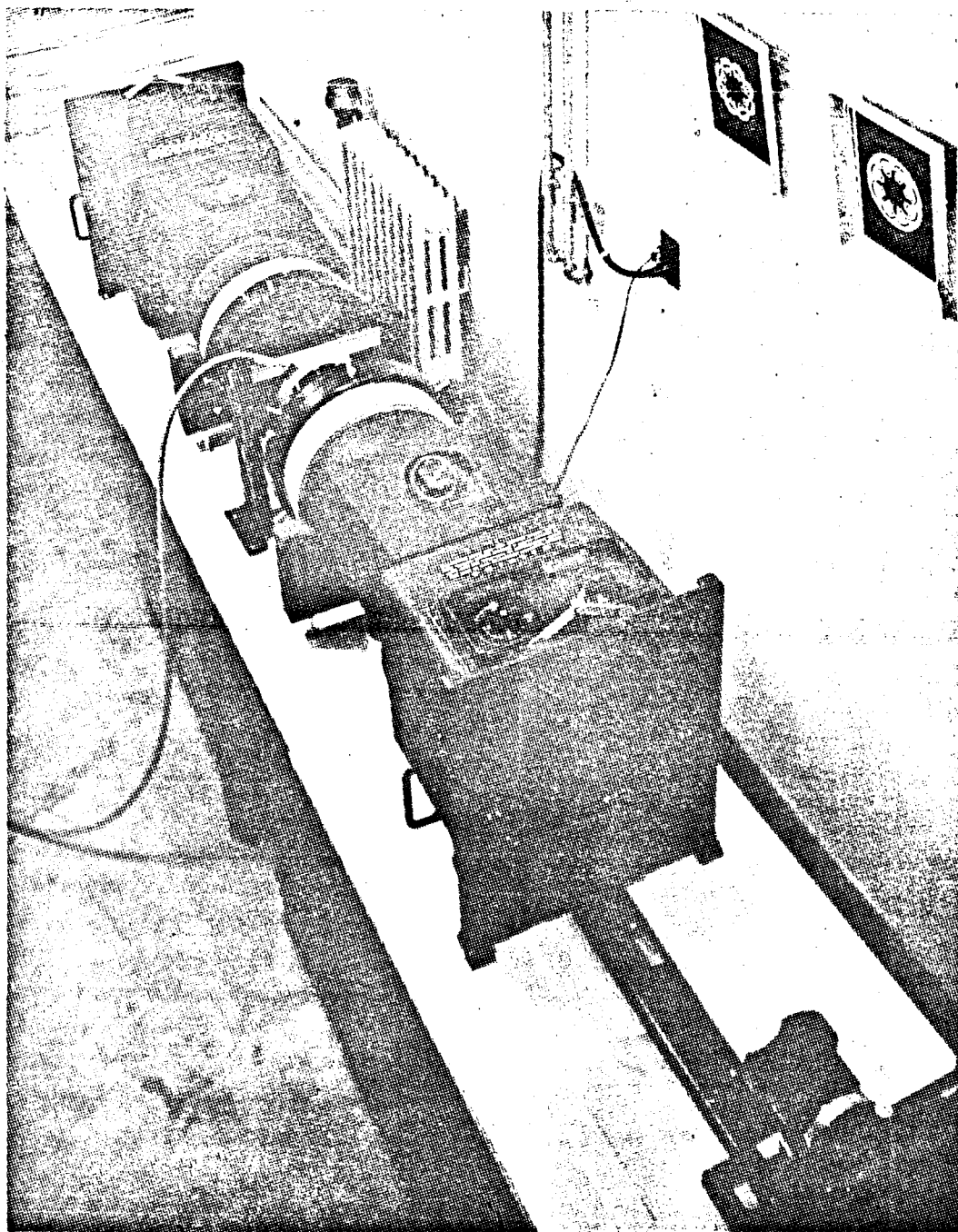
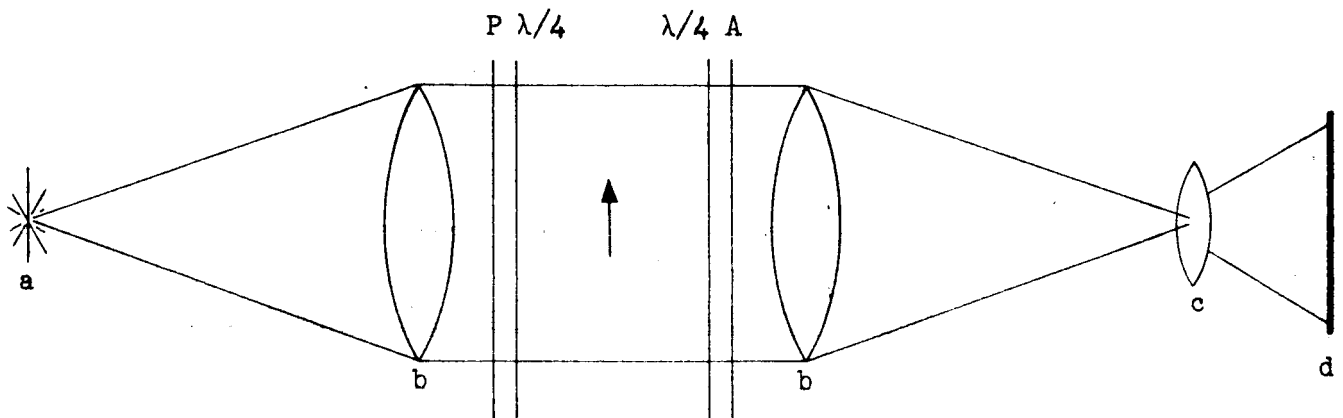Fig. A.8.1. Over-all view of optical bench.

Fig. A.8.2. Schematic Diagram of Optical Arrangement

    a - Point light source

    b - Collimating lenses - 48" focal length f/6.3

    c - Focusing lens - 20" focal length f/5.6
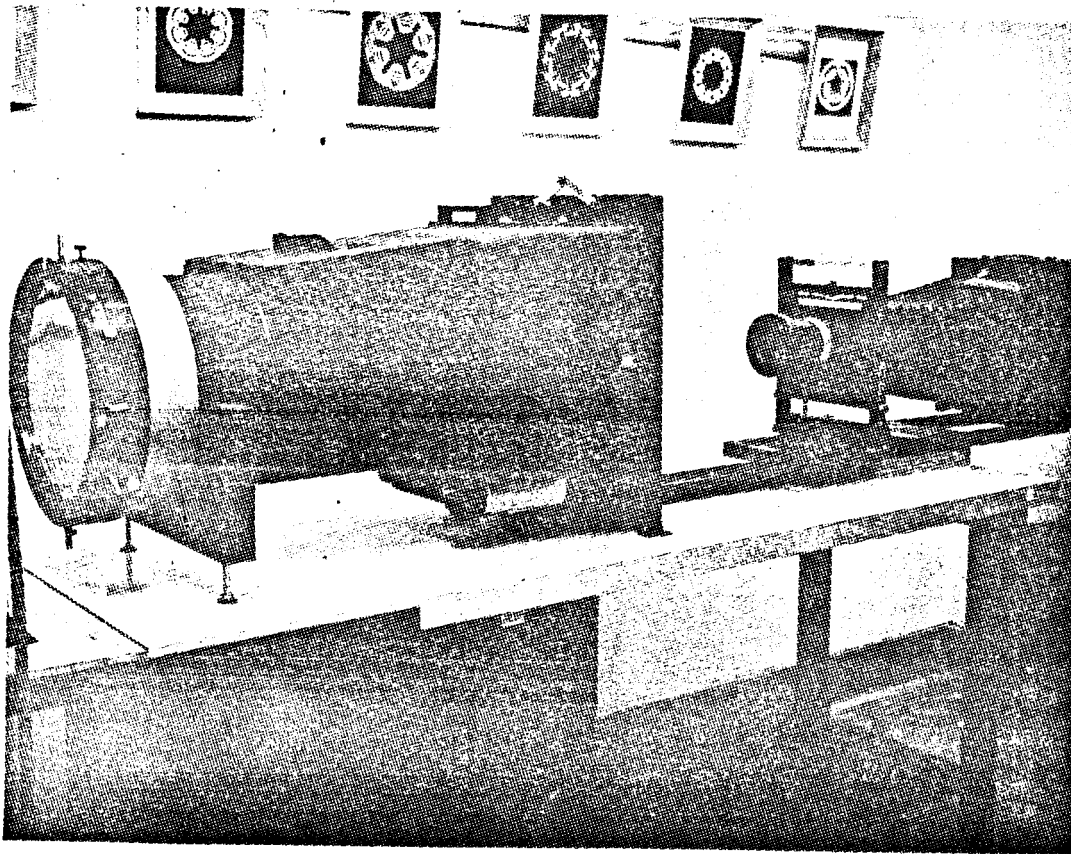
    d - Viewing device

Fig. A.8.3. Collimating lens with attached quarter-wave
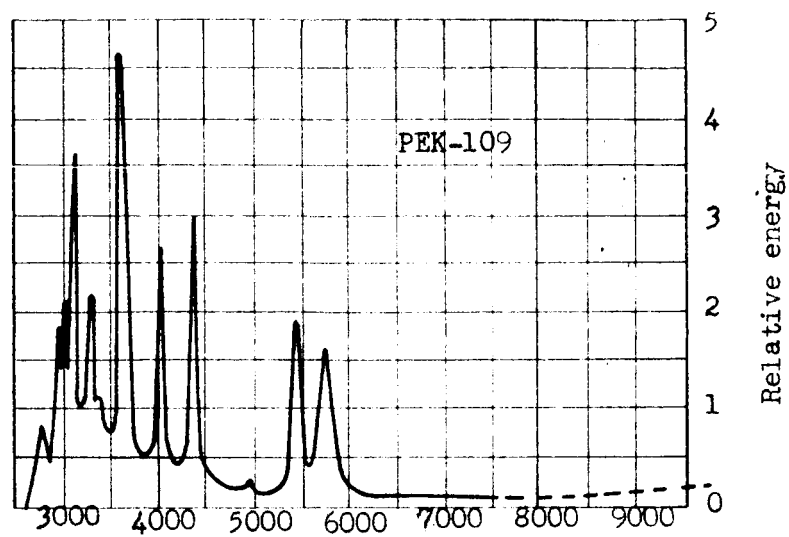plate and analyzer. Also scan arc focus.

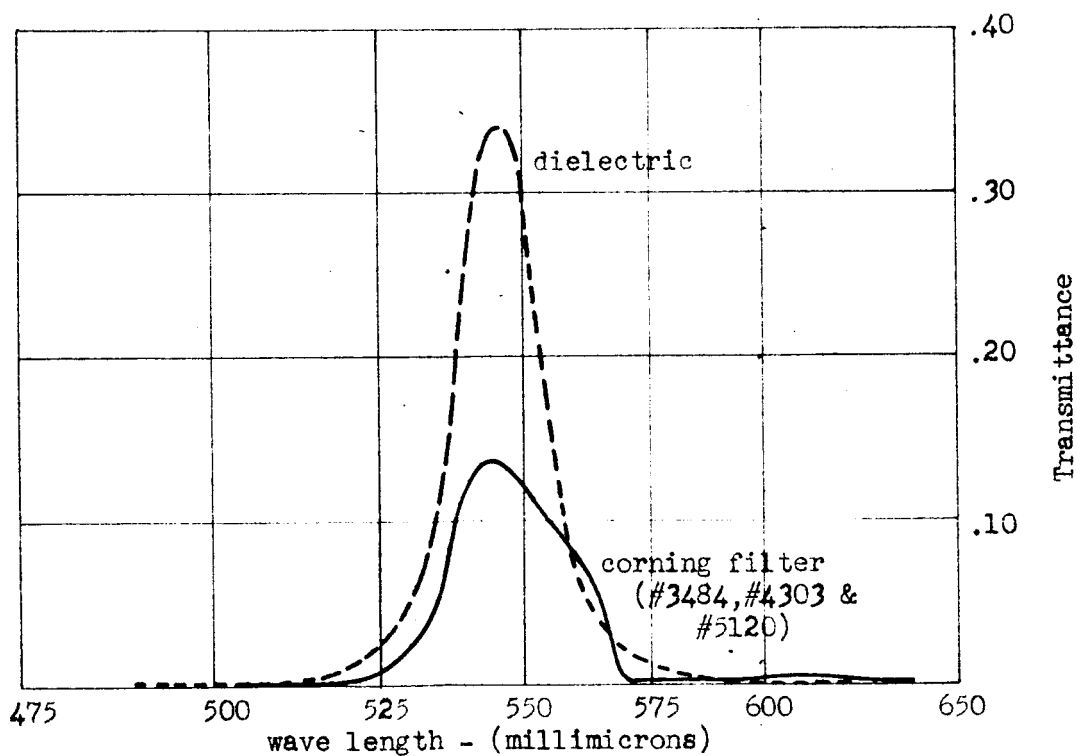Fig. A.8.4. Relative spectral energy graph for PEK-109

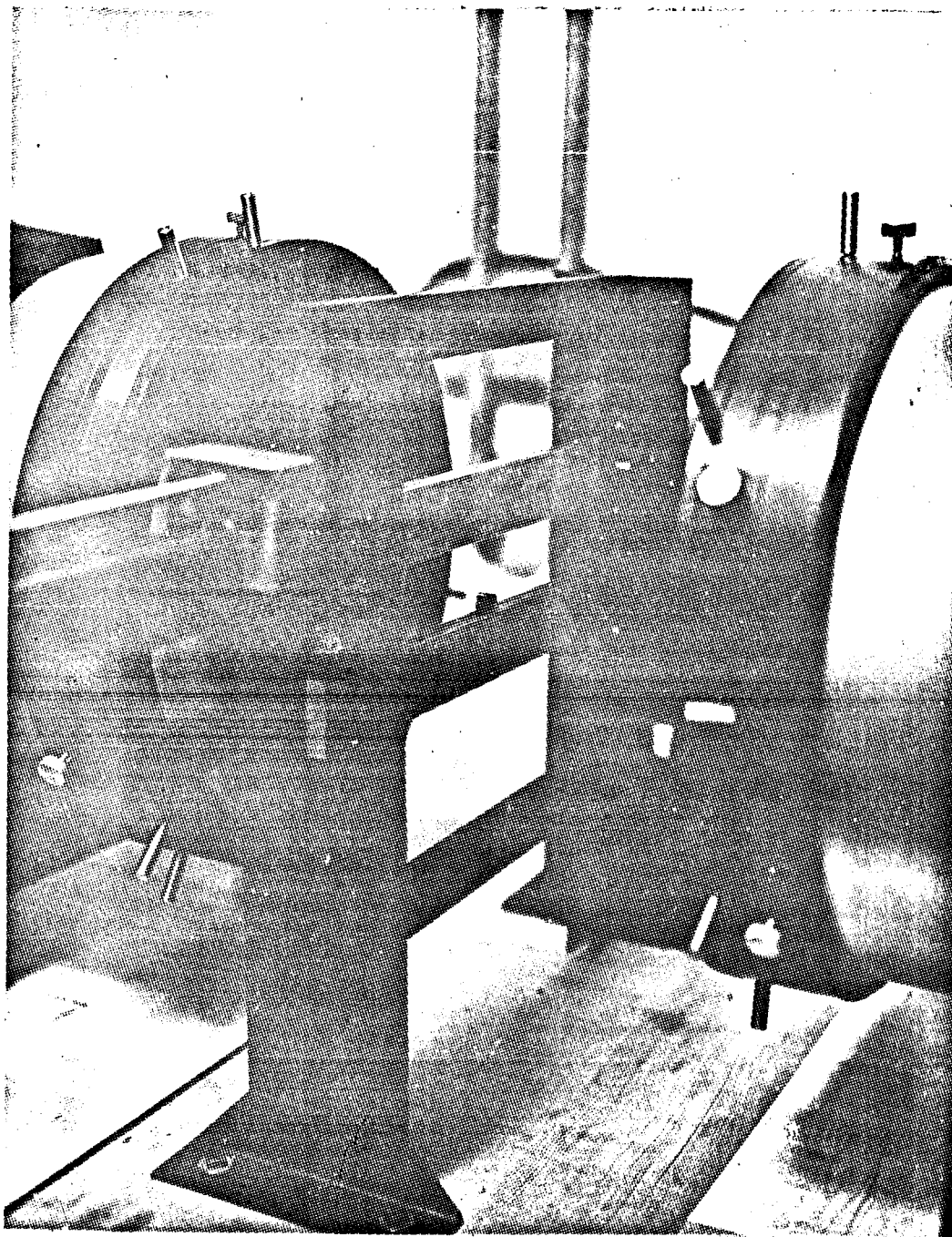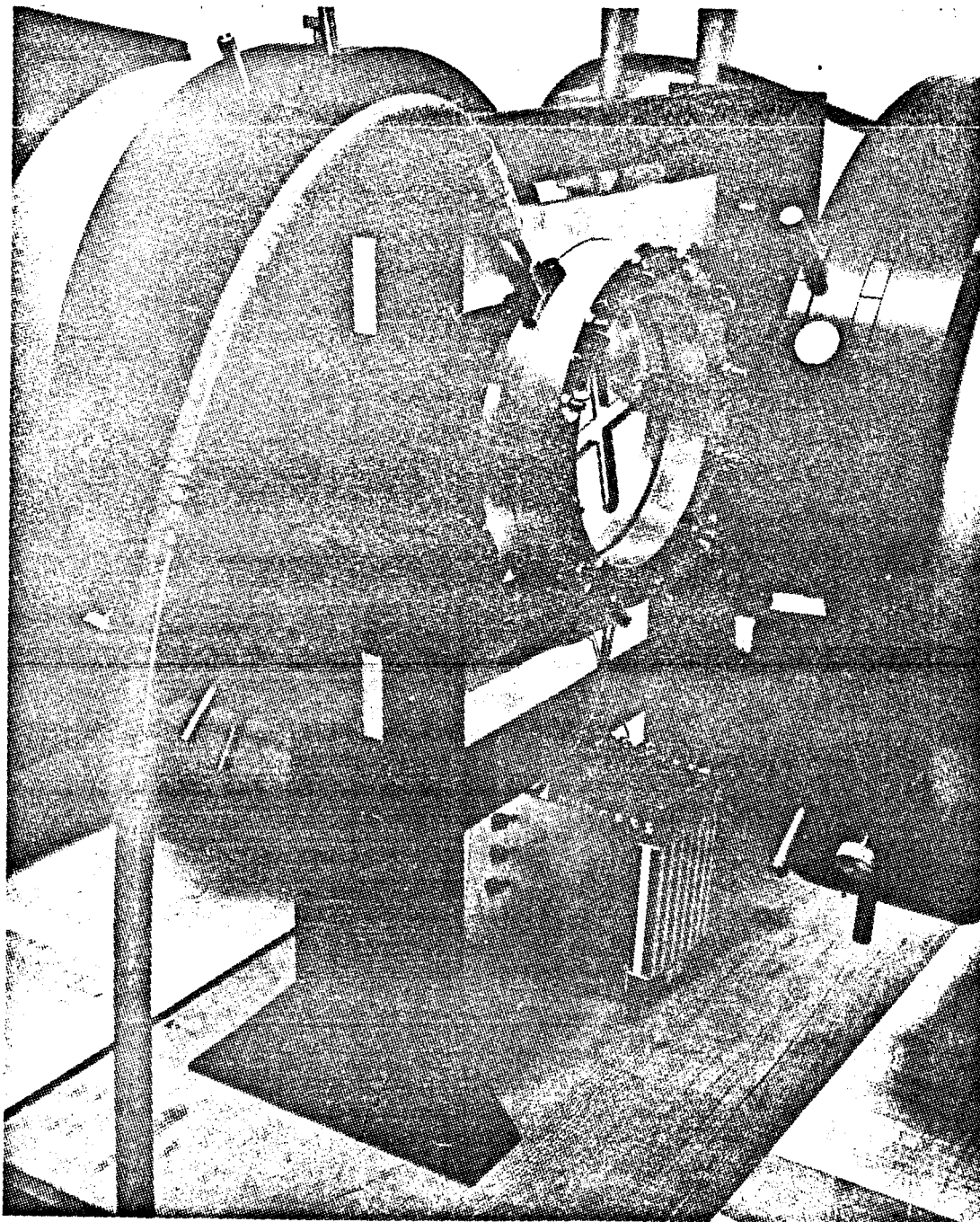Fig. A.8.5. Filter characteristics.

Fig. A.8.6 Straining Frame

Fig. A.8.7. Pressure rig with rocket grain
cross-section and binary counter.